Development and analysis of responsive polymers as sensing elements for storage conditions and freshness of food

by

Adrian David Lopera-Valle

A thesis submitted in partial fulfillment of the requirements for the degree of

Doctor of Philosophy

in

Materials Engineering

Department of Chemical and Materials Engineering

University of Alberta

Abstract

As the global population growth continues to increase the needs for higher production of food, governments, organizations, and individuals are faced with the task to implement strategies to mitigate the impact that food waste has in food security, the economy and the environment. One of the sources of this waste is directly linked to the lack of accurate information that retailers and end-consumers (individuals, hotels, restaurants, caterers, etc.) have about the storage conditions history and freshness food. In order to reduce this source of waste, tools such as active, intelligent, and smart packaging. Intelligent packaging can monitor food storage conditions and freshness, as one potential solution to mitigating waste.

Recently, responsive polymers are strong candidates to fabricate intelligent packaging given that they can show measurable changes in properties that can be used to monitor changes in storage conditions and freshness. Other advantages of responsive polymers include versatility, low weight, and inexpensive price, which make them attractive in intelligent packaging applications.

This thesis studies two particular responsive polymer systems that present potential to be used in packaging systems. These can provide information about humidity, as factor of correct packaging and handling of food, and about the concentration of amines, by-product of produce decomposition, as indicator of freshness.

The first polymer system is a conductive polymer composite (CPC), comprised of commercial silver (Ag) micro-particles that provides high conductivity to the films, and of a hygroscopic polymer matrix (poly(hydroxyethyl methacrylate)-co-poly(ethylene glycol diacrylate) (HEMA-co-PEGDA)) that responds to humidity by undergoing an increase in volume

(through swelling). The electrical resistivity and swelling behavior of the CPCs are characterized, thin films or patterned lines are fabricated to form sensors, and the effects of relative humidity on the electrical resistivity of the composite films for different compositions and geometries are investigated. To characterize the material responsive behaviour, a data acquisition system was used to measure changes in resistance while the relative humidity was controlled in a humidity chamber. When the humidity was increased from 25% to 95% RH, the resistance of the films increased up to 650%. Composites with a higher fraction of HEMA in the matrix were found to have both lower recovery times and less hysteresis than composites in which the matrix was pure PEGDA. Such materials can form the basis of inexpensive, printable humidity sensors.

The second polymer system is a functional graft-polymer of poly(lactic acid) (PLA) and succinic anhydride (SAh) to engineer colorimetric indicators that respond to the presence of amine vapours. In this graft-polymer, PLA behaves as backbone for SAh, which responds to amines by undergoing a ring opening amidation reaction. This reaction can be reported through the inclusion of a pH responsive dye. Firstly, the grafting reaction was carried by means of free radical polymerization of PLA and maleic anhydride (MAh) in ratios of PLA:MAh from 90:10 wt% to 25:75 wt%, using AIBN as free radical initiator. The characterization of the grafting reaction and of the chemical-response to amines was carried out on solvent cast polymer films that were exposed to amine vapours. The response of the PLA-g-SAh polymers with different compositions to amines was characterized by studying their thermal properties by DSC before and after exposure to the vapours from a 400 ppm methylamine solution. To engineer colorimetric sensors, the PLA-g-SAh polymers with varying composition were mixed in solution with a pH-responsive dye and air-sprayed onto paper. Colorimetric indicators were exposed to concentrations of methylamine ranging from 50 to 600 ppm at temperatures from 5ºC to 22ºC.Visible changes in color were

observed to be affected by both solution temperature and amine concentration. From this data, the kinetics of the color change reaction were studied, and rate constants were estimated. This work presents potential opportunities for the development of real-time amine sensors under different conditions of temperature and analyte concentration.

The development of responsive materials like those studied in this thesis have great potential in applications of intelligent packaging. Their further development can contribute to mitigate some of the sources of food waste that are linked to producers and consumers lacking knowledge of the storage conditions and freshness of food.

Preface

The work henceforth presented has been conducted at Dr. Elias' research laboratory, under the supervision of Dr. Anastasia Elias, at the Department of Chemical and Materials Engineering, at the University of Alberta in Canada.

A version of Chapter 3 has been published as Adrián Lopera-Valle, Anastasia Elias, *"Low-resistance silver microparticle-HEMA-PEGDA composites for humidity sensing"*, Smart Mater. Struct., Volume 27, Number 10 (105030), doi: 10.1088/1361-665X/aad355. All the major components of this manuscript: conceptualization, planning, experiment design, data collection, analysis and editing, were responsibility of the author of this thesis. It is full acknowledge that Dr. Anastasia Elias, as supervisory author of given manuscript, played an indispensable role in conceptualization, design, data analysis and composition.

A version of Chapter 4 has been published as Adrián Lopera-Valle, Anastasia Elias, *"Amine Responsive Poly(lactic acid) (PLA) and Succinic Anhydride (SAh) Graft-Polymer: Synthesis and Characterization"*, Polymers, Volume 11, Issue 9, No. 1466, doi: 10.3390/polym11091466. All the major components of this manuscript: conceptualization, planning, experiment design, data collection, analysis and editing, were responsibility of the author of this thesis. It is full acknowledge that Dr. Anastasia Elias, as supervisory author of given manuscript, played an indispensable role in conceptualization, design, data analysis and composition.

A version of Chapter 5 will be submitted for consideration of a peer-reviewed journal as Adrián Lopera-Valle, Anastasia Elias, "*Colorimetric Indicators for Volatile Amines Based on Succinic Anhydride (SAh)-grafted Poly (lactic acid) (PLA)*". All the major components of this manuscript: conceptualization, planning, experiment design, data collection, analysis and editing,

were responsibility of the author of this thesis. It is full acknowledge that Dr. Anastasia Elias, as supervisory author of given manuscript, played an indispensable role in conceptualization, design, data analysis and composition.

Acknowledgements/Agradecimientos

I would like to deeply thank my supervisor and mentor Dr. Anastasia Elias for these years of support and guidance. Her commitment to help me, and my colleagues, grow professionally made of my doctoral studies a fulfilling learning experience. I am thankful to have had the opportunity of being one of Dr. Elias trainees.

I would like to thank my friends and colleagues at Dr. Elias Lab. Their professional and personal support have helped me overcoming some of the obstacles that I faced during my courses, experiments, candidacy exam preparation, conference talks, and weeks of writing. Sharing with them long days in the lab, dinners after work, and constructive conversations in the office motivated me to be a better researcher every day.

Finalmente, quiero agradecer a mis padres, Gloria y Fernando, que desde la distancia, me acompañaron durante este largo proceso. A mi hermano, mejor amigo y héroe personal, Sebastian, por saber escucharme cuando así lo necesitaba, por animarme en tiempos difíciles y acompañarme en logros académicos y personales. A Susie, mi pareja de caminatas en el valle del rio, frías noches de invierno, e interminables aventuras de verano, por todo su soporte y amor. A mis nuevos y viejos amigos, Lina, Nikki, Linda, Shuwen, Razim, Shaina, Susana, y todos los demás: mil gracias.

Table of Content

Abstract ii

Preface v

Acknowledgements/Agradecimientos vii

Table of Content viii

List of Figures xii

List of Tables xv

Nomenclature and Abbreviations xvii

1. Introduction 1

Objectives 4

2. Background 6

2.1 Stimuli-responsive polymers in indicators 11

2.1.1 Temperature-responsive polymers for use in time temperature indicators 11

2.1.2 O_2 and humidity-responsive polymers for use in integrity indicators 16

2.1.3 Analyte-responsive polymers for use in freshness indicators (microbial or pathogen spoilage) 18

2.2 Conducive polymer composites (CPCs) for sensors 24

2.2.1 Responsive CPCs for humidity sensing applications 30

2.2.2 Responsive CPCs for amine sensing 32

2.3 Traceability and identification technology 33

3. Low-Resistance Silver Microparticle-HEMA-PEGDA Composites for Humidity Sensing. 36

3.1 Introduction 37

3.2 Experimental methods 40

3.2.1 Preparation of CPC mixture for spin coating and direct-write printing (DWP) 40

3.2.2 Percolation threshold 42

3.2.3 Synthesis of spin-coated films and printed elements 42

3.2.4 Material characterization 43

3.2.5 Electrical characterization of spin-coated films and printed lines 44

3.2.6 Equilibrium water content 45

3.2.7 Humidity response testing 46

3.2.8 Sensitivity 48

3.2.9 Statistical analysis 48

3.3 Results and discussion 48

3.3.1 Material characterization 48

3.3.2 Electrical characterization of spin-coated films and printed lines 53

3.3.3 Equilibrium water content 53

3.3.4 Steady humidity response 57

3.3.5 Cyclic humidity response 60

3.4 Conclusions 65

4. Amine Responsive Poly(lactic acid) (PLA) and Succinic Anhydride (SAh) Graft-Polymer: Synthesis and Characterization 67

4.1 Introduction 68

4.2 Experimental Methods 71

4.2.1 Polymer Synthesis and Sample Preparation 71

4.2.2 GPC 71

4.2.3 Fourier Transform Infrared Spectroscopy (FTIR) 72

4.2.4 Thermal Characterization 72

4.2.5 Hydrogen Nuclear Magnetic Resonance (^{1}H-NMR) 73

4.2.6 Amine Response 73

4.2.7 Statistical Analysis 74

4.3 Results and Discussion 74

4.3.1 Molecular Weight 74

4.3.2 Polymer Structure 76

4.3.3 Thermal Properties and Degree of Grafting 77

4.3.4 Amine Response: Polymer Structure 83

4.3.5 Amine Response: Thermal Properties 85

4.4 Comparison with Literature 88

4.5 Conclusions 91

5. Colorimetric Indicators for Volatile Amines Based on Responsive Poly (lactic acid) (PLA) and Succinic Anhydride graft-polymer 92

5.1 Introduction 93

5.2 Experimental Methods 96

5.2.1 Polymer synthesis 96
5.2.2 Fabrication of color change indicators 96
5.2.3 Scanning electron microscopy 97
5.2.4 Effect of SAh content on sensor response 97
5.2.5 Effect of amine concentration and temperature 98
5.3 Results and Discussion 100
5.3.1 Scanning electron microscopy 100
5.3.2 Effect of SAh content on sensor response 101
5.3.3 Color change performance – concentration and temperature 105
5.3.4 Color transition and sensor characterization – kinetics 107
5.4 Comparison with literature 112
5.5 Conclusions 114
6. Final remarks 115
Conclusions 115
Future work 118
References 120

List of Figures

Figure 2-1: Common structures of responsive polymers [53]. 9

Figure 2-2: Common temperature-responsive polymers and their LCST (adapted from [77]) ... 13

Figure 2-3: Common pH-responsive weak-acid polymers [77] 20

Figure 2-4: Common pH-responsive weak-base polymers [77] 20

Figure 2-5: Illustration of percolation threshold for electric resistivity in CPCs [148] 26

Figure 2-6: Influence of geometry on percolation limit [144] 27

Figure 2-7: (a) Design of RFID with the location of the responsive element (R_s); C: tuning capacitor; L: inductor (antenna); R_{IC}: resistance; and C_{IC}: capacitance of integrated circuit; (b) Poly(4-vinylpyridine)-single-walled carbon nanotubes-Fe(II) ions composite [196] 35

Figure 3-1: Processing, composition, and responsive of conductive-particle composites utilized as humidity sensing materials. 39

Figure 3-2: Typical features of conductive a) spin-coated film samples and b) printed line samples. 43

Figure 3-3: Diagram of humidity testing and data collection. The electrical resistance of the sample and the signal from a commercial humidity sensor placed within the humidity chamber were collected by a DAQ every 3 seconds as the humidity was varied. 47

Figure 3-4: Percolation threshold for resistivity of CPC with PEGDA-100/HEMA-0, PEGDA-50/HEMA-50 and pure HEMA as matrix. 49

Figure 3-5: a) Low and b) high magnification SEM image of a film sample; c) low and d) high magnification SEM image of a bulk sample; e) low and f) high magnification SEM image of a printed line sample. 50

Figure 3-6: Swelling of a) pure polymer blends and b) CPCs with 75 wt% Ag particles. Samples were immersed in water at time = 0 hrs (measured periodically), and removed from water at t = 27 hours and dried to 16% RH. 56

Figure 3-7: Variation of resistance of CPCs in the form of a) spin-coated films and b) printed lines with change in RH from 25% RH to 95% RH, in 10% RH increments for 3 cycles..... 58

Figure 3-8: Cyclic variation of relative resistance of a) spin-coated CPC films and b) printed CPC lines with cyclic change in RH from 35% to 95%..... 61

Figure 3-9: Hysteresis loop (a and c), hysteresis values, and response and recovery times (b and d) of a-b) spin-coated CPC films and c-d) printed CPC lines with different matrix compositions. 63

Figure 4-1: Proposed free radical graft-polymerization reaction between PLA and MAh, and reaction between PLA-g-SAh and methylamine to form PLA-g-Succinamic acid..... 70

Figure 4-2: ATR-FTIR curves between (a) 4000 cm^{-1} and 400 cm^{-1}, and (b) from 3200 cm^{-1} to 2700 cm^{-1} of neat PLA, neat MAh, PLA-g-SAh50, and other graft polymer samples..... 77

Figure 4-3: DSC curves of neat PLA and PLA-g-SAh with different initial contents of MAh. Vertical lines labeled as T_g and T_m mark the glass transition and melting peak temperatures of neat PLA..... 78

Figure 4-4: TGA (a) curves of neat PLA, neat MAh, a film comprised of a 50/50 blend of PLA and MAh without initiator (PLA-MAh50), and grafted polymers (n = 3), and (b) degradation temperature of PLA-g-SAh with different initial contents of MAh. Reference samples (PLA with initiator without MAh and PLA-MAh50) are denoted in red..... 80

Figure 4-5: ^{1}H-NMR spectra of neat PLA, neat MAh, and other graft polymer samples 81

Figure 4-6: Grafting degree of grafting by TGA (n =3) and ^{1}H-NMR of succinic anhydride on PLA as function of the initial content of maleic anhydride concentration in solution. 83

Figure 4-7: FTIR curves between 1300 cm-1 and 980 cm-1 PLA-g-SAh50 samples before and after exposure to methylamine vapor from a 400 ppm solution 84

Figure 4-8: XPS curves for (a, b) C_{1S} and (c, d) N_{1S} before and after exposure to vapours of 400 ppm methylamine solution..... 85

Figure 4-9: DSC curves of neat PLA and PLA-g-SAh with different initial contents of MAh before and after exposure to methylamine. Vertical lines labeled as T_g and T_m mark the glass transition and melting peak temperatures of neat PLA..... 87

Figure 5-1: Proposed free radical graft-polymerization reaction between PLA and MAh, and the color change response of PLA-g-SAh and methylamine to form PLA-g-Succinamic acid 95

Figure 5-2: Data analysis for sensor characterization..... 99

Figure 5-3: a) Low and b) high magnification SEM image of a bare paper filter; c) low and d) high magnification SEM image of a PLA-g-SAh coated filter paper..... 101

Figure 5-4: Adsorption UV-Vis spectra and images of color change indicators before and after their exposure to methylamine (n = 5)..... 102

Figure 5-5: Blank samples of a) papers sprayed with only dye (no polymer was deposited) and exposed to methylamine vapor from a 400 ppm solution as control experiment; b) neat PLA exposed to water vapour; c) PLA-g-SAh30 indicators exposed to water vapour and d) to the vapours from a 300 ppm solution of methanol 104

Figure 5-6: Characterization of PLA-g-SAh30 indicators after 24 hrs of exposure to different methylamine concentrations and temperatures. (a) Color of sensors exposed to methylamine concentrations and temperatures indicated, (b) UV-Vis spectra for samples at 22°C and different amine concentrations, and effect of (c) temperature and (d) concentration on the color of the color indicators based on UV-Vis absorbance after 24 hrs of exposure to methylamine. 106

Figure 5-7: Color change of colorimetric sensor exposed to (a) 600 ppm, and (b) 50 ppm at 22°C 108

Figure 5-8: Response of PLA-g-SAh30 indicators as a function of time. (a) Uv-Vis spectra time series for the response of colorimetric sensors exposed to 300 ppm solution at 22°C. Wavelength of the maximum absorbance peak versus time (hrs) for samples exposed to different methylamine concentrations as measured at (b) 5°C, (c) 14°C, and (d) 22°C. 109

Figure 5-9: Effect of (a) temperature and (b) concentration on the rate of color change at half-time of response. 111

List of Tables

Table 2-1: Some examples of pH indicators based on responsive polymers [75] 22

Table 3-1: Composition of CPC mixture for spin coating process (selected to achieve a final composition of 75 wt% Ag microparticles and of 25 wt% polymer after spin coating, based on preliminary studies). The name of each composite indicates the desired ratio of PEGDA/HEMA after spin-coating (excluding the mass of the filler phase). 41

Table 3-2: Composition of CPC mixture for DWP process. The name of each composite indicates the desired ratio of PEGDA/HEMA after printing (excluding the mass of the filler phase). 41

Table 3-3: Composition of CPC spin-coated films (n = 3 for each polymer blend). The ratio of polymer to Ag was determined by TGA. The total fraction of PEGDA and HEMA in the polymer matrix was then calculated from these results based on the relative fraction of each added to the mixture (as reflected by the sample names). 52

Table 3-4: Composition of CPC printed lines. The ratio of polymer to Ag was determined by TGA. The total fraction of PEGDA and HEMA in the polymer matrix was then calculated from these results based on the relative fraction of each added to the mixture (as reflected by the sample names). 52

Table 3-5: Contact Angle of Ag CPCs 55

Table 3-6: Sensitivity of spin-coated film and printed line sensing elements. 60

Table 3-7: Comparison of resistive humidity sensors based on conductive polymer composites (CPC). 65

Table 4-1: Sample composition 71

Table 4-2: Summary of GPC results (n = 3). 75

Table 4-3: Thermal properties from DSC of neat PLA and PLA-g-SAh (n = 3, P < 0.01). 79

Table 4-4: Thermal properties from DSC of neat PLA and PLA-g-SAh before and after exposure to methylamine (n = 3). 86

Table 4-5: Relevant responsive polymers that react to amines (from 2017 to 2019) 89

Table 5-1: Sample composition 96

Table 5-2: Half-time (hrs) of response of the indicators under different conditions of concentration and temperature..... 110

Table 5-3: Recent color change indicators for amines relevant to this work (from 2015 to 2018) 113

Nomenclature and Abbreviations

Symbols

ΔHm	Enthalpy of fusion
D	Density
EWC	Equilibrium water content
h	Thickness
I	Current
L	Length
m	Mass
Mn	Number average molecular weight
Mw	Molecular weight
P	Pressure
PDI	Polydispersity index
R	Resistance, electrical
RH	Relative humidity
RR	Relative resistance
t	Time
Td	Degradation temperature
Tg	Glass transition temperature
Tm	Melting temperature

V	Voltage
Vol, v	Volume
vol%	Volume percentage
W	Width
wt%	Weight percentage

Greek symbols

ρ	Resistivity
κ	Rate of reaction
λ	Wavelength

Superscripts

t	Critical exponent
p	Power of sigmoidal regression

Subscripts

0	Initial
½	Half
Ag	Silver
c	Percolation threshold
CPC	Conductive polymer composite, Composite
D	Dry
f	Final

F	Filler
m	Matrix
max	Maximum
RH	Relative humidity
s	Saturation
w	Vapour
W	Wet

Abbreviations

^{1}H-NMR	Hydrogen Nuclear Magnetic Resonance
4-VP	4-vinylpyridine
AA	Acrylamide
AIBN	2,2′-Azobis(2-methylpropionitrile)
APTES	3(aminopropyl) triethoxysilane
BA	Biogenic amines
BuMa	Butyl methacrylate
CB	Carbon black
CNT	Carbon nanotubes
CO_2	Carbon dioxide
CO_2e	Carbon dioxide equivalent
CPC	Conductive polymer composite

DCP	Dicumyl peroxide
DSC	Differential scanning calorimetry
DTA	Differential thermal analysis
DWP	Direct write printing
EMI	Electromagnetic interference
FAO	Food and agriculture organization
Fe	Iron
FLW	Food loss and waste
FTIR	Fourier Transform Infrared Spectroscopy
GPC	Gel permeation chromatography
HDPE	High-density polyethylene
HEMA	Hydroxyethyl methacrylate
KC	Kappa-carrageenan
LCST	Lower critical solution temperature
LDPE	Low-density polyethylene
MAh	Maleic anhydride
MAP	Modified atmospheres in packaging
MB	Methylene blue
MWCNT	Multiwall carbon nanotubes
NIPA	N-isopropyl acrylamide

NPTh	Nitrated polythiophene
NTCR	Negative temperature coefficient of resistance
PAA	Poly(acrylic acid)
PANI	Polyaniline
PDEAEMA	Poly(N,N-diethyl aminoethyl methacrylate)
PDLA	Poly(D-lactide)
PDMS	Polydimethylsiloxane
PEAAc	Poly(2-ethyl acrylic acid)
PEG	Poly(ethylene glycol)
PEGDA	Poly(ethylene glycol) diacrylate
PEO	Polyethylene oxide
PET	Polyethylene terephthalate
PEVA	Poly(ethylene-co-vinyl acetate)
PLA	Poly(lactic acid)
PLLA	Poly(L-lactide)
PMAA	Poly(methacrylic acid)
PNIPAA	Poly(N-isopropylacrylamide)
PP	Polypropylene
PPAA	Poly(2-propyl acrylic acid)
PS	Polystyrene

PSMA	Polystyrene-co-maleic anhydride
PTCR	Positive temperature coefficient of resistance
PTFE	Polytetrafluoroethylene
PU	Polyurethane
PVA	Poly(vinyl alcohol)
PVA	Poly(vinyl acetate)
PVC	Polyvinyl chloride
PVDF	Polyvinylidene fluoride
PVP	Poly(vinyl pyrrolidon)
QCM	Quartz crystal microbalance
RFID	Radio frequency identification
RH	Relative humidity
SAc	Succinic acid
SAh	Succinic anhydride
SE	Secondary electrons
SEM	Scanning electron microscopy
St	Styrene
TEAMPS	Tetraethylammonium
TGA	Thermogravimetric analysis
THF	Tetrahydrofuran

TTI	Temperature time indicator
TVPT	Temperature of volume phase transition
UATR	Universal attenuated total reflectance
UCST	Upper critical solution temperature
VOC	Volatile organic compounds
VP	1-Vinyl-2-pyrrolidinone
XPS	X-ray photoelectron spectroscopy
LWF	Lost and wasted food
CO_2e	Carbon dioxide equivalent
FAO	Food and agriculture organization
PEGDA	Poly(ethylene glycol) diacrylate
TTI	Temperature time indicator
CPC	Conductive polymer composite
RFID	Radio frequency identification
MAP	Modified atmospheres in packaging
TVPT	Temperature of volume phase transition

1. Introduction

The Food and Agriculture Organization (FAO) of the United Nations has repeatedly reported that, at a global level, one third of food produced for human consumption is lost or wasted. This level of waste is significantly higher in developed countries of North America and Europe than in developing countries of African and Latin America [1]. In particular, food loss and waste (FLW) in Canada has been reported to be nearly 60% of the food produced in the country, representing an alarming 35.5 MT of food every year [2]. The economic costs to business and society of FLW are linked to unnecessary transportation, energy, water, fertilizer, machinery and equipment, packaging, and landfill usage, to name a few. While the current agricultural systems produce enough food to feed the world's population, it is estimated that about four million Canadians (including 1.4 million children) have insufficient access to food, despite the enormity of avoidable FLW that occurs [2].

The environmental impacts of FLW have been shown to be equally worrying. Based on published life cycle assessments that consider production, processing, and manufacturing of food, a total of 56.5 MT of the total carbon dioxide equivalent (CO_2e) in emissions are linked to the waste of food in Canada [3]. This represents roughly 60% of CO_2e emissions of the food industry in the country and a major contributor to the national greenhouse gas emissions budget [2]. In addition, FAO has estimated that every tonne of FLW carried in Canada is directly responsible for 128,000 liters of wasted surface and ground water [4].

While all agents along the food production chain, from producers and processors to retailers and consumers, have a relevant role in the generation of food waste, losses generated between manufacturers, retailers, and consumers demand advances in packaging systems that work as tools for these players to reduce their contribution to the issue [5]. In the past half century, packaging has been positioned as an essential technology to ensure the safe production and commercialization of food, and to eliminate contamination, increase shelf-life, and satisfy consumer expectations [6]. Current needs for innovation in packaging have led active, intelligent, and smart food packaging to be growing industries with a significant potential to reduce food waste [7].

Intelligent packaging allows the monitoring of condition of food and/or the enclosed environment. It can provide dynamic feedback to the consumer on the actual quality of the product, by interacting with indirect (environmental) and/or direct factors (food components and metabolites in the headspace) to generate a response (i.e., colour change, electrical signal) that correlates with the state of the food product. This information can be a tool to reduce food waste by informing consumers about the quality and safety of food. In contrast, the current "Best Before" and "Use By" are based on averages and assumptions regarding storage conditions. Therefore, the development of dynamic intelligent packaging could offer simple information on storage conditions such as temperature, humidity, or direct freshness to users, reducing FLW [6].

While effective and accurate, electrochemical sensors, e-tongues and e-noses for food freshness monitoring are complex, require expensive instrumentation, batteries and are not suitable to be integrated into packaging [8]. These disadvantages present and opportunity for the development of inexpensive simple systems that can be printed on packaging, an can be easily used by distributors and users [6]. Recent progress in intelligent packaging includes tools such as radio frequency identification (RFID) tags, time-temperature indicators, integrity sensors, and freshness indicators that use materials that respond to particular stimuli in packaged goods. For instance, stimuli-responsive polymers and composites, which are able to respond to environmental changes such as temperature, biological molecules, ion strength, pH or electric/magnetic fields, have large potential to be used in food freshness assessment systems. The response to these stimuli include changes in modification of surface properties, shape, electrical/magnetic properties, solubility, color/fluorescence, and others. Examples of responsive polymers in intelligent packaging are those used in time temperature indicators (TTIs) that show changes in color dependent of the thermal history of food. These aim to give information on how long food has been exposed to elevated temperatures [7, 9]. In addition to active, intelligent, and smart packaging, responsive polymers and composites have the potential to be used in a wide range of applications such as medical devices, drug delivery, tissue engineering, sensors and biosensors, while allowing for simple and cheap fabrication processes [10–13].

Humidity and temperature are relevant factors for the formation and growth of spoilage microorganisms that affects the shelf-life of goods [14–16]. To prevent food loss during transportation and storage, simple sensing devices that require low operational energy and that can

detect these indirect indicators of spoilage are needed [17]. The sensing of humidity has been traditionally done using highly-sensitive hydrophilic polymers. For instance, Hamouche *et al.* presented a novel keratin (biopolymer) based capacitive humidity sensor [18]. This polymer was solution casted onto two different types of electrodes, interdigitated and rectangular spiral. The capacitance of these sensors was measured at relative humidity between 16% and 82% using an inductance-, capacitance-, and resistance- meter. The results showed that the capacitance of the polymers increased with the increase in relative humidity with very low response time and hysteresis [18]. Other examples of responsive polymers for humidity sensing include copolymers of divinylbenzene and 4-vinylpyridinium salt derivatives [19], polyaniline [20], methacrylic monomers [21], as well as polymer composites [22].

Another application of responsive polymers in intelligent packaging is the monitoring of volatile organic compounds that are directly linked to processes of food degradation and ripening (e.g. ethylene oxide [6]). In the case of meat and fish products, biogenic amines – including ammonia, dimethylamine, putrescine, dopamine, histamine and methylamine – are known markers of spoilage [23–26]. In sensing these elements, piezoelectric behavior of polymers like poly (3-hexyl thiophene) [27], changes in electrical properties of conjugated polymers [28], and change in color from polymer like nitrated polythiophene [29] have been used as response mechanisms. A key component of this system is a material that reacts selectively with amines.

The purpose of this thesis is to develop stimuli-responsive polymers and composites for the monitoring of indirect and direct indicators of food spoilage. Two systems are investigated in detail: *i)* printable responsive conductive polymer composites (CPCs) that undergo changes in electrical resistivity as response to changes in humidity for the fabrication of humidity sensors, and *ii)* grafted-polymers that respond to by-products of meat and fish spoilage and are used in color change indicators that show a visible signal to the presence of amines. These systems are required to be simple to fabricate, cheap and undergo simple to measure changes in properties as response to a particular stimulus (i.e. humidity or volatile amines). In particular, and following these two major thesis topics, the following objectives are addressed in this thesis.

Objectives

The main objectives of this thesis are addressed in 3 different chapters, as follows.

Chapter 3: *"Low-Resistance Silver Microparticle-HEMA-PEGDA Composites for Humidity Sensing"* aims

- To investigate the feasibility of using a low resistance hygroscopic-polymer-based CPCs for the fabrication of sensing elements for humidity;
- To propose and evaluate different printing methods for the fabrication of these responsive materials;
- To tailor the swelling and response of the composite by manipulating their compositions;
- To characterize the physical properties of these CPCs, and determine how both the composition and structure affect the humidity sensing properties of the materials.

Chapter 4: *"Amine Responsive Poly(lactic acid) (PLA) and Succinic Anhydride (SAh) Graft-Polymer: Synthesis and Characterization"* aims

- To develop a method for the synthesis of an amine-responsive polymer;
- To study the effect of composition of the polymer on the physical properties, including molecular weight, polydispersity index, thermal stability, and thermal properties;
- To characterize the response of these materials to methylamine amine.

Chapter 5: *"Colorimetric Indicators for Volatile Amines Based on Responsive Poly (lactic acid) (PLA) and Succinic Anhydride graft-polymer"* aims

- To investigate the feasibility of using an amine responsive polymer, coupled with a pH sensitive dye ,as color change indicator for methylamine;
- To further characterize its performance under different condition of amine concentration and temperature.

In order to give context to these thesis objectives, Chapter 2 provides a background on responsive polymers in packaging technologies. Following the background, Chapter 3 evaluates

the feasibility of using a low resistance conductive polymer composite (CPC) for the fabrication of elements for humidity sensing. Chapter 4, presents a solution-based method for the synthesis of an amine responsive polymers, and the characterization of their response. In Chapter 5, this thesis presents the use of this responsive polymer, coupled with a pH sensitive dye, as an amine-responsive material that undergoes an irreversible change in color upon exposure to small concentrations of amines in vapor. Finally, in the Conclusions chapter, the work presented in this thesis is brought to context with current developments in responsive polymers and composites for packaging applications.

2. Background

The most basic function that packaging serves is protecting a product from the external environment while working as a means of marketing and branding. Packaging serves as a way to *i)* prevent leaking or breaking of the product, and to protect it against contaminations, *ii)* provide information about the contained food product, its nutritional content, and instructions of preparation or cooking, and *iii)* allow easy transportation, storage and handling [30, 31]. Moreover, the increase of customer experience expectations, complexity of products, and national and international initiatives towards reducing food waste, while fostering a circular economy in manufactured products, has allowed innovative packaging to gain more relevance [32, 33]. For instance, current packing is aimed to decrease the amount of preservatives used in food, while meeting higher health regulations and standards, and allowing cradle-to-grave tracking of food [32]. The necessity of safer and functional packaging has led to the development of new kinds of packaging to emerge: active, smart, and intelligent packaging.

Active packaging refers to elements used for the absorption, adsorption, or release of substances from or into food or its surrounding environment to sustain quality and prolong shelf-life [5]. Advantages of using active packaging include reduction of preservatives, processing, tracking activities, and of exchange of compounds from the package to food [34]. Common examples of this type of packaging include humidity (water), oxygen, and ethylene scavengers, flavour and odour absorber/releaser, antimicrobial and antioxidant compounds [9].

While polymers like low-density polyethylene (LDPE), high-density polyethylene (HDPE), polypropylene (PP), polytetrafluoroethylene (PTFE), nylon (polyamide), polyethylene terephthalate (PET, and other polyesters), and ethylene vinyl alcohol represent the most common types of packaging, the development of polymer-based active packaging relies on partial or complete addition of other materials as active components to retain humidity, oxygen, and ethylene, as well as to release antioxidants and antimicrobial substances in order to extend the shelf-life of produce. For instance, Li *et al.* proposed the used of ZnO nanoparticles as active material in poly(lactic acid) (PLA) films for antimicrobial active packaging [35]. Their work showed that this ZnO-PLA composite allowed a significant reduction of the levels of bacterial, yeast and fungi counts in fresh-cut apple when compared with PLA alone as wrapping material

[35]. Other examples of polymers in active materials include hydroxamic acid as antioxidant agent in polypropylene (PP) [36] and poly(ethylene terephthalate) (PET) [37] packaging; gallic acid as oxygen scavenger element in low-density polyethylene (LDPE) films [38]; and TiO_2 nanoparticles as ethylene scavenger in chitosan-based films for packaging of cherry tomatoes [39]. Vilela *et al.* presented a comprehensive review of the current research on active agents for active food packaging [40].

Smart packaging comprises systems that monitor changes in a product or its environment, then acts upon these changes, and provides feedback for the control of the environment. Factors such as freshness, presence of pathogens, humidity, oxygen, carbon dioxide, ethylene gas, pH, time or temperature, are monitored. In addition to this, smart packaging actively controls the environment inside the package to increase the shelf-life of a product [41, 42]. While still in the early stages of development, traditional packaging could be coupled with nanosized capsules that release preservatives, antimicrobials, oxygen and water scavengers for food preservation as needed; as well as dyes to signal changes in storage conditions [43–45].

Intelligent packaging is used to monitor direct or indirect factors of spoilage in packaged foods, providing information on the quality of goods as they are transported and stored [9]. This information facilitates decision-making aimed at preserving and consuming food, which can ultimately extend shelf-life and improve overall food safety while decreasing waste [46]. Intelligent packaging systems include time temperature indicators (TTIs), which undergo a change in color at a temperature-dependent rate; gas detectors/indicators, which provide information around how much time has passed since a particular product was opened; freshness and/or ripening indicators, that provide information about the quality, microbial growth, and chemical changes of food; sensors, and radio frequency identification (RFID) systems, commonly used for traceability purposes [9].

Advancements in intelligent packaging during the last two decades has been driven by the development of stimuli-responsive polymers. These polymers (often referred to as *responsive polymers*) are polymeric materials that are able to undergo measurable property changes in response to a particular stimulus. The types of stimuli may be chemical (e.g. pH or the presence of a particular analyte), biological (e.g. presence of a bacteria, viruses, and biomarkers), and physical (e.g. temperature, light) [47]. The cause of a response at a large scale is linked to how

these stimuli affect the interaction between the polymer chains, and between the polymer and their environment. The wide range of responses from responsive polymers include, changes in mechanical properties, fluorescence, color, chemical, thermal, electrical and transport properties, structure (shape and dimension, refer to as conformation state), swellability, permeability, solubility (when in solution), and phase stability [48–50]. Similarly, copolymers or ionomers present similar behavior in solid state materials [51, 52]. In addition, the breaking or formation of noncovalent or covalent bonds as response to a particular stimulus can lead to measurable changes of the polymer physical properties.[53].

The structural properties of responsive polymers are as diverse as the types of stimuli and responses. Figure 2-1 shows the most common structures of stimuli-responsive polymers, including, single macromolecules in solution, self-assembled polymer systems (micelles, vesicles), polymerized systems like polymer films or bulk, and cross-linked systems like capsules and polymer gels. In addition, the modification of surfaces with responsive polymers allows the design of surfaces that change properties due to an external stimulus. This is accomplished by direct fixation of polymer chain end to a surface substrate, creating polymer brushes, or by direct surface coating process that leads to responsive polymer films. The various polymer structures and diverse responses they could present has allowed responsive polymers to be used in medical applications of drug delivery and diagnostics [11, 54], in biotechnology [53], optical systems [55], coatings and textiles [56], and sensors [57]. As discussed in the previous section, stimuli such as changes in temperature, pH, and gases inside packaging (e.g. CO_2, volatile amines) can be used as measures of food quality and safety. In addition, these polymers can be used as matrix in composite materials that can respond to a wide range of stimuli while proving new types of response, e.g. electrical.

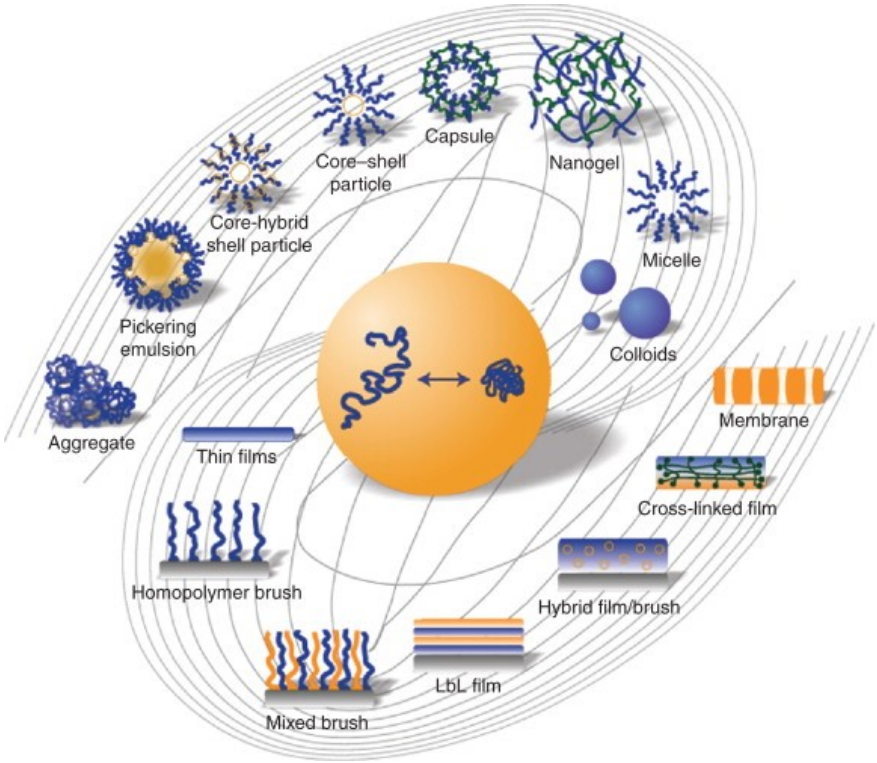

Figure 2-1: Common structures of responsive polymers [53].

Conductive polymer composites (CPCs) – materials that combine the properties of polymers with those of electrically conducting materials – can be used to engineer responsive materials that report a change in electrical properties when exposed to a stimulus that interacts with the matrix. CPCs then can be used to engineer sensors that can signal the detection of the particular analyte or report a particular stimulus [9]. In particular, CPCs can be used as sensing elements, composed of a responsive polymer and conducting elements, which enable the sensor to produce an electrical signal upon exposure to an analyte. In addition to a sensing element that selectively interacts with the analyte, sensors have two main functional parts: receptors, that react with the analyte; and transducers, which translate the interaction between the analyte and the receptor into a measureable signal, often electrical [58].

Recently, CPCs have been applied in gas sensors. For instance, Nguyen *et al.* proposed a cheap and non-toxic device for the detection and measurement of CO_2 as part of an intelligent packaging system for fresh and processed meat [59]. Their study presents details on the fabrication, characterization of electrical properties, and performance of a CNT-based gas sensor for fresh meat. The sensing mechanism of this system was concluded to be linked to the adsorption of gas

molecules on the surface of the CNTs as this, and the presence of defects, changes the overall electrical conductivity of the composites. The selectivity and sensitivity of the sensors was assessed with two gas compounds: air/CO_2 and Ar/CO_2. In commercial applications, information about the concentration of CO_2 inside the package could be processed by a transducer and perhaps transmitted using an RFID tag. Gas sensors coupled with RFID tags are discussed in section *2.3 Traceability and identification technology*.

Electrical conductive polymers have been shown to be an alternative material to CPCs for sensor for monitoring food freshness [60]. For instance, Medeiros *et al.* developed and tested a taste sensor based on polyaniline nanofibers to classify different types of orange juices. The changes in capacitance of the material enabled the estimation of the concentration of citric acid in aqueous solutions of orange juices, with a limit of detection as low as 2 ppm. These sensing elements were also efficient at separating different types of orange juice and at monitoring the aging process for different storage conditions [60]. The main sensing mechanism of these elements was the interaction between citric acid and the polyaniline nanofibers. The citric acid in the orange juice works as an electron donor, increasing the polymer conductivity, while the absorption of analyte may cause swelling and conformation changes in the polymer chains, changing the dielectric constant of the fibers, and leading to a change in the capacitance between the electrodes [60]. Other recent examples include the polyaniline-based ammonia gas sensor presented by Matindoust *et al*. [61]; and similar devices for the detection of ammonia, with varying fabrication methods, sensitivity, and limits of detection have been reported [62–64]. While the potential of conductive polymers for sensing applications is clear, these thesis will mostly focus on CPCs for this application.

The development and study of polymers and conductive polymer composites that respond to these stimuli can highly contribute to engineering indicators, sensors, and RFIDs [6, 65, 66].This section gives insights into the use of responsive polymer systems in the different types of intelligent packaging.

2.1 Stimuli-responsive polymers in indicators

Indicators are elements that display changes in storage conditions, or the presence, absence or concentration of an analyte through irreversible colour change [41, 67]. The fabrication of these indicators has been highly affected by the study of polymers that respond to temperature, pH, CO_2, volatile organic compounds and other stimuli.

2.1.1 Temperature-responsive polymers for use in time temperature indicators

Time temperature indicators (TTIs) display changes in color depending on the thermal history of the food attached to it, and can provide accurate predictions of the remaining shelf-life. TTI indicators currently available in the market are based on physical, chemical, enzymatic or biological processes [7, 68].

Due to their simplicity, TTIs are widely used commercially. For instance, 3M Monitor Mark® by 3M Company is a TTI containing a blend of a blue dye with a fatty acid ester that has a selected melting point. As the TTI is exposed to a temperature outside the critical range (-15°C to 26°C), the substance melts and diffuses through the indicator, presenting a blue colouring on the packaging [42]. Keep-it Technologies commercializes Keep-it® fresh, a TTI based on a chemical reaction between an immobilized reactant, Fe(III), and a mobile reactant, ferrocyanide. Initially contained in separate sections of the TTI, the reactants are activated by removing the sealing between the sections such that the mobile reactant is brought into contact with the immobilized reactant, resulting in a visual color change signal. This reaction is time-temperature dependent which allows the device to give information of the thermal history of the product [69]. Another TTI is Fresh-Check® by Temptime Corp. This is based on the polymerization reaction of diacetylene crystals. This time-temperature dependent reaction results in a highly coloured polymer [9]. Enzyme-based TTIs include VITSAB® by VITSAB International AB. This indicator is made of a triglycerides-pH indicator blend as a substrate and two separate compartments that contain an aqueous solution of lipolytic enzymes. After the wall between the two compartments is broken and the contents are mixed, a time-temperature dependent enzymatic hydrolysis of the substrate will lead to a colour change from green to clear yellow [70]. Other examples of commercial TTIs include OnVu™ by Ciba and Freshpoint™ and TopCryo™ by TRACEO that are based on temperature dependent photochemical and micro-organism reactions respectively.

Recently, the mechanism discussed so far have been used in TTI barcode labels like FreshCode™ by Varcode Ltd. and Tempix® by Tempix AB labels based on inks that disappear due to changes of temperature into critical ranges [70].

Outside of commercial applications, extensive research has been done in developing new methods for TTIs based on temperature responsive polymers. For instance, Lu *et al.* developed a TTI based on the diffusion of alkaline lipase enzyme though a tailored poly(vinyl alcohol) (PVA) substrate in order to monitor freshness of milk. The authors found that the TTI was stable and reliable at dynamic storage conditions and could be used to monitor the cold chain cycle of other perishable foods during their transportation. [71]. In another example, Anbukarasu *et al.* presented a temperature time indicator (TTI) based on the enzymatic degradation of a biosourced polymer-dye blend. Given that the rate of enzymatic degradation of this polymer was found to be dependent on temperature, the authors were able to correlate changes in color (as the dye was being released from the polymer matrix) with the thermal history of the indicators. Implemented as a monitoring device of food storage conditions, this device can reliably track the refrigeration history of goods, which is vital for food preservation [72–75].

Temperature-responsive polymers are by far the most commonly studied within the field of responsive polymers given their wide range of response mechanisms. A simple example of a mechanism of response to temperature changes is that of chitosan. It has been shown that hydrophobic interactions of chitosan chains and water molecules change with temperature as the electrostatic repulsion of the NH_3^+ groups in the polymer is temperature dependent. These changes lead to a competition between the hydrophobic forces and the electrostatic repulsion of chitosan (and therefore the swellability of the polymer) at a particular temperature [76]. The temperature at which this transition occurs is called critical temperature, T_{cr}, or temperature of volume phase transition (TVPT). Often, during this transition, the characteristics of intra- and inter molecular interactions in the polymer change, producing a measurable change in properties as consequence of a change in temperature. When the hydrophilic state is prevalent below T_{cr}, the polymer has upper critical solution temperature (UCST). On the other hand, if the stable state occurs above T_{cr}, the polymer exhibits a lower critical solution temperature (LCST), which is the most study type of temperature-responsive polymer. Figure 2-2 presents a summary of commonly studied temperature-responsive polymers and their LCST.

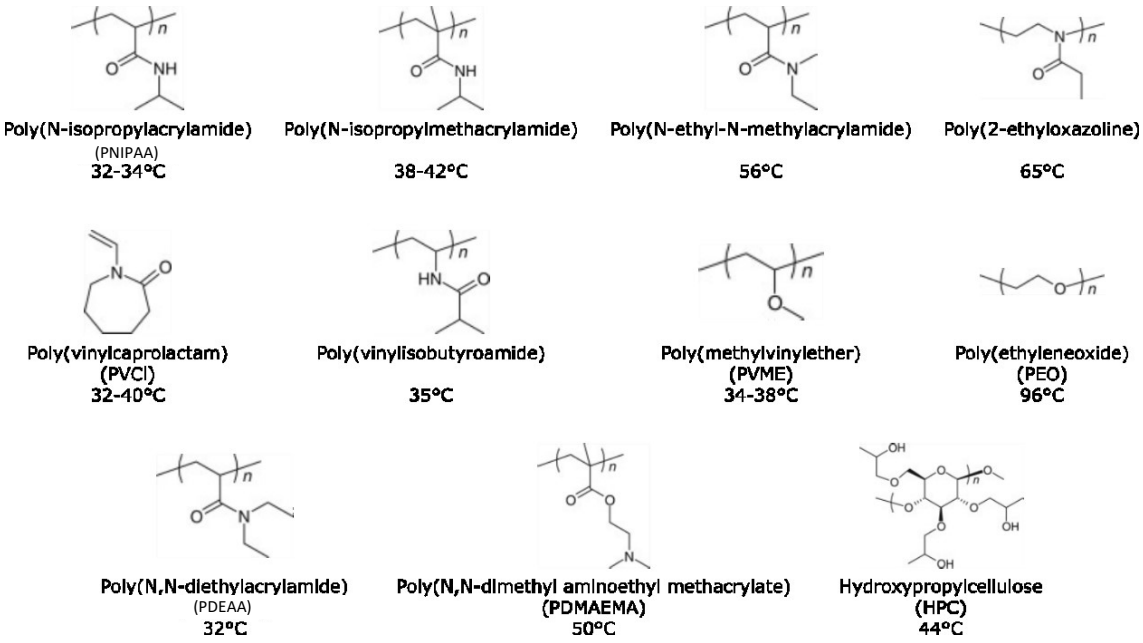

Figure 2-2: Common temperature-responsive polymers and their LCST (adapted from [47])

Depending on the application, different types of temperature-responsive polymers have been implemented. These mostly include films and micro/nano particles made with copolymers and hydrogels. Moreover, due to the high mobility that polymers have in solvents and how easily small solvent molecules can be displaced by mobile polymer chains, stimuli-responsive behavior has been widely studied and observed polymeric solutions. Gil *et al.* has presented a comprehensive review of these studies, covering a wide range of structural changes in polymers in solution [77].

Due to their extensive application in food, cosmetics, and biological applications, hydrogels are commonly studied temperature-responsive polymers. These networks of polymer chains are capable of swelling several times their weight in water [78]. An example of the temperature-responsive polymers is poly(N-isopropylacrylamide) (PNIPAA or PNIPAAm). When crosslinked using N,N′-methylene-bis-acrylamide or N,N′-cystamine-bis-acrylamide, it forms a hydrogel able to transition from a swollen to contracted state at a temperature above 37°C, which make it ideal for medical applications. This transition allows this hydrogel to quickly release any solution with which it is loaded, such as a drug in the case of drug delivery applications [79].

The development of temperature-responsive films has been also explored. Yang *et al*. [80] proposed the used of chitosan films containing polyurethane (PU) and PNIPAA as a wound healing material. The wettability and water vapor permeability of the membrane were designed to decrease

as the temperature of the films increase to that of the human body. This behavior is linked to the LCST properties of PNIPAA, which undergoes a drop in volume at higher temperatures and an increase in hydrophobicity. In their system, chitosan worked as antibacterial material while PU was used as substrate [80]. Hong *et al.* [81] proposed and assessed the fabrication of a stretchable thermosensitive film based on PNIPAA and single-walled carbon nanotubes for health monitoring applications. As the temperature of the sensing element increased, the deswelling of the PNIPAA resulted in an increase in resistivity. The thermal response of PNIPAA allowed for a high sensitivity of 6.5 %/°C within temperatures between 25°C and 45°C. In addition, a leuco dye, deposited on top of the sensing element, was used to engineer color change indicators that could show a visual temperature change [81]. In a similar example, Lavrenova *et al.* [82] reported the synthesis of a temperature sensitive film based cyano-substituted oligo(p-phenylenevinylene). This polymer was shown to change in color in response to mechanical stimulus and temperature [82].

The modification of the critical temperature, $T_{cr,}$ allows the response properties of the polymer to be tailored. To achieve this, the balance between hydrophobic and hydrophilic sections in polymer chains needs to be achieved. In the case of LCST systems, an increase in the number of hydrophilic domains causes an increased T_{cr} while more hydrophobic domains will decrease the T_{cr}. The most common method for tailoring the T_{cr} of responsive polymers is by random copolymerization of the temperature-responsive polymer with controlled amounts of hydrophilic or hydrophobic monomers in order to increase or decrease the T_{cr}, respectively. For instance, Hoffman *et al.* investigated the effect of randomly copolymerizing acrylamide (AA) (hydrophilic) or N-tert-butylacrylamide (hydrophobic) on the T_{cr} of random copolymers of NIPAA [83]. Their results suggest that concentrations of AA below 20% led to an increase of T_{cr} to above 50°C, while the addition of N-tert-Butylacrylamide produced a decrease in T_{cr} below 10°C [83]. Aside from random copolymerization, the addition of functional groups of different nature, the direct modification of the second monomer in a copolymer, and the addition of particles are some strategies used for the control of T_{cr} [47].

An increasingly relevant class of temperature-responsive polymers is shape-memory and shape-changing polymers. These polymers can be deformed into temporary shapes and then recover their original shape upon heating [84]. This interesting property is often achieved by cross-

linking a polymer with low glass transition temperature (T_g) or T_{cr} with a fixating polymer that controls the elastic recovery. The tailoring of T_g in shape changing polymers allow for the design of one or multiple temperature shapes of an element. For instance, Xie *et al.* showed that Nafion - a commercial polymer based on tetrafluoroethylene - and a perfluorosulfonic acid monomer can be programmed with up to four distinct temporary configurations [85]. This copolymer is well known to present two phase transitions, a broad glass transition at lower temperatures (60°C < T_g < 150°C), and a transition related to its ionic cross-links at higher temperatures (>240°C) [85, 86]. The first transition is linked to short-range motion between the physical ionic cross-links that are stable up to the second transition [87].

Temperature is the most used stimulus in responsive, self-healing polymers. These type of materials differ from autonomous healing polymers in that they require a stimulus (thermal activation) to undergo self-healing. Strictly speaking, any amorphous and semi-crystalline polymer can heal if the temperature is above T_g and T_m, respectively, for long enough. Moreover, the time scale required for this process to take place would make it unfit for most applications [88]. To solve this, dynamic covalent bonds can be incorporated into polymer backbones [89]. In these polymers, weaker dynamic bonds in low-molecular weight species will be broken preferably upon mechanical stress, which then can allow for easier diffusion and faster healing. While this approach allows polymer to fully recover their mechanical properties after healing, the use of weak dynamic covalent bonds leads to materials with low mechanical properties, when compared with traditional polymers [90]. Another approach to this is to use microcapsules with the monomer that, upon expose to temperature, air, or a catalyst in the main polymer can repolymerize, healing the material [91].

Chromogenic polymers are another example of temperature responsive polymers. These are polymers that respond to stimuli by changing color. Depending on the stimuli that the polymer responds to, chromogenic polymers can be classified into: thermochromic, electrochromic, photochromic, ionochromic, pizeochromic and biochromic fractions [92]. In the case of thermochromic polymers the color, intensity, and transparency depend of temperature and temperature variations. The response mechanisms of polymers like polythiophene is based on variation results in the alteration of the conjugated length of the π electrons in the backbone, which leads to changes in the absorption wavelength of absorption [93].

While a significant driver of the development of these polymers is the high interests in medical and drug delivery applications, the vast majority of these systems can be used in other applications with similar temperature ranges, for instance, food preservation [94]. As an example of this, Fucinos *et al.* studied the temperature- and pH- response of hydrogels of PNIPAA for food packaging applications. The degree of cross-linking and concentration of acrylic acid as co-monomer were evaluated to produce hydrogels with a wide range of properties, and their relationship with the swelling-collapse behaviour were studied for active packaging applications [95]. In the development of intelligent packaging systems, e.g. TTIs, temperature-responsive polymers loaded with dyes would report a visible change in color when the temperature of products was above a safe value.

2.1.2 O_2 and humidity-responsive polymers for use in integrity indicators

One of the simplest integrity indicators aims to provide information about how much time has passed since a particular product was opened. Often presented in the form of a label, the activation of indicators occurs when a seal, barrier, or devices in the pack is broken. This triggers an element that changes color as time passes. Some commercial examples are Novas® Embedded Label by Insignia Technologies Ltd., Best-by™ by FreshPoint Lab. and Timestrip® by Timestrip Ltd. [69].

In the case of meat packaging, gas indicators that detect oxygen in particular, are the most commonly used integrity indicators. They provide information on the compositions of the overhead gas inside the package, and are especially useful in the case of modified atmosphere packaging (MAP) [32]. It is common practice in MAP that meat products are packaged in a CO_2 atmosphere of 20–80% and while keeping a concentration of O_2 between 0.1% and 1%. For this reason, it is viable that a leak in a MAP package that occurs as the product is transported, stored, or consumed, can be tracked by using indicators for the high concentrations of oxygen and humidity changes.

The use of responsive polymers for the tracking of oxygen has been explored in the past. For instance, Vu *et al*. fabricated and tested an oxygen indicator based on an redox dye, thionine, an electron donor, glycerol, and UV-adsorbing semiconducting photocatalyst, P25 TiO_2, all embedded in a polymer films, zein [96]. Other examples include the work presented by Mills *et*

al., who implemented an oxygen indicator based on a low density polyethylene (LDPE) as matrix of a nano-particulate pigment particles: methylene blue (MB) and DL-threitol coated onto P25 TiO_2. The indicator changed color under the exposure to oxygen in less than 90 sec, presenting a recovery time of 2.5 days [97]. Given that the mechanism of response of most of these indicators is based on the redox dye, polymers most often play a role of encapsulation material or substrate [75].

The monitoring of humidity using responsive polymers has been addressed recently. For instance, Li *et al.* proposed the use of a crosslinked copolymer of 4-vinylpyridine (4-VP) with butyl methacrylate (BuMA) as sensing materials in a resistive polymer-based humidity sensor. In their study, the effect of copolymer composition on the humidity response were investigated. Their results suggest that the electrical conductivity in these polymers is mainly ionic while the sensing mechanism was strongly dependent on the concentration of ions and the water absorption ability of the polymer. It was found that the copolymers with higher concentration of 4-VP presented higher capacitance and sensitivity to changes in humidity [98]. In more complex systems, Lee *et al.* presented a porous structure formed via phase separation between immiscible polystyrene (PS) and polyethylene glycol (PEG), and a luminescent O_2-sensitive dye. Here, the hygroscopic PEG phase, within the PS matrix, swells with the increase in humidity, then leads to a change in the optical scattering properties of the luminescent O_2 sensing films. Given that both humidity and O_2 interact with this material, the dual response of the polymer gives it high potential in food packaging that works both as integrity indicators (by tracking high concentration of O_2 with changes luminesce) and as humidity indicator (by changing the scattering of the dye with the swelling of PEG with changes in humidity) [99]. Other examples of responsive polymers for humidity sensing include copolymers of divinylbenzene and 4-vinylpyridinium salt derivatives [19], polyaniline [20], methacrylic monomers [21], as well as polymer composites, among others [22].

2.1.3 Analyte-responsive polymers for use in freshness indicators (microbial or pathogen spoilage)

Freshness indicators are devices or systems engineered to provide information around the quality, microbial growth, and chemical changes of food. The diversity of products and ways in which their freshness change require each freshness indicator to be unique to a product. In the case of muscle foods, changes in pH, and the concentration of metabolites such as glucose, organic acids (e.g. L-lactic acid), ethanol, carbon dioxide, biogenic amines, volatile nitrogen compounds, or sulphuric compounds have been shown to be indicative of microbial activity, presenting the opportunity of using them as analytes of freshness indicators [5, 66].

While an increasing number of packaging companies have announced the future development of freshness indicators, most cases did not lead to successful commercialization [69]. After only 5 year of commercial use, Fresh Tag® by COX Technologies, a colorimetric indicator for the formation of volatile amines in fish products was discontinued in 2004 [9, 100]. In 2007, DSM NV and Food Quality Sensor International Inc. announced the development of a pH-sensing element for the release of biogenic amines from microorganisms in poultry and meat. While similar attempts have been announced by VTT Technical Research Centre of Finland and UPM Raflatac, neither of these examples are currently available at a commercial scale [66, 101].

Despite the limited number of commercial freshness indicators, a more extensive range of them, in particular those based on responsive polymers, has been proposed in the literature. Indicators based on pH changes, due to the production of specific metabolites by bacteria, are particularly well studied [66]. For instance, Choi *et al.* proposed a colorimetric pH indicator based on biopolymer films of agar and potato starch, used to encapsulate a natural dye (anthocyanin). Given that variations in pH have been widely correlated with the spoilage process of meat, the indicators were designed to change color from an initial spoilage pH value of 6.28, shown to be in the range of the pH of fresh pork, between 5.18 and 6.16, to a final stage of 7.42, for spoiled pork. This color change was then attributed to different molecular structures of anthocyanins that depend on pH. Their work then suggest that similar methods can be used in other meat products [102].

The response of polymers to changes in pH, mostly as structural changes, has been widely studied in biology and biomedical applications. In these polymers, the changes in structural

properties and hydrophobicity depend on intra- and intermolecular interactions (hydrogen bridge bonds, charge attractions) that are affected by pH. In the synthesis of polymers, the inclusion of ionisable functional groups that can accept and donate protons depending on the concentration of ions in the environment would lead to pH-responsive polymers. In particular, weakly acidic and basic groups with protonation/deprotonation in the pH range between 4 and 8 are commonly used [47]. As the value of pH approaches the transition point of protonation and deprotonation of the polymer, critical pH (pH_{cr}), the degree of ionization will be changed dramatically. As this change takes place, the now uncharged macromolecule collapses (when in solution) or deswells (when polymerized) given that the hydrophobic interactions within the polymer backbones becomes dominant. As charges are transferred to the polymer, this produces an expanded conformation due to the electrostatic repulsion and hydration processes takes place [47]. A significant increase in swelling behaviour occurs in the polymer with charged groups as the osmotic pressure from mobile counter ions increases [103, 104]. Similar to temperature-responsive polymers, the structural configuration and its equilibrium in pH-sensitive polymers is directly dependent of the balance between hydrophobic domains and ionizable groups [77]. Tonge *et al.* presented a highly detailed review of the structures and properties of responsive hydrophobic associating polymers [105].

Polymers containing carboxylic groups are the most commonly studied pH-responsive weak-acid polymers (Figure 2-3). Within this group, poly(acrylic acid) (PAA) and poly(methacrylic acid) (PMAA or PMAAc) are the most frequently investigated pH-responsive polymers [106, 107]. In the case of PMAA, the inclusion of hydrophobic methyl group causes the polymer to exhibit a more compacted conformation in the uncharged state as well as a sharp phase transition compared to PAA. Similarly, poly(2-ethyl acrylic acid) (PEAA) and poly(2-propyl acrylic acid) (PPAA) transition into more compact structures at low pH and have more abrupt property changes.

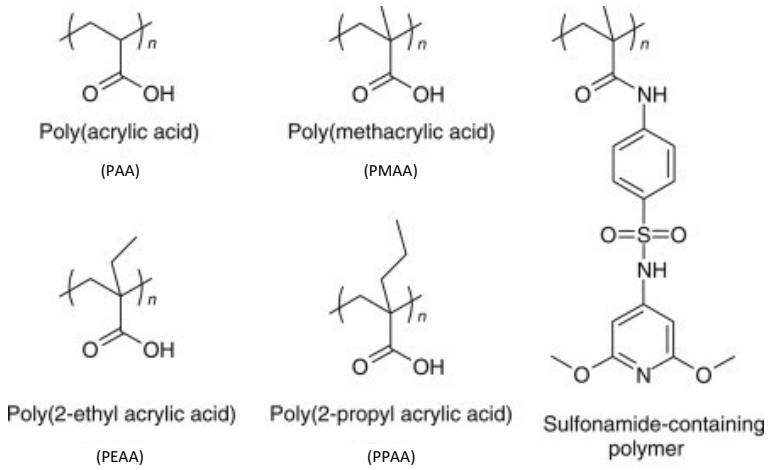

Figure 2-3: Common pH-responsive weak-acid polymers [47]

Representative examples of weak-base polymers are shown in Figure 2-4. These include some tertiary alkyl amines and aromatic amines. In general, the amine groups are able to accept protons at low pH levels, making the polymer charged. On the other hand, they do not affect the polymer at higher pH. Poly(N,N-diethyl aminoethyl methacrylate) (PDEAEMA) – a common example of these polymers – has longer hydrophobic alkyl chains than poly(N,N-dimethyl aminoethyl methacrylate) (PDMAEMA) which makes PDEAEMA able to engage in compacted conformations at high pH, suggesting stronger hydrophobic interactions at these pH values. At pH less or equal to 7.5, PDEAEMA precipitates due to protonation [108]. In addition to the reliable response to pH, PDMAEMA has been reported to show sensitivity to temperature, similar to PNIPAA [109].

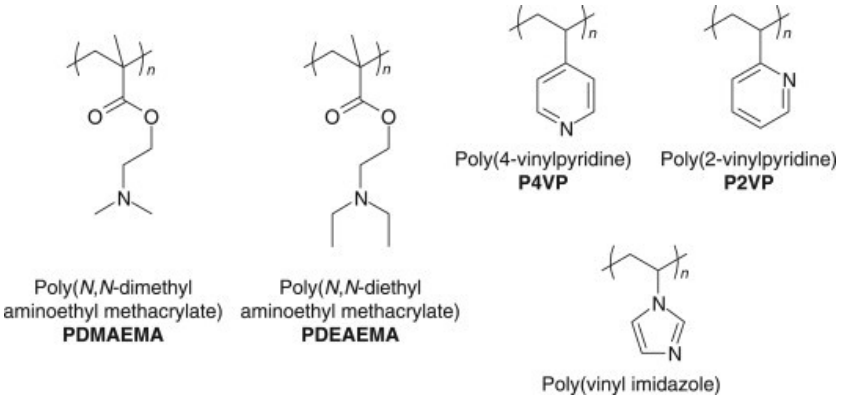

Figure 2-4: Common pH-responsive weak-base polymers [47]

In some cases, the pKa (pH at which the protonated and deprotonated groups in a polymer are equal [110]) of a particular ionisable polymer can be tailored by changing the design of the polymer itself. For instance, polymers that contain sulfonamide (Figure 2-3) are easily acidified to give a weakly acidic polymer, given that amide hydrogen is readily ionized and the electron-accepting nature of the SO_2. On the other hand, electron-donating groups like the methoxy group (Figure 2-3) will lead to an increase in pKa of the sulfonamide group. Park *et al.* used sulfamethazine to modify the pKa of DMAA by free radical copolymerization. This structure modification in DMAA lead to changes in pKa values ranging from 3 to 11. Following modification with sulfonamide groups, the polymers exhibit a more abrupt phase transition and a higher sensitivity to pH changes than pure DMAA [111]. In addition, pH_{cr} can be modified by incorporation of hydrophobic groups to a polymer by copolymerization with hydrophobic monomers. For instance, Philippova *et al.* proposed the modification of PAA by copolymerizing it with hydrophobic n-acrylates (Figure 2-4). The resulting pH-responsive gel exhibit a higher critical pH value than PAA [103].

The use of polymers in packaging applications for indicators that are based on pH changes due to the production of specific metabolites by bacteria continues to grow [66]. Based on the natural changes in pH of food, and given that the pH_{cr} of pH-responsive polymers can be tailored, the loading of dyes in these polymers can lead to simple color changes indicators for the spoilage of products. For instance, the work Choi *et al.* on colorimetric pH indicators based on biopolymer films of agar and potato starch, used to encapsulate a natural dye (anthocyanin) described above. In their work, the polymer plays the role of substrate for the dye, which is the active component of the system [102]. In addition, the significant change in volume in temperature- and pH-responsive polymers as they deswell can be leveraged as a signal in conductive polymer composites.

In addition, changes in pH have been associated with the release of volatile amines; therefore, pH can be used as freshness indicator in muscle foods, particularly in fish [58]. Responsible for the characteristic smell of fish, volatile amines are the natural by-product from the degradation of trimethylamine oxide by microorganisms [112]. For instance, Boscher *et al.* proposed the use of a metalloporphyrin-based coating applied to poly(ethylene terephthalate) (PET) for the detection of trimethylamine, trimethylamine, and dimethylamine amines [113].

Similarly, Pacquit *et al.* proposed the use of a colorimetric dye-based indicator to track the increase in volatile amines as an indicator of fish spoilage. The indicators were prepared by mixing pH-sensitive dyes within cellulose acetate, such that once in contact with basic volatile amines in the package headspace, the amines would permeate the polymer matrix and react with dye, leading to a change in color [114, 115]. Other studies have leveraged the same principle for a wide variety of pH-based freshness indicators for other muscle foods [116–119]. The table below presents additional examples of responsive polymers for pH indicators in food packaging.

Table 2-1: Some examples of pH indicators based on responsive polymers [75]

Material	pH	Food	Ref.
Polyvinyl alcohol, chitosan nanoparticles & mulberry extracts	1-3	Fish	[120]
Polylactic acid, poly (ethylene oxide) & phycocyanin	3.6-4 5.6-6.2	Citrus Meat	[121]
Black rice bran anthocyanins, oxidized-chitin nanocrystals and chitosan matrix	1-12	Seafood	[122]
Tamarind seed polysaccharide & litmus lichen	4-10	Milk	[123]
Chitosan, blueberry and blackberry pomace	4-7	Meat	[124]

Another stimuli for freshness indicators has been the production of carbon dioxide (CO_2), by-product of microbial growth [125, 126]. For instance, Saliu *et al.* investigated the performance of a CO_2 indicator based on a homogenous blend of an amino acid (L-Lysine), a polymer matrix (ε-poly-l-lysine, EPL) and a natural dye. Their study showed that the polymer blend changed from blue to intense purple color as response to the presence of CO_2 in concentrations up to 2.5%. The mechanism of CO_2 indicating was proposed to initiate by the reaction of CO_2 with lysine and the subsequent pH transition of cyanidin. In low concentrations of CO_2, the lysine is partially protonated due the production of the hydroxide salt, shifting the pH to the basic region. Moreover, when the concentration of CO_2 increases, the pH dramatically decreases and the lysine is partly converted to its carbamate and bicarbonate salt [127].

The synthesis of CO_2 responsive polymers is often addressed using monomers that contain tertiary amine groups such as PDMAEMA, and poly(N,N-diethylaminoethyl methacrylate) (PDEAEMA) [128, 129]. For instance, Wang *et al.* proposed the use of POEGMA-b-P(DEAEMA-

random-4-(2-methylacryloyloxyethylamino)-7-nitro-2,1,3-benzoxadiazole) for the fabrication of a high response fluorescent sensor for CO_2 [128]. The fluorescence of these copolymers was found to change as result of the lone pair electrons of the tertiary amine of PDEAEMA. These sensors showed good reversibility. In the design of these polymers, groups containing amidine, imidazole, guanidine groups and others have been explored in the synthesis of CO_2 responsive polymers [130, 131]. These type of materials have the potential to be used a gas indicators in MAP applications as well as freshness indicators as concentrations of CO2 can provide information about the microbial activity in food.

As briefly discussed above, monitoring changes in pH can provide information about the presence of amines. Moreover, the direct detection of organic compounds (e.g. CO_2, amines NH_3 or chlorinated gases), and of volatile organic compounds (VOCs) (e.g. alcohols such as methanol, 2-propanol and 1-octanol, and volatile amine groups) is also interesting. Recent research has been done in sensors for these types of compounds, using piezoelectric behavior [27], changes in electrical properties (impedance, capacitance and resistance) [132], electrochemical measurements [133]. Other examples of these polymers include polyfluorene/Pd tetraphenylporphyrine, and 2-amino-4,6-dimethylpyrimidine-co- 4-dimethylaminobenzaldehyde which respond to the presence of amines by charges in fluorescence and other optical properties [134, 135].

The response of polymers to particular stimulus is dependent on changes in chemical and physical properties of the polymer. For instance, changes in electrical properties of resistive and capacitive sensors are commonly due to a preferential adsorption of, or reaction of functional groups with, different analytes such as NH_3, H_2S or CO. In general, changes in color, luminescence, or opacity depends on selective chemical reactions between the analyte and the polymer or on weak on/off interaction within the polymer that change with presence of the analyte. The advantage of color and other optical responses in that they can be easily identified by the naked-eye [136].

Recently, different polymer-based methods to monitor amines have been presented. For instance, He *et al.* [137] proposed the use of an alkaline earth metal–organic coordination polymer as a luminescent indicator for methylamine, dimethylamine, and trimethylamine. The response of this material relies on the amines combining with unsaturated carboxylic groups in the polymer. As consequence of this, the carboxylic group can no longer vibrate, increasing the rigidity and

reducing the loss of non-radiation energy of the ligand, causing an increase of the fluorescence emission intensity. This change intensity allows for an on/off change in fluorescence with initial and final peaks at 525 nm and 612 nm which requires a UV lamp to be evaluated. In more simple systems, Jin *et al.* [29] proposed nitrated polythiophene (NPTh) films as indicators for ethylenediamine, putrescine, cadaverine, spermidine, phenethylamine, and histamine. In this system, the biogenic amine (BA) easily diffuses into the polymer film and forms charge transfer complexes with NPTh. These $NPTh^{\delta+}$-$BA^{\delta-}$ complexes lead to a fast change in color of the films from light brown to a highly deep dark brown. Aiming to provide consumers with simple sensing elements, polymers-based sensors and indicators must rely on simple responses like change in color or opacity. Azzouz *et al.* recently reviewed the current advances in colorimetric and optical sensing for gaseous volatile organic compounds [138]. In addition, Sanjuan *et al.* presented a review on the recent developments in sensing devices based on polymeric systems [139].

The design of sensing elements that generate an electrical signal in response to a stimulus can be addressed by adding conducive elements into a stimulus-responsive polymer matrix. The following section develops on basic concepts of conductive polymer composites (CPCs) and on some their applications on the sensing of humidity and volatile organic compounds.

2.2 Conducive polymer composites (CPCs) for sensors

Conductive polymer composites (CPCs) were developed as a solution to the high specific weight, tendency to corrosion, relative low formability into complex shapes, and cost of metallic materials for electromagnetic interference (EMI) and other electric shielding applications [140]. A way of overcoming these problems was found by incorporating and dispersing a small volume fraction of an electrically conducting phase into a polymeric matrix, resulting in a conductive polymer composite (CPC) [141, 142]. Conventionally, metallic and carbonaceous materials in the form of particles, fibers, flakes, thin layers, and rods have been used as fillers in micro- and nano-sized scales [143]. The incorporation of these conductive fillers at a sufficient volume ratio in a polymeric matrix results in filler-linked paths through the material which allow the conduction of electrons, resulting in an electrically conductive polymer composite [140, 143]. The electrical properties of these materials are highly dependent on the interplay between the filler and matrix, and the sensitivity to various parameters can be leveraged to form novel sensors.

As with traditional composite materials, combining a polymer matrix with electrically conductive materials results in a set of tailorable combination of features of the different components in the composite. Some of these features include high formability, low weight, high corrosion resistance, flexibility, and good mechanical properties which make CPCs feasible materials for several applications. In particular, properties such as flexibility, positive temperature coefficient of resistance (PTCR), hygroscopicity, functionalization, processability, among others, have been highly beneficial for the development of CPC-based sensors [144]. On the other hand, the addition of conductive reinforcements of significant size and volume ratio may be detrimental to the processability, density, and mechanical properties of the matrix. Therefore, a solution to diminish these disadvantages is to add filler materials with size in the micro- and nano- scale in the lowest ratio possible [140, 142]. The minimum filler content at which the isolated conductive elements get in contact creating conductive paths is usually refer to as the percolation threshold (Figure 2-5) and is dependent on the geometry of the fillers, the blending method, and the components of the composite [145–147]. Statistical percolation theory is particularly effective in the estimation of electrical properties of composite, heterogeneous, materials such as CPCs. The dependency of conductivity on filler concentration takes the simple form of a scaling law according to Eq. 1.

$$\rho_{CPC} = \rho_F(v_F - v_c)^t \qquad \text{Eq. 1}$$

where ρ_{CPC} is the resistivity of the composite, ρ_F the resistivity of the filler, v_F and v_c the volume fraction of the filler and that one of the percolation threshold respectively, and t is the critical exponent, calculated from experimental results [144, 145, 147]. When used in sensing, CPCs requires the formation of stable conductive paths between conductive particles which are achieved with filler concentrations above that of the percolation threshold, therefore, estimating the percolation content limit is useful for the fabrication of CPC blends.

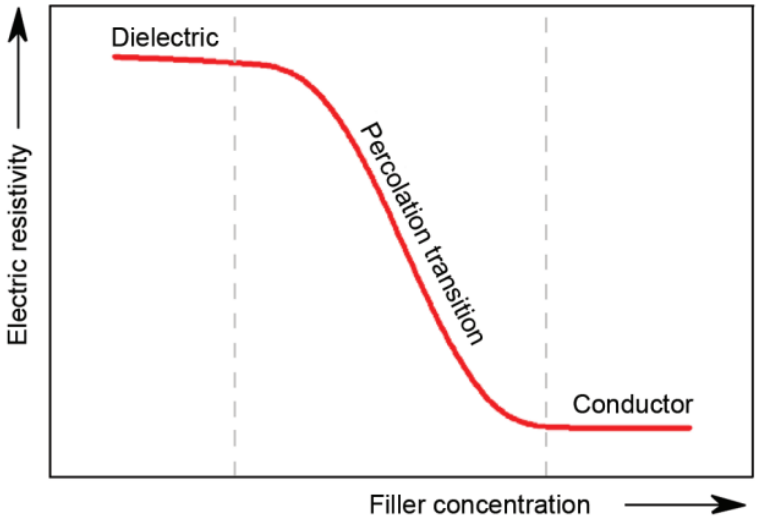

Figure 2-5: Illustration of percolation threshold for electric resistivity in CPCs [148]

The conduction of electrons, or charge carriers, in CPCs takes place mainly thought two processes, ohmic conduction and tunnelling conduction. The first occurs when the content of fillers is above the percolation threshold and is due to the direct contact between the conductive filling elements in the composite. On the other hand, tunnelling conduction occurs when the content of conductive fillers is slightly below the percolation threshold and the mean free path between particles is not larger than 10 nm. In this case, electric field assisted tunnelling can transport carriers between filler neighbours though the thin insulating barrier [144, 149].

In practice, the materials used as conducting elements in CPCs present a broad spectrum of properties and morphologies that drastically affect the resulting electrical and mechanical properties of the composite. Geometric factors such as shape and size have been found to be significant factors to consider in the study of electrical properties of CPCs [147, 150, 151]. Figure 2-6 shows the effect of geometric factors such as, dispersion level and shape factor, on the percolation threshold. While most of the models for percolation threshold and prediction of electrical properties are based on spherical particles, the conductive fillers often include elements with aspect ratios different to 1, such as fibers, flakes, carbon nanotubes, mono- and multi- atomic graphene, among others. For instance, fillers with a high aspect ratio (length-to-width ratio) have been found to present lower percolation thresholds given that the probability of creating conductive paths are higher as the length of the fillers increase with respect to the width [141, 147, 150]. Grossiord *et al.*, found that the percolation limit content decreased in 20 wt% with the increase of

the aspect ratio of multi-wall carbon nanotubes in a PE-based composite, from ~40 to ~120 [152]. In addition to the decrease percolation limit, the increase of the aspect ratio has been found to increase the in the maximum conductivity that can be achieved in the composite as the concentration increases [153]. However, high aspect ratio fillers have been found to agglomerate easily and dispersion techniques are required to disperse the conductive filler into conductive networks [154]. In addition to geometric factors, the inherent electrical conductivity and surface energy of the fillers affect the resultant electric conductivity of the CPC. Fillers with higher inherent conductivity are more suitable to have a higher maximum conductivity with lower percolation limit [155]. It has been shown that factors such aspect ratio, geometrical morphology, and inherent electrical conductivity affect the electrical properties and percolation limit of CPCs.

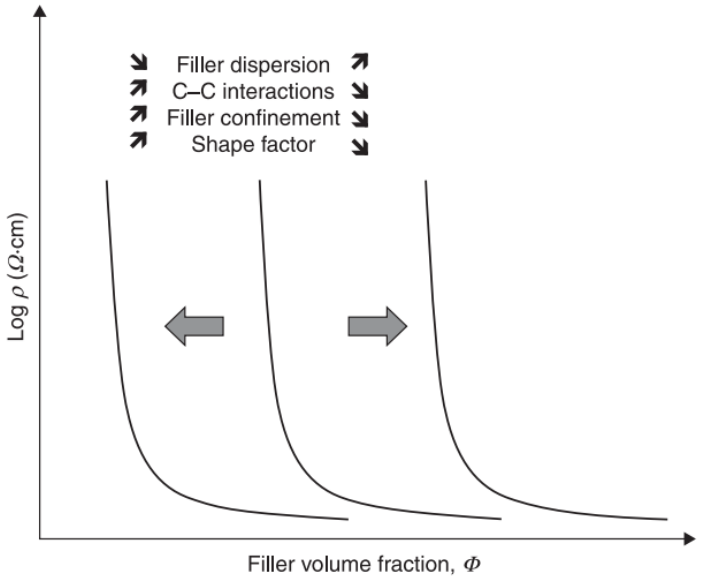

Figure 2-6: Influence of geometry on percolation limit [144]

The sensing of analytes by CPCs can be associated with the response properties of the polymer matrix, the reinforcing element, or both. While relaying on the response of the polymer matrix is common, applications of composites with carbon nanotubes (CNTs), multiwall carbon nanotubes (MWCNT), carbon black (CB), and others as conducting element, often leverage their high surface energy to produce sensing elements [156, 157]. The response from some CPCs can also come from measureable changes in properties of the reinforcing conductive element, instead of the matrix itself. For instance, Liu *et al*. fabricated and tested a flexible temperature sensor of polyethyleneimine and reduced graphene oxide CPC by spraying it onto a polyimide substrate.

The main mechanism of sensing of this composite was based on the thermal excitation of the charge carriers in rGO. As the temperature in the sensor increases, the limited carrier hopping carrier tunneling between rGO sheets transport are increases, leading to higher probability of barrier overcoming for carriers. As consequence of this, the carrier mobility of sensing film increases remarkably with the increase of temperature [158]. Other examples include the CNT-based RFID systems by Nguyen *et al.* discussed above [59], and the graphite-polyethylene oxide (PEO) and polyvinylidene fluoride (PVDF) composite, and the graphene-gelatine composite for temperature sensing by Huang *et al.* [159] and Nassira *et al* [160], respectively.

Other CPCs (those that use the polymers as responsive element) produce a signal that is linked to the way the arrangement of conductive paths of fillers changes inside the material upon a particular stimulus, such as, changes in humidity, temperature, mechanical deformation, presence of organic vapours, and corrosion [141]. While the electrical properties of CPCs are strongly determined by the conductive fillers, the response to these stimuli is mainly linked to changes in the polymer matrix and in various applications to the junction of the response of both matrix and filler [144, 161]. This section develops on mechanisms behind the most relevant applications of CPCs on sensing applications.

The simplest implementation of CPC sensor to understand is a strain sensor. In this system, the change in conductivity of CPCs upon external stress is due to the change in mean free path of the conductive fillers, which increases due to the overall strain of the sensor body [162]. While the sensing of strain using CPCs is theoretically feasible, it requires CPCs with high filler content that provides stable conductive channels which is detrimental for the flexibility and resilience of the composite, properties that are preferred in the fabrication of strain reusable sensors [141, 163]. However, previous works established a balance between conductivity and mechanical properties for the design of strain sensor for different CPCs materials. For instance, Levin *et al.* [163] proposed the use of polyaniline nanoparticles in a poly(vinyl acetate) latex matrix (PVA–PANI) as high strain sensing element [163]. This study found the interaction between conductive participles to be weak, which allows the disconnection of conductive paths upon an overall strain, increasing the sensitivity of the sensor. With conductive percolation limits as low as 0.6 wt%, the PVA–PANI sensing elements were able to sense cyclic strain of up to 1%, as well as in static strains of 5% [163].

Temperature sensing, temperature protection, self-regulating heating, among other applications are based on the changes in resistivity in devices due to the positive (PTCR) and negative (NTCR) temperature coefficient of CPCs [164]. The abrupt change in volume of the polymer matrix of the composite as the temperature increases and eventually reaches melting point leads to the change in mean free path between conductive fillers resulting in a change in resistivity [165]. In self-regulating heating, the conductive filler paths generate heat by means of Joule, or resistive, heating that increases the temperature in the CPCs. The volume in the polymer increases as consequence of the increase in temperature resulting in the interruption of conductive paths, and therefore, the interruption of the resistive heating. The flow of electrons and generation of heat would continue once the temperature is decreases and the conductive paths are connected as consequence of the decrease in volume [166, 167]. In sensors, the variation in electrical resistivity due to PTC and NTC works as response toward changes in temperature.

One class of sensor relevant to packaging is chemical sensors. Chemical sensors leverage surface adsorption to detect of the presence, activity, composition and concentration of particular chemicals or gases. Following adsoption, an electrical signal is generated by an active or passive actuator [41]. In the case of gas sensors for food packaging applications, the most common analytes include oxygen, carbon dioxide, water vapour, ethylene gas and ethanol. The mechanism of reaction to these analytes depends on the materials used as sensing elements. These materials include metal oxide semiconductors, organic conducting polymers, responsive polymers, conductive polymer composites (CPCs), and piezoelectric crystal sensors [9]. For instance, Wei *et al.* [167] presented the fabrication of a vapour/gas sensor based on MWCNTs/polylactic acid (PLA) conductive polymer composite thin films. The sensing properties of the films were tested with chloroform ($CHCl_3$) vapour. The response of the films was found to be linear, repeatable, and dependent on the molecular weight of the PLA matrix. Their work successfully improved the response time of the films by taking advantage of the high surface area of MWCNTs and by using thin films which high surface-to-volume ratio provides them with high sensitivity and analyte permeability [167]. This is an updated example of vapour sensing by implementing CPCs.

The change in the overall electrical properties, such as resistance, in a sensing device is generated by the presence of a given analyte, two main components contribute to the overall change in electrical properties. On one hand, the adsorption of vapour or liquid molecules changes

the electrical properties of the CPC conductive paths of fillers by creating insulting layers between particles. Secondly, similar to PTC, the resistance of CPCs increases as consequence of the increase in specific volume of the polymer matrix produced by the swelling, this produces an increase in the mean free path between particles, reducing the quality and quantity of conductive paths within the volume of the composite. Furthermore, the overall conductivity of the CPC sensing device changes as combined result of these two phenomena.

As the main interest of this thesis is in humidity and amine sensing applications, and in the most relevant responsive polymers that can be used as matrix for sensing CPCs, the following section will only cover responsive CPCs for humidity and amines sensing applications. This work will then focus on CPCs in sensing applications where the response comes mostly from the polymer matrix instead of the conductive elements.

2.2.1 Responsive CPCs for humidity sensing applications

The measurement of humidity has been of interest for various industry applications, including, monitoring of environment conditions for experiments, window defogging in automobile industry, industrial drying, and environment control in textiles, human comfort, and electronics, among others [168, 169]. In the processing and storage of food stuff, humidity, in addition to temperature, is a relevant factor for the formation and growth of spoilage microorganisms that affect the storage time of goods. Therefore, the monitoring of humidity during the processing and storage of products in food industry is important in order to prevent food loss during production and storage [17].

Humidity, in its basic definition, is the content of water in a gas. In a more detailed fashion, humidity can be defined in two ways. The absolute humidity is the measure of mass of water vapour in a unit volume and relative humidity is the ratio of water-vapour pressure present to the saturated water-vapour at a given temperature or, usually expressed as the ratio of the mass of water vapour in a unit volume compared to the mass of water vapour in a unit volume if the vapour were saturated at a given temperature. RH is typically expressed as:

$$RH = \frac{P_w}{P_s} \times 100\% \qquad \text{Eq. 2}$$

where P_w and P_s are the vapour and saturation pressures, respectively [168].

Generally, the measurement of humidity is done in integrated circuits by measuring changes in electrical properties of sensing element with the adsorption of water molecules on several materials like metal oxides, porous ceramic, electrolytes, and polymers. Some limitations are linked to sensitivity, energy requirements, response time, and hysteresis [170, 171]. Attempts to solve these issues have been done with composite materials based on nanomaterials as they offer high sensitivity. Moreover, complexities linked to high hysteresis and fabrication methods can make some of these applications unviable [170, 172]. A viable solution to these problems can be found in composite materials based on the blend of electrically conductive particles into polymers matrixes that respond to changes in humidity, usually by swelling. These conductive particles create conductive pathways throughout the polymer matrix and that facilitate the monitoring of humidity by changes of electrical properties [173].

Notably, hydrophilic polymers are good candidates for the matrix in a humidity sensing CPC. Hydrogels, for instance, are three dimensional cross-linked polymer networks that can swell up to 99% of their weight without dissolving [174, 175]. The inert nature of hydrogels minimizes the interaction with specific proteins and cells which makes hydrogels great candidates for various biological and chemical applications [174, 176–181]. Poly(ethylene glycol diacrylate) (PEGDA) is a hydrogel that has been implemented in various biological and battery applications [178–181]. PEGDA can be functionalized [182] and cross-linked [183, 184] which allow it to be used in various applications. In the fabrication of sensors, Lee *et al.* [185] has proposed and tested the use of PEGDA-embedded polydiacetylene for the fabrication of a colorimetry biosensor. While the sensing response was found to be low, this study successfully tested multiple α-cyclodextrin solutions with different concentrations [185]. Similar to Lee *et al.* [185], Havens *et al.*[186] has used PEGDA for the fabrication of sensors with embedded sensing material. In this case, functionalized multiwall carbon nano-tubes (MWCNT) were used in the detection of acetaminophen and ascorbic acid. The sensing elements were found to be responsive to the analytes in aqueous solution [186]. In both examples, the swelling of solution containing specific analytes allowed the analytes to diffuse through the polymer, interact with the sensing constituent and generate a signal [185, 186]. While PEGDA has been widely implemented in various applications, the study of the effect of this hydrogel on the electrical and sensing properties of

CPCs, particularly in humidity sensing applications, has been limited and not necessarily representative of the potential that the hydrophilic and hygroscopic properties offer toward producing sensors and other electronics with these composites [174].

The fabrication of CPCs for sensing applications and other electronic devices has included conductive polymers, carbonaceous materials, and metallic particles in the micro- and nano- scale particles [187]. While carbonaceous materials have shown good performance in these applications, they present limited conductivity in thin film applications and the tendency to agglomerate in various other applications. Metallic materials, such as gold (Au) [188], copper (Cu) and silver (Ag) [189], micor/nano- particles have been well-established in the fabrication of CPCs. In the case of Ag, the high electrical conductivity, high stability, low cost, and antioxidant properties have allowed this material to be a good candidate to be a conductive element in CPCs [190]. Various studies have used Ag as conductive element in CPCs; however, there have not been enough studies on Ag-CPCs applied in sensing elements and on the effect that this conductive filler has on the selectivity and sensitivity of sensors for humidity and more complex applications.

2.2.2 Responsive CPCs for amine sensing

The detection and quantification of bacterial activity and volatile organic components have been of interest for fields of medicine, biology, chemistry, among others. In food industry, the detection of spoilage bacteria activity has been addressed in an attempt to discard hazardous spoiled food before human consumption as well as the waste of food stuff. The development of cheap, portable, accessible, sensing elements has been previously proposed as a solution to these disadvantages. These sensors can be attached to food packages and food containers for the sensing of humidity, pH, temperature, or volatile gasses [191–193]. In the sensing of amines, Fiddes *et al.* [191], proposed a method for chemically sensing biogenic amines present in spoiled food stuff by integrating a sensitive CPC to an radio-frequency identification (RFID) antenna. The sensing material was composed of graphene, maleic anhydride, and poly(ethylene-co-vinyl acetate) (PEVA), acted as conductive element, sensing element, and swelling polymer matrix, respectively. The CPCs was found to be sensitive to putrescine, histamine, cadaverine, spermine, and spermidine which are volatile molecules present in food during the spoilage process [191]. Their work aimed to propose a simple CPC-based sensing element for volatile components produced

during food spoilage. In addition, Lorwongtragool *et al.* [194], tested the performance of CNTs mixed with different polymers, polyvinyl chloride (PVC), cumene terminated polystyrene-co-maleic anhydride (PSMA), poly(styrene-co-maleic acid) partial isobutyl/methyl mixed ester (PSE), and polyvinylpyrrolidon (PVP) in the detection of the amines, dimethylamine, dipropylamine, pyridine, and ammonia solution inside a vapour chamber. Their work found that CNT/PSE sensing elements increased their resistivity in approximately 10% when exposed to a 1000 ppm of the different tested amines. These studies are examples of the detection of food amines by using the adsorption properties of the polymer matrix and the conductive properties of the fillers in a CPC.

As discussed previously, numerous designs and methods for sensing freshness and integrity in food packaging have been proposed by researchers and packaging companies. Moreover, freshness indicators continue to stay at development stages, without significant penetration to the market. Unfortunately, proving information about the actual freshness of food has become a risk to the image of processors, which has become a limitation for the wider development of these freshness indicators. As consequence of this, the integration of food sensors to RFID systems could be a more likely solution to this image issue as producers and retailers, and not consumers, could have information about the actual freshness of food.

2.3 Traceability and identification technology

As the risk of public scrutiny for high standards in food safety increases, food producers are more interested in technologies that allow them to trace general information about products. In order address this issue, radio-frequency identification (RFID) tags use radiofrequency electromagnetic fields to store and transmit information of the product for product identification and traceability [7, 69]. RFID devices are composed of an integrated circuit to store information and an antenna that allows the communication and transition to an external reader [195]. Compared with other identification techniques, such as barcodes, RFID presents the advantage to allow a remote control and retrieve information of multiple items at the same time while providing information about origin, process, commercial information, date of packaging, and others [42]. Traditional RFIDs were initially designed to store limited information about the identification, origin, date of production and others. Currently, responsive CPCs can be integrated in the antenna

or the integrated circuit of the RFID, to fabricate devices that can communicate current information about the storage conditions and freshness of food [69].

Commercially, a group of companies, EPSILIA (Canada), RFID Enabled solutions Inc. (USA), and HRAFN Ltd. (Sweden), have collaborated with the meat and fish industries to advance the implementation of RFID technology [69]. Furthermore, the development of responsive polymers used in freshness indicators and sensors has allowed the integration of other functions into the RFID tags, including gas sensing, time temperature indicators, and biosensors, to monitor and communicate factors of food freshness to producers [195]. The integration of time temperature responsive materials into the integrated circuit of an RFID represents the most common used of RFIDs with sensors. The combination of these technologies has allowed to collect information about the cold chain during production and transportation.

Recent research has presented RFID tags with sensing functions in their integrated circuit, additional to those of commercial time temperature tags. In order to monitor the quality of muscle foods, for instance, Zhu *et al.* [196] reported the use of an RFID system to report changes in the concentration of O_2 in MAP based on the aerobic oxidation of FeII ions (Figure 2-7). The sensing element in the integrated circuit of this RFID was a poly(4-vinylpyridine)-single wall nanotubes-Iron II ions (P4VP-SWCNT-FeII) composites that worked as chemiresistors. Initially, the response to oxygen of the sensing element in the RFID was done by immobilizing the P4VP-SWCNT-FeII on a glass surface. Finally, the performance of this device to ambient air ingress was assessed in a food package [196].

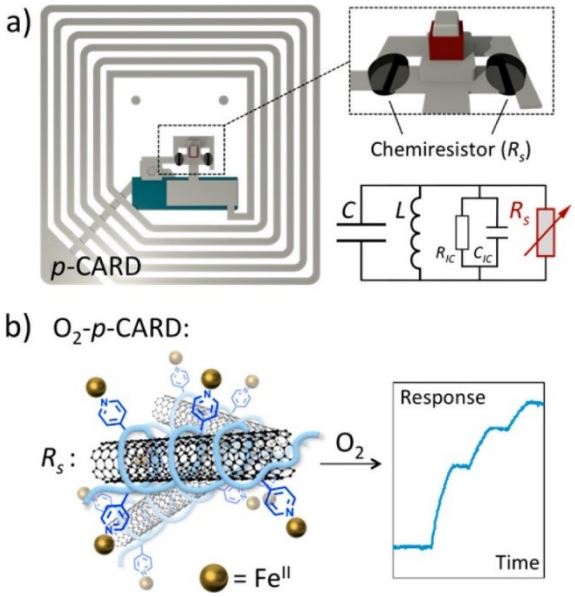

Figure 2-7: (a) Design of RFID with the location of the responsive element (R_s); C: tuning capacitor; L: inductor (antenna); R_{IC}: resistance; and C_{IC}: capacitance of integrated circuit; (b) Poly(4-vinylpyridine)-single-walled carbon nanotubes-Fe(II) ions composite [196]

CPCs can also be integrated into the antenna of RFIDs to measure variables in food packaging such as temperature, humidity, oxygen, and other gases such as volatile amine compounds [196–198]. For instance, Oprea *et al.* proposed the use of polyethylene-naphthalate and polyimide on flexible RFID labels for a capacitive humidity sensors with high sensitivity of 21 fF/%RH for relative humidity between 20% and 90% [199]. A similar study was presented by Salmerón *et al* [200]. They presented a humidity sensor based on polyimide substrate to be coupled to ultra-high frequency RFID tags. The response of these sensors was linked to the changes in electrical permittivity of the polyamide substrate with humidity. The design of the electrodes, in form of serpentine, on the polyamide substrate, gave a sensitivity of 100 fF/%RH, significantly higher than that by Oprea *et al.* [199, 200]. Babi *et al.* presented an overview of RFID technology and some leading materials and fabrication techniques, with some comprehensive examples of responsive polymers as sensing material [195].

The design, development, and commercialization of intelligent food packaging for muscle foods requires of cheap, simple, lightweight materials that can respond to changes in temperature, pH, or freshness of food. Stimuli-responsive polymers and conductive composites based on them have a large potential to cover these requirements.

3. *Low-Resistance Silver Microparticle-HEMA-PEGDA Composites for Humidity Sensing* [1]

ABSTRACT: We present a printable smart material that undergoes a large and reversible change in resistance in response to changes in relative humidity. This material is a conductive polymer composite (CPC), comprised of commercial silver (Ag) micro-particles that provide high conductivity to the films, and of a hygroscopic polymer matrix (poly(2-hydroxyethyl methacrylate)-co-poly(ethyleneglycol diacrylate) (HEMA-co-PEGDA)) that responds to humidity by undergoing an increase in volume (through swelling). We characterized the electrical resistivity and swelling behavior of the CPCs, formed sensors comprised of either thin films or patterned lines, and investigated how relative humidity affects the electrical resistivity of the composite films for different compositions and geometries. To characterize the material's responsive behaviour, a data acquisition system was used to measure changes in resistance while the relative humidity was controlled in a humidity chamber. When the humidity was increased from 25% to 95% RH, the resistance of the films increased up to 650%. Composites with a higher fraction of HEMA in the matrix were found to have both lower recovery times and less hysteresis than composites in which the matrix was pure PEGDA. Such materials can form the basis of inexpensive, printable humidity sensors.

[1] A version of this chapter has been published as Adrián Lopera-Valle, Anastasia Elias, "*Low-resistance silver microparticle-HEMA-PEGDA composites for humidity sensing*", Smart Mater. Struct., Volume 27, Number 10 (105030), doi: 10.1088/1361-665X/aad355. Refer to the preface of this thesis for more information.

3.1 Introduction

The measurement of humidity using simple, lightweight, portable sensors, is of interest for various industrial applications, including monitoring of environment conditions, window defogging in automobile industry, industrial drying and environment control in textiles, human comfort, and electronics [168, 169]. For instance, in the processing and storage of food products, humidity — in addition to temperature — is a relevant factor for the formation and growth of spoilage microorganisms that affects the storage time of goods [14–16]. Therefore, in order to prevent food loss during production and storage, simple sensing devices that require low operational energy are needed [17]. Lightweight and inexpensive sensors based on responsive materials could even be incorporated directly into food shipments or packages.

Humidity is traditionally measured by means of optical, gravimetric, piezoresistive, magnetoelastic, capacitive, and resistive techniques [201–203]; the last two of these represent more than 75% of the humidity sensors on the market [168, 204, 205]. A variety of materials have been employed for use in humidity sensors, including porous ceramics, electrolytes, polymers, and composites [171]. In recent years, conductive polymer composites (CPC) —comprised of conductive fillers in a polymer matrix — have been used in the fabrication of humidity sensors; carbon-based conductive fillers materials have been employed in particular due to their intrinsically high conductivity and high surface area [206–208]. The sensing of humidity using CPCs usually relies on the hygroscopic properties of the polymer matrix. This matrix swells as the relative humidity (RH) increases, leading to an increase in the distance between the conductive elements, (e.g. particles, flakes, whiskers), resulting in a change in electrical properties such as resistance [147, 175]. For instance, Peng *et al.* studied the performance of kappa-carrageenan (KC) – CNTs as humidity sensing material, and implemented devices that exhibited high performance during the humidity measurements, hysteresis, and stability tests [209]. In this material, the resistance *decreased* as a function of humidity, due to interactions directly between water and the surface of the CNTs. The hysteresis was found to be less than 4%, and good stability was observed during 30 days of testing at humidity levels between 35% and 90% RH [209]. However, the baseline resistance of the CPC-based humidity sensors — like those presented by Peng *et al.* and others [168, 173, 210] — is large (≥1000 Ω), which may limit the efficient implementation of these

materials in portable devices as larger power supplies or sensitive electronics are therefore required to achieve measurable currents [209].

When hygroscopic polymers are exposed to water vapor, an osmotic pressure associated with their hydrophilicity causes these materials to absorb water and swell. In response to this swelling osmotic force a reactive elastic force develops, opposing the stretching of the polymer volume [211–214]. When equilibrium is achieved, the elastic and osmotic forces reach a balance and no additional swelling occurs [211]. Hydrogels and other highly hygroscopic polymers are good candidates for the matrix in a humidity sensing CPC given that they can swell to over 100% and of their weight without dissolving [174, 175]. The hydrophilicity of the polymers such as poly(ethylene glycol) diacrylate (PEGDA) and 2-hydroxyethyl methacrylate (HEMA) — due to polar ether groups (–C–O–C–) and hydroxyl groups (–OH), respectively — make them attractive for use in CPC for humidity sensing applications [215, 216]. These two polymers may also be blended [183, 184, 217]; polymers based on PEGDA and HEMA blends have been widely studied in biomedical applications due to their biocompatibility and tunable properties such as swelling ratio, mechanical properties, and cytotoxicity [218]. PEGDA-based composites have been implemented in a variety of sensors. Lee *et al.* [185] demonstrated a colorimetric biosensor comprised of PEGDA-embedded polydiacetylene. In their study, the intensity of the colorimetric response was tuned by varying the concentration of α-cyclodextrin (the polysaccharide responsible of color signal) [185]. Similarly, Havens *et al.* [186] used PEGDA for the fabrication of electrochemical sensors in which the responsive elements were immobilized in a hydrogel matrix. In their work, functionalized multiwall carbon nanotubes (MWCNT) within the PEGDA were used to detect both acetaminophen and ascorbic acid by cyclic voltammetry. In both examples, analytes from the solution diffused through the water-swollen polymer to interact with the sensing constituent and generate a signal (e.g. optical or electronic) [185, 186].

A variety of fillers have been investigated for sensing applications, including conductive polymers, carbon-based, and metallic particles in the micro- and nanoscale [187]. While carbon-based materials (such as carbon nanotubes and graphene) have shown good performance in these applications, they present limited conductivity in thin film applications and can be difficult to disperse. The use of metallic materials, such as gold (Au) [188], copper (Cu) and silver (Ag) [189] micro/nanoparticles has been well-established in the fabrication of CPCs. In the case of Ag, the

high electrical conductivity, high stability, low cost, and antioxidant properties have led this material to be used as the conductive filler in a number of CPCs [190]. In general, CPCs can be processed by means of a wide range of manufacturing techniques [141] including both spin coating, which produces films with thickness determined by viscosity of the solution and spin-speed, [219, 220] and direct-write printing (DWP), in which a material is dispensed through a pressurized syringe over a substrate that can be moved within the x-y plane to produce lines and other shapes or patterns [190, 221].

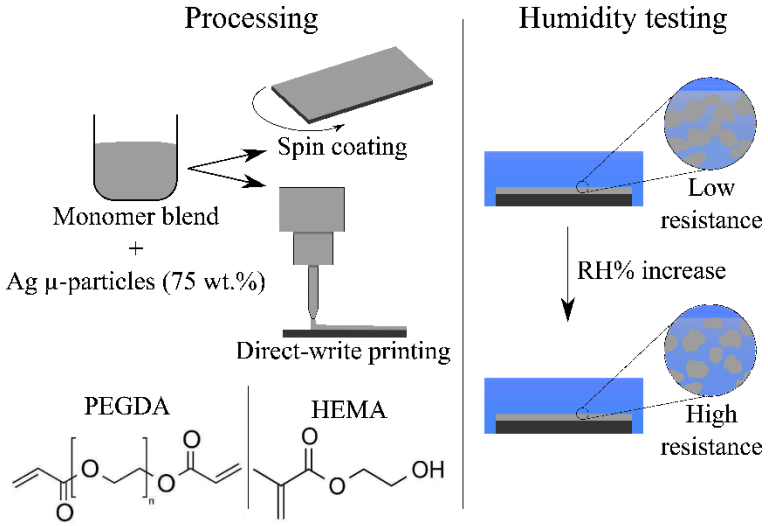

Figure 3-1: Processing, composition, and responsive of conductive-particle composites utilized as humidity sensing materials.

In this study, we investigate the feasibility of using a low resistance silver-HEMA-PEGDA composite for the fabrication of elements for humidity sensing. In these materials, the hydrogel matrix swells upon exposure to water vapor, causing a physical separation of the conductive silver particles, thereby increasing the resistance of the material (Figure 3-1). CPCs were formed using Ag microparticles as the conductive filler and blends of the polymers HEMA and PEGDA as the matrix. Ag microparticles with a flake-like shape were selected as the conductive filler based on their relative high stability (as compared with Ag nanoparticles) and due to the fact that flake-like particles are known to exhibit good connectivity within a CPC [147]. For the matrix, blends of HEMA and PEGDA were selected, and the ratio of these components was varied to tailor the swelling and response of the composite. We first developed a methodology to produce sensing elements for humidity based on Ag-HEMA-PEGDA using spin coating to produce films and

direct-write printing (DWP) to produce lines. We then characterized the physical properties of these CPCs, including morphology and swellability**.** Finally, we determined how both the composition of the hydrogel and the type of structure (films vs. lines) affected the humidity sensing properties of the materials, including responsivity and hysteresis in the measured signal.

3.2 Experimental methods

3.2.1 Preparation of CPC mixture for spin coating and direct-write printing (DWP)

Conductive polymer composite (CPC) mixtures for spin coating and direct-write printing (DWP) were obtained by mechanically mixing different ratios of 2-hydroxyethyl methacrylate (HEMA, average Mn 130 Da) (No. 128635, Sigma-Aldrich, St. Louis, MO, USA) with poly(ethylene glycol)-diacrylate (PEGDA, average Mn 750 Da) (No. 437468, Sigma-Aldrich, St. Louis, MO, USA). These blends of miscible polymers, hereafter referred to as PEGDA-100/HEMA-0, PEGDA-75/HEMA-25, PEGDA-50/HEMA-50, and PEGDA-25/HEMA-75, were comprised of 100/0, 75/25, 50/50, 25/75 wt% of PEGDA/HEMA, respectively. To enable free radical polymerization of monomer mixtures, 0.3 wt% of thermally-degradable free radical initiator, 2,2′-Azobis(2-methylpropionitrile) (AIBN) (No. 441090, Sigma-Aldrich, St. Louis, MO, USA) was added to the mixtures. No water was used in the polymer blend, as the addition of water was found to decrease the viscosity of the mixture, which sometimes resulted in the precipitation of the Ag particles. The polymers and initiator were mixed using a stirring plate (Isotem Basic Stirring Hotplate, Fisher-Scientific, Pittsburgh, PA, USA) at 600 RPM for over 2 hours to ensure that a uniform mixture was produced. Following polymer mixing, silver conductive particles (No. 6105, Methode Development Co., Chicago, IL, USA), with nominal diameters of 10-12 μm [222] were added in different ratios to the polymer solutions. Mixing was achieved using a 40 kHz ultrasonic bath at 21°C (CPXH Heated Ultrasonic Cleaning Baths, Fisher-Scientific, Pittsburgh, PA, USA) for as long as 3 hours to fully disperse the particles in the polymer blends.

As the concentration of particles in a solution are known to vary during the spin-coating process [223–226], preliminary experiments were required to determine the composition of solutions for spin-coating that would result in samples with the final desired composition: 75 wt% Ag. A range of solutions were prepared, spin-coated, and crosslinked, and the content of Ag was analyzed by thermogravimetric analysis (as described in section *3.2.4 Material characterization*).

The content of PEGDA, HEMA, and Ag required to achieve 75 wt% (24 vol%) Ag in the spin-coated samples is shown in Table 3-1. In this table, the sample names represent the final ratio of PEGDA:HEMA in the hydrogel matrix of the composite (excluding the mass of the filler phase). As can be seen from Table 3-1, it was generally necessary to add less Ag than desired in the final film. This trend has been reported and explained in previous studies [223–226]; due to the low viscosity of the monomer solution, this mixture is spun off preferentially with respect to the filler particles, resulting in coatings of higher wt% of the filler. Table 3-2 lists the content of PEGDA, HEMA, and Ag in each CPC solution used for DWP. No material is lost during the DWP process (unlike the spin-coating process), therefore the composition of the solution directly matches the desired composition of the sample. The ratios of PEGDA:HEMA summarized in Table 3-1 and Table 3-2 reflect the composition of the polymer blend *prior* to co-polymerization and do not represent the final composition of each co-polymer after free radical polymerization.

Table 3-1: Composition of CPC mixture for spin coating process (selected to achieve a final composition of 75 wt% Ag microparticles and of 25 wt% polymer after spin coating, based on preliminary studies). The name of each composite indicates the desired ratio of PEGDA/HEMA after spin-coating (excluding the mass of the filler phase).

	Mixture content required for spin-coating		
Composite	PEGDA	HEMA	Ag
PEGDA-100/HEMA-0/Ag	30 wt% (80 vol%)	0 wt% (0 vol%)	70 wt% (20 vol%)
PEGDA-75/HEMA-25/Ag	30 wt% (65 vol%)	10 wt% (21 vol%)	60 wt% (14 vol%)
PEGDA-50/HEMA-50/Ag	25 wt% (45 vol%)	25 wt% (45 vol%)	50 wt% (10 vol%)
PEGDA-25/HEMA-75/Ag	14 wt% (23 vol%)	41 wt% (69 vol%)	45 wt% (8 vol%)

Table 3-2: Composition of CPC mixture for DWP process. The name of each composite indicates the desired ratio of PEGDA/HEMA after printing (excluding the mass of the filler phase).

Composite	PEGDA	HEMA	Ag
PEGDA-100/HEMA-0/Ag	25 wt% (76 vol%)	0 wt% (0 vol%)	75 wt% (24 vol%)
PEGDA-75/HEMA-25/Ag	19 wt% (57 vol%)	6 wt% (19 vol%)	75 wt% (24 vol%)
PEGDA-50/HEMA-50/Ag	12.5 wt% (38 vol%)	12.5 wt% (38 vol%)	75 wt% (24 vol%)
PEGDA-25/HEMA-75/Ag	6 wt% (19 vol%)	19 wt% (57 vol%)	75 wt% (24 vol%)

3.2.2 Percolation threshold

The percolation threshold of the electrical resistivity was studied by adding Ag particles in concentrations from 0 to 80 wt% (30 vol%) in PEGDA-100/HEMA-0, PEGDA-50/HEMA-50, and pure HEMA polymer matrices. Bulk samples were prepared by casting the solutions in silicone molds, as described in section *3.2.6 Equilibrium water content,* and electrical resistivity was characterized by four-point probe as described in section *3.2.5 Electrical characterization of spin-coated films and printed lines*. The morphology of specimens of CPC casted samples was characterized as described in section *3.2.4 Material characterization*.

3.2.3 Synthesis of spin-coated films and printed elements

Polymer composite films, shown in Figure 3-2a, were deposited by spin coating. Glass microscope slides (No. 12-550-A3, Fisherbrand Pittsburgh, PA, USA), 25.4 mm × 76.2 mm x 1 mm (width x length x thickness) were used as substrate for spin coating. To facilitate electrical connections to the composites, sections of conductive copper tape (No. 1181, 3M, St. Paul, MN, USA) approximately 20 mm in length and 12.7 mm in width were placed 40 mm apart on one of the sides of the glass. The substrates were cleaned with isopropyl alcohol and placed on the chuck of the spin coater (Model WS 650-8B- 23 NPP, Laurell Technologies Corporation, North Wales, PA, USA). Approximately 3 mL of CPC mixture was applied on the surface of the substrate. The coating process was conducted in two steps: 1) a spreading step in which the substrates spun at a speed of 500 RPM for 30 seconds (to disperse the mixture over nearly the entire surface of the substrate), 2) a spin step at a velocity of 1400 RPM for 15 seconds (to control the thickness of the final film). Finally, to activate the initiator and polymerize the samples, the CPC-coated glass substrates were placed inside an oven (Isotemp Standard Oven, Pittsburgh, PA, USA) set at 80°C for 6 hours.

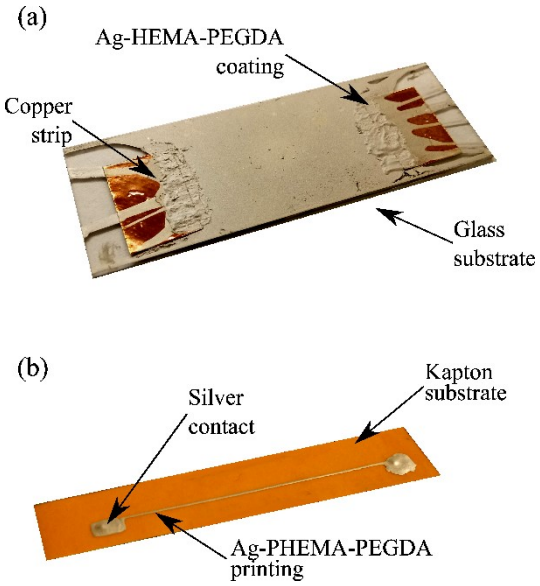

Figure 3-2: Typical features of conductive a) spin-coated film samples and b) printed line samples.

The printed lines, shown in Figure 3-2b, were deposited by a direct-write printing (DWP) technique. Sections of KAPTON® tape, 50 mm in length and 12.7 mm in width, were affixed to strips of bond paper to create self-standing thin substrates for the printing of sensing lines of CPC. The KAPTON® substrates were cleaned with isopropanol as described above. Following cleaning, a printing system (I&J F2200, I&J Fisnar Inc., Germantown, WI, USA), equipped with a pneumatic syringe for material deposition and a programmable x-y stage, was used to pattern lines. The mixture was dispensed through a gauge no. 26 needle in a straight line with 40 mm of length. In order to print consistent lines, the distance between the substrate and the needle tip was set to be approximately 200 μm, while the speed of printing was set to 30 mm/s at a feeding air pressure of 3 psi. Finally, the printed lines were cured inside an oven set at 80°C for 6 hours. Following curing, the spin-coated films and printed lines were placed into a desiccator for as long as 8 hours to remove any water molecules that might have been absorbed during the fabrication process.

3.2.4 Material characterization

The morphology of spin-coated thin films and printed lines was evaluated using a field emission scanning electron microscope (SEM) (Zeiss Sigma 300 VP-FESEM, Zeiss, Cambridge, UK). Images of the un-coated CPC elements were captured using secondary electron (SE) mode.

In addition, a two-dimensional surface topography profiler (Alpha-Step IQ, KLA Tencor, Malpitas, CA, USA) was used to accurately measure the thickness of the spin-coated films and construct profiles of the cross section of the printed lines. The profiler is equipped with a 5 μm radius stylus used to profile the contour of the lines at a speed of 50 μm/sec under an applied force of 12.5 mgf.

The composition of the CPC in the cured spin-coated films and printed lines was investigated to verify that the concentration of Ag was similar in all samples. Based on previous studies [223–226] and preliminary tests, the concentration of Ag was expected to vary subsequent spin-coated process. The Ag volume fraction (V_{Ag}) of the composite was determined by thermogravimetric analysis in accordance with ASTM Standards ASTM D2584 [227] and ASTM D3171 [228]. A thermogravimetric analyzer (TGA/DSC Model 1, Mettler Toledo, Columbus, OH, USA), equipped with an ultra-micro balance cell and differential thermal analysis (DTA) sensors, was set at a heating rate of 10 °C/min under nitrogen atmosphere. The Ag volume fraction of each sample was calculated by using the following formula shown in Eq. 3 [229]:

$$Vol_{Ag} = \frac{\frac{m_{Ag}}{D_{Ag}}}{\frac{m_{Ag}}{D_{Ag}} + \frac{m_m}{D_m}} \quad \text{Eq. 3}$$

where *m* is the mass, *D* is the density, and the subscripts Ag and *m* represent the Ag particles and matrix, respectively. The values of the densities of PEGDA, HEMA, and the Ag particles were taken as 1121 kg/m^3 [230], 1150 kg/m^3 [231], and respectively 10490 kg/m^3 [232].

3.2.5 Electrical characterization of spin-coated films and printed lines

Electrical characterization of samples was performed using both two- and four- point probes. A four-point probe (Signatone S-302-4, Lucas Signatone Corporation, Gilroy, CA, USA), coupled with a sourcemeter (Keithley 2401 SourceMeter, Solon, OH, USA), was used to apply 10 μA current and to measure the resulting voltage between the 1.5 mm spaced probes. The electrical resistivity of the film samples was calculated using Eq. 4 [233]:

$$\rho = \frac{\pi h}{\ln(2)}\left(\frac{V}{I}\right) \qquad \text{Eq. 4}$$

where ρ is the material resistivity, h is the film thickness, V is the voltage measured in the probe and I is the applied current applied with the sourcemeter. Due to their reduced sampling area, characterization of the printed lines could not be undertaken using a four-point probe. Alternatively, a sourcemeter (Keithley 2401 SourceMeter, Solon, OH, USA) was set in two-point measurement mode to record the resistance between the two silver points in the extremes of the printed line, as shown in Figure 3-3. In the case of printed lines, the material resistivity is given by Eq. 5 [234]:

$$\rho = \frac{Wh}{L}\left(\frac{V}{I}\right) \qquad \text{Eq. 5}$$

where ρ is the material resistivity, h is the line thickness, W is the line width, L is the line length, V is the voltage measured in the probe and I is the applied current applied with the sourcemeter.

3.2.6 Equilibrium water content

Studies of equilibrium water content (EWC) were performed to determine the swellability and affinity of the CPCs to water. The equilibrium content was studied by preparing samples with Ag particles in concentrations of 0 or 75 wt% (24 vol%) in hydrogel matrices with the following compositions: PEGDA-100/HEMA-0, PEGDA-75/HEMA-25, PEGDA-50/HEMA-50, PEGDA-25/HEMA-75. The preparation of the CPC mixtures was the same as for the samples described in section *3.2.1 Preparation of CPC mixture for spin coating and direct-write printing (DWP)*. However, rather than spin-coating or printing the mixtures, the samples for the study of equilibrium water swelling content were fabricated by casting roughly 4 ml of the CPC mixture in disk-shaped silicone containers and then curing this material inside an oven set at 80°C for 6 hours. Following the fabrication of the samples, hereafter referred to as the 'bulk samples', their initial mass was measured and recorded. The samples were then immersed in a 50 ml glass beaker with no less than 40 ml of DI water. Over 27 hours, the bulk samples were periodically removed from

the DI water, the water from the surface of the samples was removed using a light stream of air followed by blotting, and the mass of the samples was then measured and recorded. After 27 hours of immersion, the samples were removed from the DI water and dried at 16% RH; similar mass measurements were then taken. Assuming that the Ag particles do not contribute in the absolute increase in mass by water swelling, the swelling content of the hydrogel component of the samples could be calculated using Eq. 6:

$$EWC = \frac{(m_W - m_D)100}{(100 - wt\%_{Ag})m_D} \quad \text{Eq. 6}$$

where m is the mass, $wt\%_{Ag}$ is the weight content of Ag particles, 0 or 75 wt%, and the subscripts W and D represent the wet and dry states of the samples, respectively.

The hydrophilicity and wettability of the CPC and their polymer blends was investigated by using water-in-air contact angle measurements. Previous studies have suggested that the adsorption and affinity of a material to water can be investigated by means of studying its wettability [235, 236]. For instance, Muster *et al.*[235] stablished a correlation between the water absorption and the bulk wettability of silica particles, where particles with lower contact angles were found to have higher water adoption [235]. In this study, a video system analysis tool for contact angle (FTA 200 Dynamic Contact Angle Analyzer, First Ten Angstroms, Inc., Portsmouth, VA, USA) was used to characterize the hydrophilicity of the pure PEGDA:HEMA blends and the PEGDA:HEMA:Ag CPCs at 23°C. Bulk samples of pure PEGDA:HEMA were fabricated as described above in this section. Films of CPC were fabricated as described in section *3.2.3 Synthesis of spin-coated films and printed elements*.

3.2.7 Humidity response testing

The response of the spin-coated films and printed lines to the changes of relative humidity (RH) was investigated by placing the samples inside a controlled humidity chamber (Thermotron S-1.0-3200, Thermotron Inc., Holland, MI, USA) at a constant temperature of 25°C, and monitoring the changes in their electrical resistance as the humidity inside of the chamber was varied. As shown in Figure 3-3, within humidity chamber, a data acquisition system (NI USB-

6216, National Instruments, Austin, TX, USA) was used to measure the resistance of the active material in a two-probe configuration, while a commercial IC humidity sensor (HIH-5030, Honeywell, Golden Valley, MN, USA) was utilized as a reference probe. Measurements were collected every 3 seconds. The response of the CPC elements was investigated by placing the samples, Figure 3-3, inside the humidity camber set at various levels of RH ranging from 25% RH to 95% RH, with 10% RH steps, for as long as 90 minutes for each step. The stability of the sensing elements was evaluated by setting the samples in a 60% RH environment for as long as 5 days while their resistance was monitored. In addition, the response and recovery times of the sensors were evaluated by exposing the samples to 10 cyclic changes in humidity from 35% RH to 95% RH. The response of the samples to changes in humidity was studied in the form of relative change in resistance (RR) as described in Eq. 7:

$$RR = \frac{R_{RH} - R_0}{R_0} \times 100\% \qquad \text{Eq. 7}$$

where, RR is the percentage change in electrical resistance, R_{RH} is the electrical resistance at a given RH in ohms, and R_0 is the electrical resistance of the samples after 8 hours inside a desiccator at a relative humidity of 16% RH in ohms.

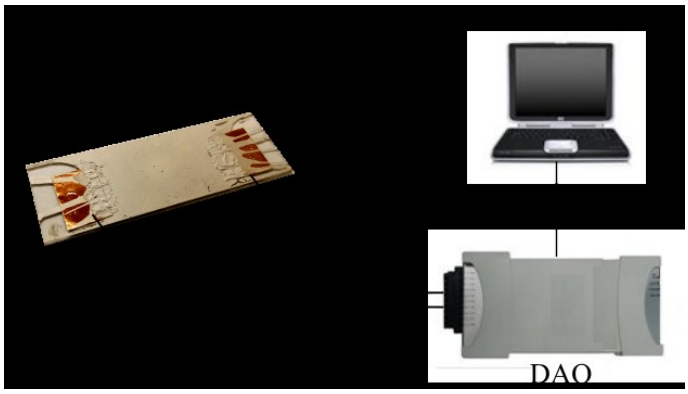

Figure 3-3: Diagram of humidity testing and data collection. The electrical resistance of the sample and the signal from a commercial humidity sensor placed within the humidity chamber were collected by a DAQ every 3 seconds as the humidity was varied.

3.2.8 Sensitivity

A simple linear regression was used to model the sensitivity (i.e. the relationship between RR and RH) of the responsive elements. RR was plotted as a function of RH and the slope of the data, termed the regression coefficient, was calculated within the evaluated range of RH. The coefficient of determination (r^2) for the regression lines of the experimental data points was at least 0.95 or greater for both the spin-coated films and printed lines.

3.2.9 Statistical analysis

A t-test analysis was performed using commercial software (STATISTICA for Academia, StatSoft Inc., Tulsa, OK, USA) to evaluate the statistical differences between sets of results. Unequal variances and a significance level of $\alpha = 0.05$ were used in the evaluations, corresponding to a 95% confidence interval.

3.3 Results and discussion

3.3.1 Material characterization

Samples were prepared by both spin-coating and direct write printing. To determine the concentration of Ag in the hydrogel matrix, composites were initially prepared at a range of concentrations, and the resistivity of the samples were measured (Figure 3-4). The percolation threshold was found to be around 45 wt% (with some variation depending on the blend of polymer in the matrix); a loading of 75 wt% was selected for all subsequent CPCs. In some responsive CPCs, the wt% loading is chosen to be near to the percolation threshold in order to maximize the response [187, 237]. However, such systems can also have non-linear responses, requiring complex signal processing and electronics that can operate over a wide range of currents, as discussed in Lee *et al.* [173]. Here a higher value was chosen to ensure that the initial resistivity would be low, ensuring that characterization could be taken using simple electronics and a low voltage power supply.

Figure 3-4 shows the electrical resistivity of different concentrations of Ag in PEGDA-100/HEMA-0, PEGDA-50/HEMA-50, and pure HEMA polymer matrixes. The percolation threshold of the CPC with pure HEMA was determined to be around 15 wt% (2.6 vol%)

composition, at which concentration the resistivity of the composite decreases from 220 Ωcm to 0.02 Ωcm. In the case of the PEGDA-100/HEMA-0 polymer matrix, the percolation threshold was found to be around 45 wt% (9.7 vol%), where the resistivity of the CPC decreased from 56300 Ωcm to 0.2 Ωcm. In the case of the PEGDA-50/HEMA-50 polymer matrix, the percolation threshold was found to be around 30 wt% (4.3 vol%), where the resistivity of the CPC decreased from 320 Ωcm to 0.03 Ωcm. The values of resistivity found in this work are significantly larger than that one of pure bulk Ag, 1.6×10^{-10} Ωcm, due to both the insulating effects of the polymer matrix and its interaction with the conducting particles.

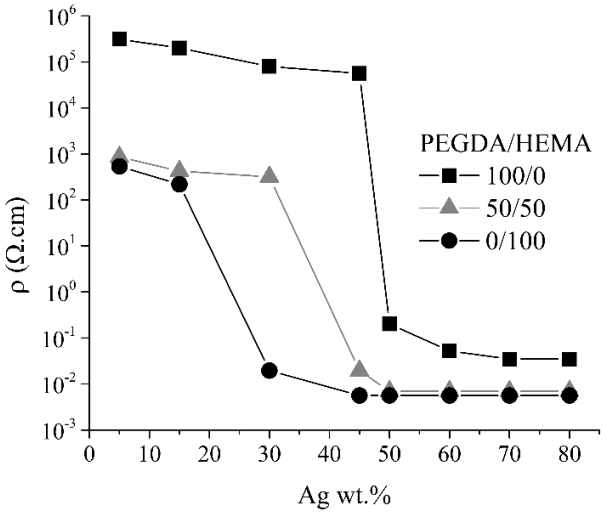

Figure 3-4: Percolation threshold for resistivity of CPC with PEGDA-100/HEMA-0, PEGDA-50/HEMA-50 and pure HEMA as matrix.

Low magnification SEM images were used to characterize the morphology of the spin-coated films and printed lines, as shown in Figure 3-5. Figure 3-5a shows a representative low magnification image of the spin-coated film samples (top view). The films – comprised of 25 wt% polymer and 75 wt% Ag microflakes – appear to be homogenously coated on the surface of the glass substrate (as observed by eye and by microscope inspection). While some voids were observed on the surface of the spin-coated films, (Figure 3-5a) the volume of these voids was not significant in comparison with the overall volume of the film. Apparent agglomeration or clustering of Ag microparticles in the polymer matrix was not seen (by visual inspection or by SEM). While the high content of silver microparticles can be detrimental to the mechanical integrity of the polymer composite, visual inspection of the films and lines did not reveal any

adhesive or cohesive failure of the sensing elements (Figure 3-5). This may be due to the mechanical support that the glass and KAPTON® substrates provide to the composite films and lines. The low magnification image of the top view of the bulk sample (Figure 3-5c, formed by casting the CPC in a silicone mold) is very similar in appearance to the spin-coated film. However, some differences in the orientation and morphology of the particles in the spin-coated and bulk samples can be seen in the high magnification images (Figure 3-5b and Figure 3-5d, respectively). A range of particle sizes — as large as 12 µm — was observed. The orientation of the Ag particles in the spin-coated films (Figure 3-5b) was observed to be partially aligned in-plane direction of the glass substrate, whereas the orientation of the particles in the bulk sample appear more random and globular (Figure 3-5d). The partial orientation could be related to the spin coating process and shape of the particles. In spin coating, the rotation of the substrate leads to uniformity of the resultant film while the excess of mixture is eliminated. In the case of particulate suspensions and immiscible polymer blends, the centrifugal forces in spin coating have been found to significantly affect the orientation and distribution of particles present in suspension [238–241].

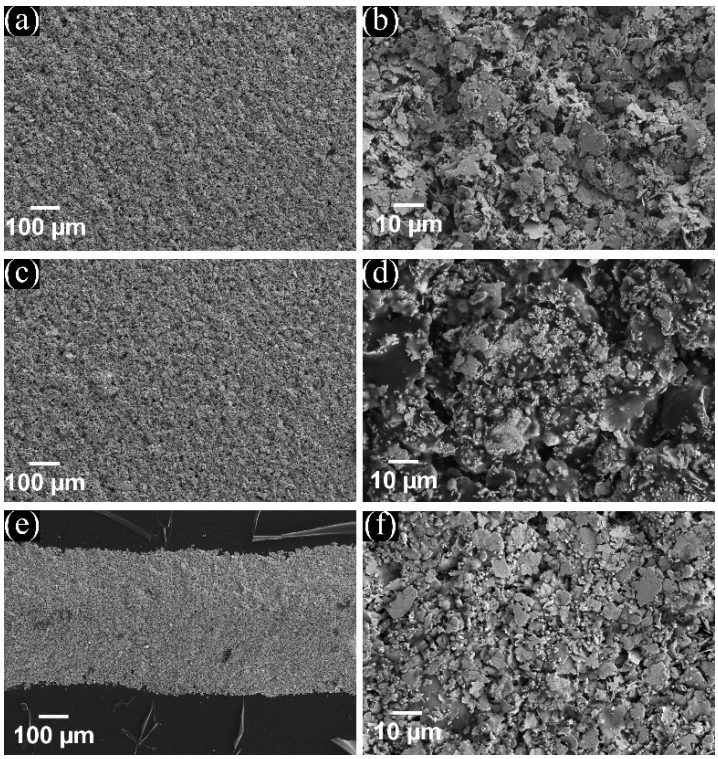

Figure 3-5: a) Low and b) high magnification SEM image of a film sample; c) low and d) high magnification SEM image of a bulk sample; e) low and f) high magnification SEM image of a printed line sample.

Figure 3-5e and Figure 3-5f show representative low and high magnification SEM images of the printed lines. At low magnification, the lines appear dense and similar to the other two samples (films and bulk). At high magnification, the particles in the printed lines can be seen to be highly oriented parallel to the plane of the substrate. With respect to DWP, extensive research has concluded that the shear forces involved in the flow of the mixture throughout the deposition needle can lead to alignment of the particles [242–244]. At high magnification, it can be seen that the particles in the spin-coated films (Figure 3-5b) and printed lines (Figure 3-5f) appear to be aligned in the plane of the substrate, whereas those in the bulk samples (Figure 3-5d) appear to be more randomly oriented.

Surface profilometry was used to measure the width and thickness of both spin-coated films and printed lines. The average thickness of the spin-coated films was found to be 13 μm ± 3 μm (n = 20, 4 measurements in 5 samples). In comparison, the width and thickness of the printed lines was found to be 435 μm ± 14 μm (n = 20, 4 measurements in 5 samples) and 27.8 μm ± 3.5 μm (n = 20, 4 measurements in 5 samples), respectively. In the case of the printed lines, the low standard deviations of the thickness and width suggests that these features were homogeneous throughout the samples.

In order to ensure that the content of Ag was consistent in all samples, ASTM D2584 [227] and ASTM D3171 [228] were used to determine the Ag weight fraction in the CPC spin-coated films and printed lines, and the results are shown in Table 3-3 and Table 3-4. In this table, the content of HEMA and PEGDA values were calculated from the weight fraction of the polymer matrix determined by TGA based on the ratio of HEMA or PEGDA in the initial solution. These results show that, as expected, the average Ag fraction in the film specimens was 78 wt% (27 vol%) which was higher to that of the CPC mixtures utilized for spin-coating (as described in Table 3-1). For instance, the concentration of Ag in the composite with blend PEGDA-100/HEMA-0 as matrix changed from 70 wt% (20 vol%) prior spin coating to 77 wt% (26 vol%) in the films, and from 45 wt% (8 vol%) to 78 wt% (28 vol%) for those films with PEGDA-25/HEMA-75 as polymer matrix. The trend of increased concentration of particle filler in the spin-coated film with respect to the concentration of particles of the initial mixture has been previously reported and explained in previous studies [223–226]; due to the low viscosity of the monomer solution, this mixture is spun off preferentially with respect to the filler particles, resulting in

coatings of higher wt% of the filler. In contrast, the composition of the lines deposited by DWP does not change substantially since the material that is printed is the material that is cured. The content of Ag in the spin-coated films and DWP lines was nearly the same: 77.3 wt% ± 1.4 wt% (n = 12) and 75.8 wt% ± 0.8 wt% (n = 12), respectively. The slight differences were not found to be statistically significant. In our work the content of the mixtures was selected to keep the wt% Ag as constant as possible while varying the composition of the hydrogel matrix (e.g. the ratio of PEGDA to HEMA). Some variation in the Ag wt% can be seen in Figure 3-5, however the variation in the wt% between the different sample types was much less than the difference between the wt% of PEGDA or HEMA in the matrix.

Table 3-3: Composition of CPC spin-coated films (n = 3 for each polymer blend). The ratio of polymer to Ag was determined by TGA. The total fraction of PEGDA and HEMA in the polymer matrix was then calculated from these results based on the relative fraction of each added to the mixture (as reflected by the sample names).

Composite	PEGDA	HEMA	Ag
PEGDA-100/HEMA-0/Ag	23 wt% (74 vol%)	0 wt% (0 vol%)	77 wt% (26 vol%)
PEGDA-75/HEMA-25/Ag	16 wt% (53 vol%)	5 wt% (18 vol%)	79 wt% (29 vol%)
PEGDA-50/HEMA-50/Ag	13 wt% (38 vol%)	12 wt% (37 vol%)	75 wt% (25 vol%)
PEGDA-25/HEMA-75/Ag	6 wt% (19 vol%)	16 wt% (54 vol%)	78 wt% (28 vol%)
Max SD = ± 1.4 wt% (± 1.6 vol%)			

Table 3-4: Composition of CPC printed lines. The ratio of polymer to Ag was determined by TGA. The total fraction of PEGDA and HEMA in the polymer matrix was then calculated from these results based on the relative fraction of each added to the mixture (as reflected by the sample names).

Composite	PEGDA	HEMA	Ag
PEGDA-100/HEMA-0/Ag	24 wt% (75 vol%)	0 wt% (0 vol%)	76 wt% (25 vol%)
PEGDA-75/HEMA-25/Ag	19 wt% (57 vol%)	6 wt% (19 vol%)	75 wt% (24 vol%)
PEGDA-50/HEMA-50/Ag	11.5 wt% (37 vol%)	11.5 wt% (37 vol%)	77 wt% (26 vol%)
PEGDA-25/HEMA-75/Ag	7 wt% (19 vol%)	19 wt% (57 vol%)	75 wt% (24 vol%)
Max SD = ± 1.1 wt% (± 1.3 vol%)			

3.3.2 Electrical characterization of spin-coated films and printed lines

The electrical resistivity of the spin-coated films and printed lines was investigated using 4- and 2- point probe respectively. The overall resistance of the spin-coated film samples was 3.8 Ω ± 0.3 Ω, and that of the DWP lines was 42.5 Ω ± 1.6 Ω (values averaged across all types of polymer matrix blends). The resistivity of the samples with PEGDA-100/HEMA-0 as polymer matrix was 1.6 mΩ·cm ± 0.4 mΩ·cm for both films and lines, while that of the composite with PEGDA-25/HEMA-75 polymer blend was 1.3 mΩ·cm ± 0.5 mΩ·cm. In a t-test analysis, a p-value of 0.27 was found when comparing the resistivity of the PEGDA-100/HEMA-0 and that of the PEGDA-25/HEMA-75 films, indicating that the difference between these values was statistically negligible ($p > 0.05$). The low resistivity of this CPC is desirable as it would allow these materials to be implemented in low power applications such as food storage systems.

While the electrical resistivity of the films and lines at the selected concentration (~76 wt% or 25.9 vol%) were similar to each other (1.3 to 1.6 mΩ·cm), these values differed from the electrical resistivity of the bulk samples (as measure for the electrical percolation study described in section *3.3.1 Material characterization*, ~ 6 mΩ·cm at a similar concentration). The difference between these values can be attributed to differences in the distribution and orientation of the particles. The SEM images of the films and printed lines revealed that the Ag particles had some orientation in the plane of the substrate (likely caused by the flow dynamics during the spin coating and DWP processes), whereas the Ag particles in the bulk films were more randomly oriented. These results suggest that the orientation of the Ag particles in the direction of the substrate decrease the resistivity of CPCs, as particles in this orientation can form a more connected and continuous network through which the electrons can travel. These results are in agreement with previous studies from the literature, which have shown that the orientation of anisotropic particles can lead to an enhancement in properties such as thermal conductivity and mechanical strength [150, 241, 243].

3.3.3 Equilibrium water content

The swelling dynamic of the polymer blends was studied by immersing bulk samples in DI water while their mass was measured, and the results are shown in Figure 3-6. Figure 3-6a depicts the gain in mass in time due to swelling of water of the polymer samples *without* Ag particles (as

calculated using Eq. 6, above). After approximately 12 hrs of immersion, the sample mass reached a steady state, achieving an increase in mass of 51.7% ± 1.4%(n = 12); this value remained relatively constant until the samples were removed from water after 27 hrs of immersion. As shown in Figure 3-6a, the EWC was not significantly affected by the composition of the polymer blend in those samples without Ag particles. These values are generally in agreement with previous work from the literature: Hirota *et al.* [245] and Wu *et al.* [246] reported the EWC values of polymerized HEMA and PEGDA (average Mn 700 Da) networks as 44.9% and 49.2%, respectively. Other articles from the literature have shown that higher EWC can be achieved when the monomers are polymerized in the presence of water, which results in a more porous and swollen structure [246, 247]. Here, we opted not to mix water with the monomer solution in order to maintain a high viscosity for DWP, and to prevent phase separation of the components.

Figure 3-6b depicts the equilibrium swelling ratio of CPCs (containing 75 wt% Ag). As only the polymer fraction (and not the silver fraction) of the blend absorbs water, this value has been scaled by the wt% of the polymer matrix. As shown in Figure 3-6b, the inclusion of Ag particles in the polymer blends affected the water absorption capacity of the CPC matrix for most of the polymers. An exception was seen for the samples containing 100 wt% PEGDA in the matrix: the EWC of pure PEGDA-100/HEMA-0 and the EWC of PEGDA-100/HEMA-0/Ag were similar (52.1% ± 1.6% and 51.68% ± 1.3%, respectively), indicating that PEGDA absorbs the same amount of water with and without silver present. In contrast, the pure PEGDA-25/HEMA-75 matrix had a significantly higher EWC than the analogous CPC (53.8% ± 0.5% vs 41.4% ± 0.4%). Lower EWCs were also seen for the CPCs than for the pure polymers for the two other polymer compositions (PEGDA-75/HEMA-25 and PEGDA-50/HEMA-50). These results suggest that the inclusion of Ag microparticles (which are themselves hydrophobic) in the different polymer blends leads to decreased hydrophilicity in samples with higher content of HEMA in their polymer matrix when compared with those without Ag. Similar increases in hydrophobicity upon the addition of silver flakes were reported by Bayer *et al.* [248], who proposed to blend silver flakes into poly(vinyl chloride-co-vinyl acetate-co-vinyl alcohol) coatings in order to make them superhydrophobic. Their results showed that the addition of silver flakes in 50 wt% to the polymer matrix led to an increase in the contact angle from 75° to 164° ± 4° [248]. Contact angle data for our polymer blends and CPCs are shown in the Table 3-5. While all composites (without Ag) had similar initial contact angles 28° ± 1.9° (n = 48), the values for the CPCs ranged from 45° ± 2.1°

(n = 12) for PEGDA-100/HEMA-0/Ag to 62° ± 2.7° (n = 12) PEGDA-25/HEMA-75/Ag. These results indicate that hydrophobicity of all samples increased with the addition of Ag, with the largest increase occurring for the sample with highest HEMA content.

The contact angle results for the PEGDA:HEMA bulk samples and CPCs are shown in Table 3-5. The results for the PEGDA:HEMA bulk samples of each composition were similar, and the average value of the bulk samples (without conducting particles) was 28° ± 1.9° (n = 28) for the CPCs, the contact angle of the film samples varied with the composition of the CPC polymer matrix. For instance, the contact angle of the spin-coated film with matrix PEGDA-100/HEMA-0 was 45° ± 2.1° (n = 12) and that of PEGDA-25/HEMA-75 was 62° ± 2.7° (n = 12). The contact angle was found to increase in roughly 38% from PEGDA-100/HEMA-0 to PEGDA-25/HEMA-75 polymer blends, showing that the material became more hydrophobic as the proportion of HEMA was increased.

Table 3-5: Contact Angle of Ag CPCs

CPC Polymer matrix	Polymer blend only	Contact Angle (n = 12)
PEGDA-100/HEMA-0	29° ± 1.4°	45° ± 2.1°
PEGDA-75/HEMA-25	29° ± 2.0°	50° ±1.8°
PEGDA-50/HEMA-50	28° ± 1.6°	57° ± 2.3°
PEGDA-25/HEMA-75	26° ± 1.1°	62° ± 2.7

Overall, the differences in EWC and contact angle for composites containing Ag particles may be due to interactions between functional groups in the HEMA monomer and the Ag conducting particles. While some previous studies have reported that the addition of HEMA, due to its –OH groups, increases the hydrophilicity of PEGDA-HEMA hydrogels [216], here we observed a decrease in the hydrophilicity of the CPCs as the content of HEMA increases, evidenced by both a decrease in contact angle and a decrease in EWC. A reason for this might be associated with specific interactions between the –OH groups and the Ag particles. Previous studies, such as that by Siddiqui *et al.* [249], have suggested that the hydrophilic –OH groups and C=O in HEMA can easily create hydrogen-bond of the OH···OH and C=O···HO types [249, 250]. Not only OH···OH dimers, but –OH···OH···OH···OH– aggregates and as well as Ag+···OH bonds have been reported during polymerization of solid polymers and HEMA-Ag nanocomposites [249–251]. When OH- interacts with Ag+ instead of forming hydrogen bonds, an

increase in hydrophobicity and a decrease in the EWC may result. This may help to explain our results. In agreement with the findings in this work, Lee *et al.* [252] and Chandra *et al.* [253] showed that the EWC of 1 vinyl-2-pyrrolidone/N,N0-methylene-bisacrylamide, and sodium carboxymethyl cellulose/ poly(acrylamide-co-2-acrylamido-2-methylpropane sulphonic acid) polymers, respectively, could be reduced by the inclusion of Ag particles.

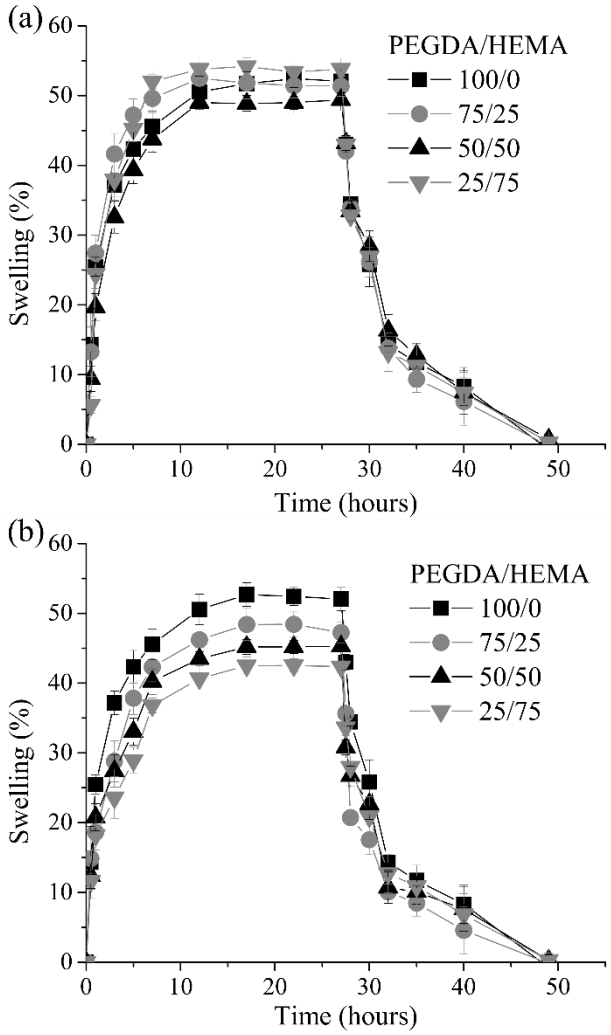

Figure 3-6: Swelling of a) pure polymer blends and b) CPCs with 75 wt% Ag particles. Samples were immersed in water at time = 0 hrs (measured periodically), and removed from water at t = 27 hours and dried to 16% RH.

3.3.4 Steady humidity response

In this work, the CPC is comprised of conductive Ag particles embedded in a hygroscopic polymer that has been previously reported to swell upon changes in RH [217, 254]. As consequence of this swelling, an increase in the effective distance between the conductive particles was expected to occur, leading into a change in the resistivity of the CPC material. The response of the CPC film and line sensors was assessed inside a humidity chamber as the relative humidity (RH) was varied from 25% to 95% RH. The relative resistance (RR (%)) is given by equation Eq. 7, above, is plotted as a function of RH in Figure 3-7.

In Figure 3-7a, which depicts the response of the films, the relative resistance of all compositions showed a *linear* increase when the relative humidity increased. As expected, the swelling of the polymer matrix led an overall increase in resistance, likely resulting from an increase in separation between conductive particles. In our work, the response of the films to changes in RH was different for each material, despite the fact that the content of Ag filler was nearly the same for all films (~76 wt% or 25 vol%). The results shown in Figure 3-7a suggest that the composition of the polymer blend in the films has an effect on the magnitude of the change in resistance of the material. For instance, the relative resistance of the PEGDA-75/HEMA-25/Ag samples was 86% ± 1.7%(n = 3) at 25% RH and 338% ± 8%(n = 3) at 95% RH. In general, the value of the relative resistance increased with increasing RH, reaching a maximum at RH 95%. For instance, at 95% RH, the RR was 521% ± 9%(n = 3) for PEGDA-100/HEMA-0/Ag, 338% ± 8%(n = 3) for PEGDA-50/HEMA-50/Ag, 137% ± 3%(n = 3) for PEGDA-50/HEMA-50/Ag and 95% ± 2%(n = 3) for PEGDA-25/HEMA-75/Ag polymer blends. The increase in resistance was mainly driven by the swelling of the polymer matrix. As the humidity increased and the content of water in the CPC sensing elements increased, the polymer swelled, increasing the main free path between the Ag particles, which alters the conductive paths within the CPC, therefore increasing the relative resistance of the material.

As shown in Figure 3-7a, the relative resistance of the spin-coated CPC films exposed to 95% RH increased with the concentration of PEGDA. For instance, the value of relative resistance at 95% RH for PEGDA-100/HEMA-0/Ag was 521% ± 8%(n = 3), while the relative resistance for PEGDA-25/HEMA-75/Ag was only 95% ± 2%(n = 3). This difference in behavior can be attributed to higher hydrophilicity of the CPC PEGDA-100/HEMA-0/Ag as compared with the

sample containing HEMA in the matrix. As discussed in section *3.2.6 Equilibrium water content*, the water absorption results showed that the CPC samples with the highest content of PEGDA (PEGDA-100/HEMA-0/Ag) underwent more swelling than those with HEMA in their composition. Therefore, these samples also exhibited the highest change in resistance when exposed to 95% RH.

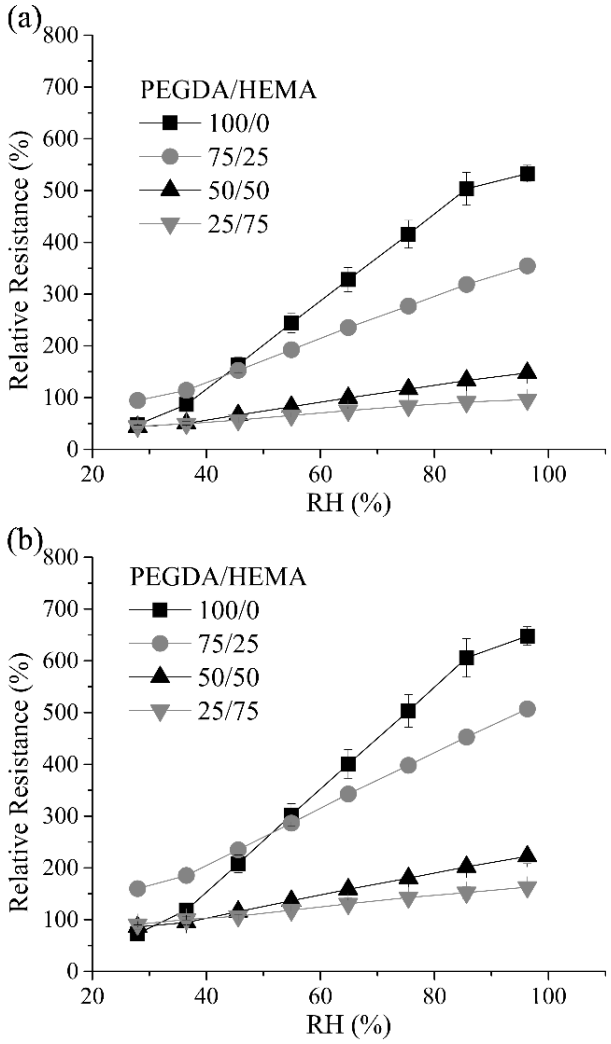

Figure 3-7: Variation of resistance of CPCs in the form of a) spin-coated films and b) printed lines with change in RH from 25% RH to 95% RH, in 10% RH increments for 3 cycles.

The response of the printed lines was evaluated as per the methods described above for film samples. Figure 3-7b shows the response, in terms of relative resistance, of the printed lines upon changes in RH inside the humidity chamber. In the case of lines of PEGDA-100/HEMA-0/Ag, for instance, the RR of the samples changed from 53% ± 5%(n = 3) to 630% ± 10% (n = 3) when the

RH in chamber changed from 25% RH to 95% RH. On the other hand, the RR of the PEGDA-25/HEMA-75/Ag printed sample increased from 83% ± 2%(n = 3) to 157% ± 3%(n = 3) when the RH inside the humidity chamber changed from 25% RH to 95% RH. Similar to the response of thin films, the relative resistance increased linearly with the increase of RH. In addition, the composition of the CPC polymer matrix was found to have an effect in the magnitude of the response of the printed sensing elements. The composite which underwent the largest response (PEGDA-100/HEMA-0/Ag) was also the most hydrophilic (with the largest EWC and contact angle). To determine the stability of the networks, the RR of a sample kept at 60% RH was measured every 3 seconds for as long as 5 days; a slight increase in the measurement of 4.3% was found over the time period of measurement. This indicates that the samples are relatively stable, even in conditions of relatively high humidity.

While the response of the spin-coated films (Figure 3-7a) and printed lines (Figure 3-7b) was found to be similar in behaviour (with the response of each sample increasing with increasing composition of PEGDA in the polymer matrix), the magnitude of the response differed for each geometry. For instance, the value of RR of the spin-coated film with PEGDA-100/HEMA-0/Ag was 521% ± 8%(n = 3), while the printed lines presented a RR value of 630% ± 10% (n = 3). A similar trend was observed for each matrix composition: larger responses were measured for the lines than for the films. In terms of geometry, the average width and thickness of the printed lines were 435 µm ± 14 µm (n = 20) and 27.8 µm ± 3.5 µm (n = 20), while those of the spin-coated films were 25.4 mm and 13 µm ± 3 µm (n = 20). The lines were therefore thicker than the films (by a factor of ~2), while the films had a much larger size in the plane of the substrate. The difference in thickness are not expected to affect the response; while the larger thickness of the lines would allow a higher overall swelling to occur in response to the water vapor, the *relative* change in resistance should be the same (assuming homogenous behaviour throughout the material). Differences in the overall geometry of the sample types are expected to contribute more substantially to differences in behaviour: while the films are constrained in the plane of the film (allowing them to swell in only one direction), the lines are able to expand in both width and height in response to the water vapor. This added degree of freedom may contribute to the higher change in resistance observed for the lines, as these structures are subject to fewer boundary conditions.

The sensitivity, *S*, of a sensor is defined as the ratio between the change in RR and any change in RH ($S = RR/RH$). The values of sensitivity of the spin-coated films and printed lines were determined from the data shown in Figure 3-7, and the results are summarized in Table 3-6. As discussed above, sensing elements with higher concentration of PEGDA showed higher sensitivity given the higher compatibility to water. As was qualitatively observed from the graphs, lines fabricated from a given CPC exhibited higher sensitivities than films of the same material.

Table 3-6: Sensitivity of spin-coated film and printed line sensing elements.

Polymer blend	Spin-coated films (%/RH)	Printed lines (%/RH)
PEGDA-100/HEMA-0/Ag	8.06	9.43
PEGDA-75/HEMA-25/Ag	4.15	5.44
PEGDA-50/HEMA-50/Ag	1.66	2.15
PEGDA-25/HEMA-75/Ag	0.9	1.19

3.3.5 Cyclic humidity response

To test the cyclic response of the sensing elements, the RR of films and lines were characterized as the RH was periodically varied from 35% to 95%. This range of humidity was chosen to span the values reported for the storage of fresh grains, produce, and meat [15, 16, 255]. Each humidity cycle lasted 180 mins (90 mins at 35% RH and 90 mins at 95% RH); transitions between the two states typically took 120 sec to achieve. The results of five cycles of testing for films and lines are shown in Figure 3-8a and Figure 3-8b respectively. In each case, a relatively fast change in relative resistance was observed when the humidity was increased or decreased, and a steady state was then reached. The average values of RR in cyclic tests were consistent with those found in the steady state tests (shown in Figure 3-7a and Figure 3-7b). For instance, the average value of RR in steady state and cyclic tests of PEGDA-100/HEMA-0/Ag spin-coated films at 35% RH was 88% ± 7%(n = 10) and 552% ± 17%(n = 10) at 95% RH. On the other hand, the average value of RR in steady state and cyclic tests of PEGDA-100/HEMA-0/Ag printed lines at 35% RH was 115% ± 12%(n = 10) and 665% ± 32%(n = 10) at 95% RH. The small differences between these values can in part be attributed to hysteresis (discussed below). As was observed in the study of the steady-state response, the magnitude of the response, and therefore of the sensitivity, of the printed lines sample was roughly 27% higher than those of the spin-coated film

samples. As argued above, the sample geometry affects the sensitivity and the magnitude of the response of the CPC samples.

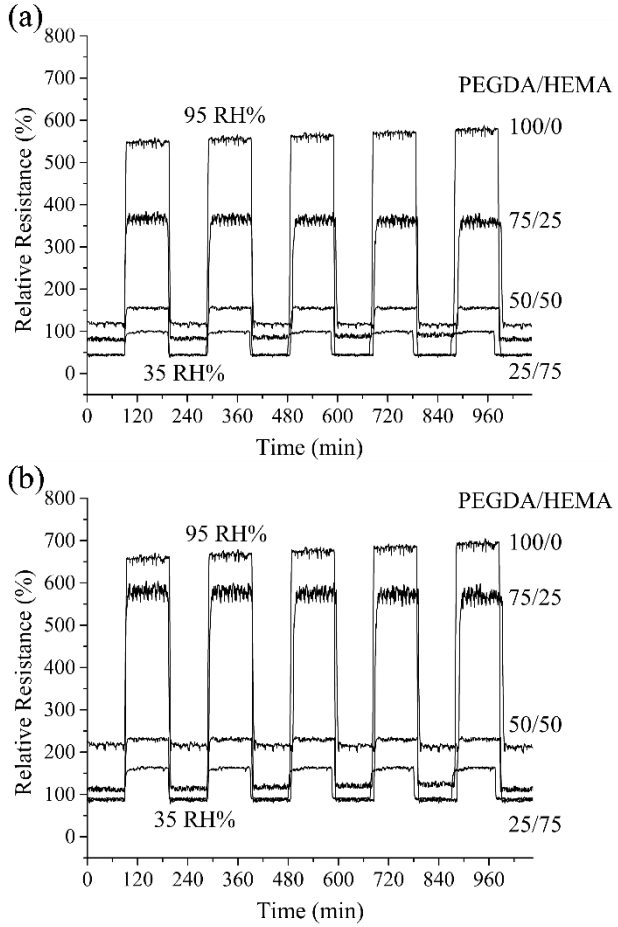

Figure 3-8: Cyclic variation of relative resistance of a) spin-coated CPC films and b) printed CPC lines with cyclic change in RH from 35% to 95%.

The recorded values of RR during the cyclic changes of RH showed evidence of hysteresis, exhibiting slightly but progressively higher relative resistance values at a given state from cycle to cycle. Representative hysteresis loops are shown in Figure 3-9a and Figure 3-9c for films and lines. The hysteresis for each sample composition was calculated by the change in RR after each low-to-high humidity cycle, using the first cycle as reference, and the results are shown in Figure 3-9b and Figure 3-9d for films and lines, respectively. Hysteresis was observed particularly in spin-coated films and printed lines with PEGDA-100/HEMA-0/Ag polymer blend, for which the values of RR for the spin-coated films increased from 552% ± 17%(n = 10) in the first cycle to 587% ± 22%(n = 10) after 10 cycles. Notably lower hysteresis effects were observed in samples with higher

concentration of HEMA in their polymer blend, e.g. PEGDA-25/HEMA-75/Ag, for which the values of RR for the spin-coated films increased from 94% ± 7%(n = 10) in the first cycle to 97% ± 2%(n = 10) after 10 cycles. As argued above, the sensing mechanism of the spin-coated films and printed lines is that as the film swells upon exposure to water, the change in volume causes the distance between conductive particles to increase, leading to a measurable increase in resistance. The permanent change in resistance suggests that part of the conductive paths along the volume of the sample were permanently changed after exposure to high levels of humidity. As has been discussed previously by Ahmad *et al.* [256], Farahani *et al.* [257] and others, hysteresis in the electrical properties of CPCs exposed to humidity — evidenced by a permanent change in RR — may be attributed to the formation of clusters of absorbed water in pores in the volume of the polymer matrix or at the filler-polymer interface.

The time required to reach a steady state RR value after a controlled changed of RH inside the humidity chamber was estimated. The time required for the RR to increase and reach steady state following an increase in RH from 35% to 95% is referred to as response time, whereas the time is required for the RR to decrease and reach steady state following a decrease in RH from 95% to 35% is referred to as recovery time. These parameters were calculated by taking the time derivative of RR, ${}^{dRR(t)}/_{dt}$, and measuring the time taken from the control change in RH inside the humidity chamber to the time at which this derivative decreased to less than 0.05. The results are shown in Figure 3-9a-b and Figure 3-9c-d for both the spin-coated films and printed lines, and, as for other parameters, the time of response of the CPC samples was affected by the matrix composition. For instance, the average response time of the PEGDA-100/HEMA-0/Ag spin-coated film samples was 226 sec ± 8 sec (n = 10), while that of the PEGDA-25/HEMA-75/Ag was 325 sec ± 5 sec (n = 10). The film samples with the highest response (highest overall change in RR) were also the samples with the fastest response time; this behavior can likely be attributed for the high affinity of water to these materials (samples with this composition were also the most hydrophilic). These samples also exhibited the longest recovery times, indicating that more time was required to remove the water from the network once the relative humidity dropped; this also results from the comparatively high hydrophilicity of the samples. This is likely due to the hygroscopic properties of the samples: once water was absorbed into the more hydrophilic samples (containing the highest proportion of PEGDA) the high affinity of the water for the network

resulted in the longest time to remove the water from the network once the RH dropped. Conversely, as the proportion of PEGDA decreases in the samples (and the proportion of HEMA therefore increases), the overall response (RR at 95% RH) decreases, the response times become longer, and recovery times become faster; this results from the decreasing hydrophobicity of the samples.

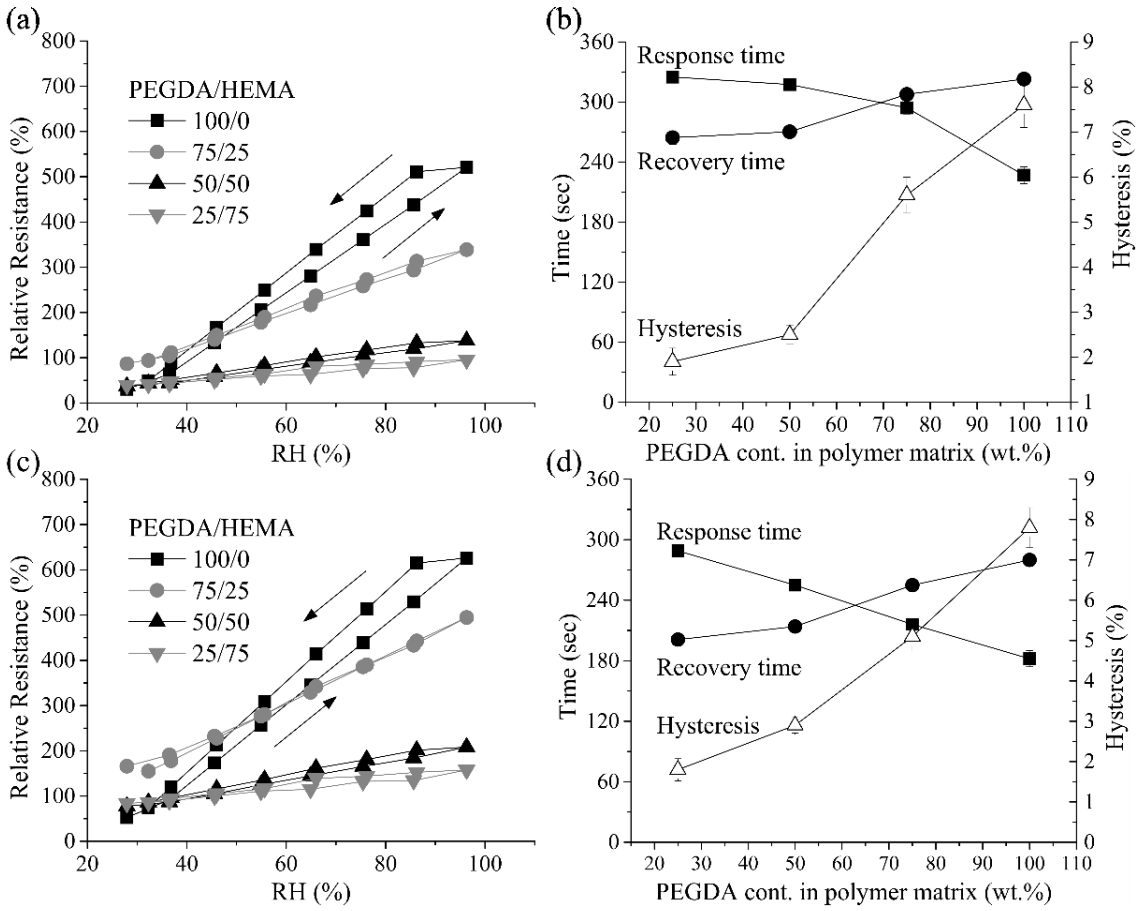

Figure 3-9: Hysteresis loop (a and c), hysteresis values, and response and recovery times (b and d) of a-b) spin-coated CPC films and c-d) printed CPC lines with different matrix compositions.

In general, both the response and recovery time were shorter for the printed lines than for the films. For instance, while the PEGDA-50/HEMA-50/Ag and PEGDA-75/HEMA-25/Ag spin-coated film samples required 294 sec ± 6 sec (n = 10) and 317 sec ± 6 sec (n = 10) of response time, the printed samples for equal compositions required only 255 sec ± 5 sec (n = 10) and 216 sec ± 5 sec (n = 10) respectively. This represents an average decrease in response time of 20%. Similarly, the recovery times of the films was found to be longer than those of lines of the sample

material: the recovery time of PEGDA-50/HEMA-50/Ag and PEGDA-75/HEMA-25/Ag spin-coated films was 307 sec ± 6 sec (n = 10) and 270 sec ± 6 sec, respectively, whereas the recovery times of the printed lines of the same materials were only 255 sec ± 6 sec (n = 10) and 214 sec ± 6 sec (n = 10), respectively. These findings provide additional evidence that the geometry of the sensing elements, particularly the cross-sectional area, affects the sensing properties. The material comprising patterned lines is generally more accessible to water vapor than the material comprising a thin film, as the vapor can diffuse inward from more than one direction (i.e. from both the sides and top rather than simply from the top). These modified boundary conditions result in a higher response. Similar effects in resistive sensors were observed by Ahmadipour *et al.* [258], who examined the effect of the thickness of resistive sensors, based on calcium copper titanate (CCTO) films on the response and recovery times for humidity change from 30% to 90% RH. An increase in thickness — and therefore in volume of the sample — from 200 nm to 600 nm, led to the increase in response time from 12 seconds to 35 seconds, and an increase in recovery time from 500 sec to 650 sec. In the case of response and recovery times, lower volume of printed lines leads the sensing elements to reach equilibrium more quickly. Through variation of the thickness, it may be possible to tune and balance the response time and thickness of the line-like sensing elements [258, 259].

In establishing a comparison between the current work and other CPC-based resistive humidity sensors, Table 3-7 summarizes sensing properties, such as relative sensitivity, and response/recovery time, of this work with other recently demonstrated materials. While some other CPCs materials were found to have a higher absolute change in resistance when exposed to high levels of relative humidity, the initial or base-line resistance of these materials is significantly larger (≥1000 Ω) than the CPC films and printed lines presented in this work. For instance, Tripathy *et al.* [208] presented a polydimethylsiloxane (PDMS)-Armalcolite nanocomposite as humidity sensor with a sensitivity of 8×10^5 Ω/%RH and an initial resistance of 8×10^7 Ω. This large resistance requires the use of electronics that can resolve resistances that vary over orders of magnitude. On the other hand, if the *relative* change in resistance is considered, the CPCs presented in this work is higher than others, with an approximately 10%/%RH, which is higher than that of the (Tetraethylammonium 2-acrylamido-2-methyl-1-propanesulfonate) -co- 1-Vinyl-2-pyrrolidinone/Ag (TEAMPS-co-VP/Ag) composite presented by Park *et al.* [210], and the poly(acrylic acid)-multiwall carbon nanotubes (PAA-MWCNTs) composite by Lee *et al.* [173].

Despite their low resistance and high sensitivity, the response time of the HEMA-PEGDA-Ag composites presented here was comparable or longer than other composites; the fastest times were shown by Tripathy *et al.* [260], Xu *et al.* [206] (utilizing Polyvinyl alcohol nano-fibrillated cellulose graphene oxide (PVA-NFC-rGO) composites), and Peng *et al.* [209] (utilizing Kappa-carrageenan-carbon nanotube (KC-CNT) composites).

Table 3-7: Comparison of resistive humidity sensors based on conductive polymer composites (CPC).

Material	R0 (Ω)	Abs. Sensitivity (Ω/RH)	Rel. Sensitivity (%/RH)	Response (sec)	Recovery (sec)	Ref.
HEMA-PEGDA-Ag Films	3.8	0.31	8.06	227	323	Current
HEMA-PEGDA-Ag Lines	45	4.24	9.43	182	280	Current
PAA-MWCNTs	100	6.85	6.85	670	380	[173]
TEAMPS-co-VP/Ag	8.1×105	1.2×104	-1.53	180	195	[210]
PVA-NFC-rGO	3.7×106	1.3×105	-3.47	120	120	[206]
KC-CNTs	2.6×105	3.1×103	-1.19	100	130	[209]
PDMS-Armalcolite	8×107	8.3×105	-1.04	10	15	[260]

3.4 Conclusions

In this study, the feasibility of using Ag-HEMA-PEGDA/Ag for the fabrication of elements for humidity sensing was investigated. These materials exhibited low electrical resistivity and high response to changes in RH when compared with similar CPCs from the literature [173, 209, 210], although the response times of the materials was relatively high.

The composites explored in this thesis were simple to prepare and could easily be patterned on arbitrary samples by dispensing them through a pressurized syringe onto a moving stage. Due to their low overall resistance, the CPCs investigated in this study may be useful for integration into low-power and portable devices. For example, inexpensive sensors could be fabricated to monitor storage conditions of food and other humidity-sensitive consumer products as they travel through the supply chain. Such sensors would consist of the printed responsive material, and an external power supply and a current meter r ohmmeter. To ensure their utility, future work should focus on determining the selectivity of these sensors with respect to stimuli such as temperature

and pressure. While this study focused on polymer matrices which swelled in response to water, in future work the composition of the matrix could be tailored to enable sensing of other materials.

4. Amine Responsive Poly(lactic acid) (PLA) and Succinic Anhydride (SAh) Graft-Polymer: Synthesis and Characterization[2]

ABSTRACT: Amines are known to react with succinic anhydride (SAh), which in reactions near room temperature, undergoes a ring opening amidation reaction to form succinamic acid (succinic acid-amine). In this work, we propose to form an amine-responsive polymer by grafting SAh to a poly(lactic acid) (PLA) backbone, such that the PLA can provide chemical and mechanical stability for the functional SAh during the amidation reaction. Grafting is performed in a toluene solution at mass content from 10 wt% to 75 wt% maleic anhydride (MAh) (with respect to PLA and initiator), and films are then cast. The molecular weight and thermal properties of the various grafted polymers are measured by gel permeation chromatography and differential scanning calorimetry, and the chemical modification of these materials is examined using infrared spectroscopy. The efficiency of the grafting reaction is estimated with thermogravimetric analysis. The degree of grafting is determined to range from 5% to 42%; this high degree of grafting is desirable to engineer an amine-responsive material. The response of the graft-polymers to amines is characterized using X-ray photoelectron spectroscopy, infrared spectroscopy, and differential scanning calorimetry. Changes in the chemical and thermal properties of the graft-polymers are observed after exposure to the vapors from a 400 ppm methylamine solution. In contrast to these changes, control samples of neat PLA do not undergo comparable changes in properties upon exposure to methylamine vapor. In addition, the PLA-g-SAh do not undergo changes in structure

[2] A version of this chapter has been published as Adrián Lopera-Valle, Anastasia Elias, "*Amine Responsive Poly(lactic acid) (PLA) and Succinic Anhydride (SAh) Graft-Polymer: Synthesis and Characterization*", Polymers, Volume 11, Issue 9, No. 1466, doi: 10.3390/polym11091466. Refer to the preface of this thesis for more information.

when exposed to vapors from deionized water without amines. This work presents potential opportunities for the development of real-time amine sensors.

4.1 Introduction

Sensors based on smart materials, which undergo visible and gradual changes in color in response to a stimulus of interest, can be used effectively to monitor both storage conditions and analytes indicative of food safety. For example, time-temperature indicators – which undergo gradual changes in color at a temperature-dependent rate –can reliably track the refrigeration history of goods, which is vital for food preservation [72]. While storage conditions such as temperature, humidity, and oxygen are indirect indicators of freshness, it is also desirable to monitor direct analytes such as chemicals released during food ripening (e.g. ethylene oxide [6]). In the case of meat and fish products, biogenic amines including ammonia, putrescine, dimethylamine, putrescine, dopamine, histamine and methylamine are known markers of spoilage [23–26]. The concentration of amines present in an enclosed fish package, for instance, has been shown to increase from 130 ppm to 350 ppm at 4°C with time as food decreases freshness [4,7]; gaseous and liquid amines potentially represent direct indicators of food freshness and safety.

The concentration of amines in solution, gas, or vapour phase can be measured by high performance liquid chromatography [8,9], electrochemical sensors [10,11], electrical-based sensors [266], and optical detection methods [3,13]. Most of these methods require lab-scale analytic equipment and trained personnel. However, smart materials, that undergoes a specific and sensitive reaction to a stimuli, can be used for the detection of amines. For instance, Jin *et al.* proposed the use of nitrated polythiophene (NPTh) for the detection of a wide range of biogenic amines (BAs). In this system, the BAs easily diffuse into the polymer film and forms charge transfer complexes with NPTh, leading to a change in in color of the film, [29]. A key component of this system is a material that reacts selectively with amines.

Amine-selective reactants that have been incorporated into electrically-responsive smart materials are anhydrides such as maleic anhydride (MAh) and succinic anhydride (SAh). As reported previously, in the first step of the reaction between the amine and MAh or SAh, the lone electron pair of the amine conducts a nucleophilic attack on the C=O π bond of the anhydride to

form a tetrahedral intermediate, while the second carbonyl becomes part of the leaving group on the other side of the anhydride ring [268–275]. This is followed by the removal of a proton from the leaving group by the amine and the donation of an electron from the carboxylate group back to the C=O π bond, which is much less electrophilic than in an acid anhydride [268–273]. While the reaction between MAh or SAh and amines has been used as initial step for classical approaches to the synthesis of maleimide and succinimide, this process requires the dehydration of the intermediate acid, usually promoted by acids and temperature [21,23,24]. At room temperature, the most likely pathway is that the ring-opening reaction converts the anhydride into the corresponding dicarboxylic acid monoamide, maleamic acid or succinamic acid for MAh and SAh, respectively [15,17,21]. As reviewed by Sun *et al.* [278], polymers that undergo molecular structural changes - in this case the ring opening of SAh upon contact with methylamine - have high potential as stimuli responsive materials. Such transitions could potentially be leveraged in smart material-based systems, using a pH indicator dye, as the acidity of the anhydride changes, or using an electrochemical set up to monitor the creation of H+ ions in the anhydride-amine reaction, or changes in the water solubility of the compound, as MAh and SAh are not soluble in water while maleamic and succinamic acids are.

In order to engineer amine-responsive materials based on succinic anhydride, chemically-stable materials compatible with food packaging must be produced. In the literature, a number of thermal processing methods have been demonstrated for grafting SAh onto various polymer chains, including polystyrene [19,25], poly(N-isopropyl acrylamide) (NIPA) [280], and polyethylene glycol [281]. One polymer of interest for use in food-based sensors is polylatic acid (PLA). Polylatic acid (PLA, Figure 4-1a) is a bio-sourced, food compatible, biodegradable, and recyclable thermoplastic with high commercial attention given that, as a biopolymer, it can help mitigate the polymer waste problem, particularly in food packaging [28,29]. One advantage of PLA is that it has functional groups such as –OH, and –CH in its chain, which makes possible to chemically couple it with reactive polymers such as maleic and succinic anhydrides [30,31], oxazoline, and epoxide [31,32]. In addition to reacting with amines (as described above), maleic anhydride (MAh) is one of the most widely used reactive compatibilizers in polymer processing due to its good chemical reactivity, low toxicity and low potential to form dimers, trimers, and polymers under free radical grafting conditions [287]. While the in-situ melt graft-polymerization of PLA and MAh, to form PLA-g-SAh, by means of free radical polymerization has been studies

and reported in the past by Hwang *et al.* [285], Detyothin *et al.* [288, 289], Ma *et al.* [290], Du *et al.* [291], Csikós *et al.* [292], Birnin-Yauri *et al.* [293], and others, these methods typically utilized melt-based processes and achieved only very low grafting degree (below 3%). To maximize the response of the materials, a large grafting degree is desired.

In this work, we develop a solution-based method for the synthesis of responsive polymers with SAh in their structure, and characterize the response of these materials to a fish degradation biogenic amine: methylamine. Firstly, MAh is grafted with poly(lactic acid), to form PLA-g-SAh, Figure 4-1. In this system, the PLA acts as a backbone/scaffold for the responsive component of material (i.e. the succinic anhydride) (Figure 4-1a). The method proposed in this work aims to achieve a high grafting rate of SAh to PLA chains. We then study the effect of initial MAh content in the graft-polymer on the physical properties, including molecular weight, polydispersity index, thermal stability, and thermal properties. In order to monitor and prove the responsive behavior of SAh in the graft-polymers, samples are exposed to the vapours from a 400 ppm methylamine solution in water under room conditions (Figure 4-1b). Following exposure to amines, FTIR and XPS are used to confirm and characterize the reaction between amines and SAh. In addition, the thermal properties of the polymer were compared with those of the films prior amine exposure.

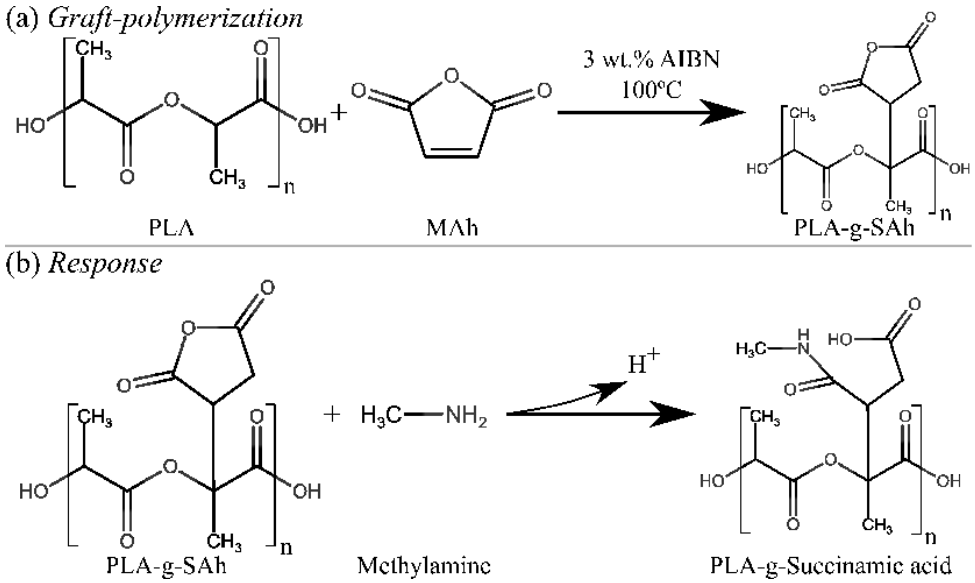

Figure 4-1: Proposed free radical graft-polymerization reaction between PLA and MAh, and reaction between PLA-g-SAh and methylamine to form PLA-g-Succinamic acid.

4.2 Experimental Methods

4.2.1 Polymer Synthesis and Sample Preparation

Poly(lactic acid) (PLA, 4042D, NatureWorks LCC, Minnetonka, MN, USA) pellets (comprised of 92% L-lactide and 8% D-lactide units) were dried in an oven at 70°C for at least 8 hours in order to remove absorbed water from the environment. Following drying, a 40 mg/ml PLA solution in toluene (No. 244511, Sigma-Aldrich, St. Louis, MO, USA) was prepared in an air-cooled reflux setup at 100°C for 1.5 hours. The graft-polymers were synthetized by adding maleic anhydrite (MAh, No. 63200, Sigma-Aldrich, St. Louis, MO, USA) and 3 wt% Azobisisobutyronitrile (AIBN, No. 441090, Sigma-Aldrich, St. Louis, MO, USA), as free radical initiator (Figure 4-1). The PLA-MAh solution was kept at 100°C for one hour in order to guarantee the complete decomposition of the free radical initiator. Table 4-1 lists the composition of the blends of PLA and MAh used in this study.

Table 4-1: Sample composition

Sample Name	PLA *wt%*	MAh *wt%*	AIBN *wt%*
Neat PLA	100	0	0
PLA-g-SAh10	87	10	3
PLA-g-SAh25	72	25	3
PLA-g-SAh50	47	50	3
PLA-g-SAh75	22	75	3

Once the polymer solution was prepared and brought to 50°C, approximately 3 ml was poured onto a pre-heated microscope glass slides (No. 12-550-A3, Fisher brand, Pittsburgh, PA, USA), 25.4 mm × 76.2 mm, and 1 mm of thickness, and maintained at 50°C until the complete evaporation of the solvent was achieved. The films casted by these means were used for characterization purposes following the methods described below.

4.2.2 GPC

Molecular weight and molecular weight distribution of PLA-g-SAh were evaluated using gel permeation chromatography (GPC). The GPC instrument was equipped with a mixed bed

column (T6000M, 300 × 8 mm, 10 μm, Malvern Panalytical, Malvern, UK), a dual detector (Viscotek GPC 270 Max, Malvern Panalytical, Malvern, UK), a refractive index detector (Viscotek VE 3580, Malvern Panalytical, Malvern, UK). The molecular weight of the samples was obtained from calibration curves using 99 kDa polystyrene and 235 kDa polystyrene for verification. Tetrahydrofuran (THF) was used as eluent at a constant flow of 0.5 mL/min. The PLA-g-SAh samples were dissolved using tetrahydrofuran (THF, sample concentration of 3 mg/mL), and filtered before injection using a 0.2 μm filter.

4.2.3 Fourier Transform Infrared Spectroscopy (FTIR)

The FTIR spectra of the polymer samples were recorded using a Fourier Transform Infrared Spectrometer (Agilent Cary 600 Series FTIR Spectrometer, Agilent Technologies Inc., Santa Clara, CA, USA) instrument equipped with a universal attenuated total reflectance (UATR) accessory. The spectra were recorded between 4000 cm^{-1} and 400 cm^{-1}, and between 3200 cm^{-1} and 2700 cm^{-1} frequency ranges.

4.2.4 Thermal Characterization

Thermal analysis was performed using a differential scanning calorimeter (DSC Model 1, Mettler Toledo, Columbus, OH, USA), under a nitrogen flow of 20 mLmin-1. Typical sample mass was 15 mg. Analysis was performed in open Al pans. Samples were initially equilibrated at -10°C for 5 minutes, heated from -10°C to 210°C at 10 °C/min, held at a temperature of 210°C for 5 minutes, and then cooled from 210°C to -10°C, at a cooling rate of 10 °C min^{-1}. From the DSC heating scans, glass transition temperature (Tg), melting temperature (Tm), and enthalpy of fusion (ΔHm) were determined.

The thermal stability of the graft-polymers was studied by using a thermogravimetric analyzer (TGA/DSC Model 1, Mettler Toledo, Columbus, OH, USA), equipped with an ultra-micro balance cell and differential thermal analysis (DTA) sensors, set at a heating rate of 10 °C/min under 20 mL/min nitrogen atmosphere, and a heating cycle from 25°C to 380°C. The thermal stability of the polymer films was defined as the onset temperature of the thermal degradation process (Td) in TGA, extracted from the Mettler Toledo STARe thermal analysis software (Mettler Toledo, Columbus, OH, USA), by taking the intercept between lines drawn

tangent to the flat portion of the curve where the weight changes very little and the steep portion of the curve once the mass begins to drop.

To enable the estimation of the degree of grafting, additional reference samples were prepared and analyzed using the same TGA method. These include: neat PLA, neat MAh, PLA-MAh50 (a 50/50 blend of PLA and MAh dissolved in toluene and cast without initiator) and PLA-AIBN3 (PLA dissolved in toluene with 3 wt% AIBN and cast).

4.2.5 Hydrogen Nuclear Magnetic Resonance (^{1}H-NMR)

Hydrogen Nuclear Magnetic Resonance (^{1}H-NMR) spectra were obtained in a Nanalysis 60 MHz NMReady-60 spectrometer (Nanalysis Corp., Calgary, AB, Canada). The equipment was pre-calibrated with deuterated toluene (No. 434388, Sigma-Aldrich, St. Louis, MO, USA). For the measurement, 10 mg of the polymer sample were dissolved in 1 mL deuterated toluene and placed in NMR tubes. Data was collected from 0 to 12 ppm with 512 scans per sample and 4096 points were recorded per scan. An analysis of the ratios of the peaks associated with MAh, PLA, and SAh was used to estimate the degree of grafting.

4.2.6 Amine Response

The response of the PLA-g-SAh graft-polymer was studied by exposing the polymer films (2.5 cm × 7.6 cm) to the vapours from a 400 ppm methylamine (No. 426466, Sigma-Aldrich, St. Louis, MO, USA) solution in water contained in a closed cylindrical glass container (25 cm diameter × 8 cm tall) containing 300 mL of amine solution at 20°C for 8 hours. The samples were then placed on a stainless steel platform inside the glass container such that they were suspended about 20 mm above the level of the amine solution. The reaction between the SAh-grafted polymer and methylamine, shown in Figure 4-1, was characterized by using FTIR techniques as per described in section *4.2.3 Fourier Transform Infrared Spectroscopy (FTIR)* with scanning range from 1300 cm^{-1} and 980 cm^{-1}. In addition, X-ray photoelectron spectroscopy (XPS) survey scans were performed using an X-ray photoelectron spectrometer (Kratos AXIS 165, Kratos Analytical Ltd, Manchester, U.K.) equipped with dual magnesium (Mg, Kα radiation hv = 1253.6 eV) and aluminium (Al, Kα radiation hv = 1486.6 eV Al), and monochromatic Al X-ray sources. XPS was performed in order to quantify the content of methylamine on the surface of the PLA-g-SAh

samples after exposure to amines, as well as to collect further evidence of the reaction between them and SAh. The XPS scans were analyzed using an XPS processing software (CASAXPS 2.3.19PR1.0, Casa Software Ltd, Teignmouth, U.K.). Finally, the changes in thermal properties of the PLA-g-SAh after exposure to methylamine were measured using DSC as described in section *4.2.4 Thermal Characterization*. In addition, a set of specimens was then exposed to water vapor (without methylamine) in order to check for selectivity of the polymer response.

4.2.7 Statistical Analysis

To test for statistically significant differences within groups of data, an analysis of variance, ANOVA with Fisher LSD post-hoc test, was performed (using STATISTICA for Academia, StatSoft Inc., Tulsa, OK, USA) , and *P*-values < 0.05 were considered statistically significant. To compare differences in properties within a certain sample type before and after exposure to amines, t-test analysis was performed using commercial software (STATISTICA for Academia, StatSoft Inc., Tulsa, OK, USA). *P*-values < 0.05 were considered statistically significant.

4.3 Results and Discussion

4.3.1 Molecular Weight

The molecular weight and polydispersity of both neat PLA and of the PLA-g-SAh samples with compositions described in Table 4-1 were measured by means of GPC. The results are summarized in **Error! Reference source not found.**. The average molecular weight (M_w) of the eat PLA was found to be 159 kDa ± 8 kDa, and the number average molecular weight (M_n) and polydispersity index (PDI) were found to be 122 ± 9 kDa and 1.3 ± 0.03, respectively. For each sample, the M_W, Mn, and PDI was found to be statistically significantly different with respect to neat PLA. Initially, we expected to observe an increase in M_W after grafting corresponding to the amount of SAh grafted onto the PLA. However, for the PLA reacted with 10 wt% (PLA-g-SAh10 samples) and 25 wt% initial MAh (PLA-g-SAh25 samples), the molecular weight of each decreased significantly to 131 kDa (corresponding to an 18% decrease). Composition with initial concentrations of initial MAh of 50 wt% (PLA-g-SAh50) exhibited a slightly lower M_w than neat PLA (141 kDa ± 2 kDa). The samples reacted with 75 wt% MAh (PLA-g-SAh75 samples) exhibited the highest Mw of all: 279 kDa ± 19 kDa. While the graft-polymerization, as a process

of chain addition, was expected to increase the M_w, it was found to have an opposite effect for initial MAh concentrations equal to or less than 50 wt%. As argued in previous studies, this decrease in M_w can be due to chain scission of the polymer chains caused by the free radicals in the polymer solution. This chain scission occurs when AIBN radicals undergo side reactions with ester groups in PLA that cause the sectioning of PLA chains [34,36,37]. For instance, Detyothin *et al.* [288] reported a significant decrease in the molecular weight of PLA, from about 70 kDa to 15 kDa after it was melt copolymerized with 7 wt% MAh by means of free radical polymerization with 2,5-bis(tert-butylperoxy)22,5-dime-thylhexane (Luperox 101) [288]. While this phenomenon is likely to occur at all initial concentrations of MAh, the overall values – which generally increase with MAh content – likely reflect a combination of chain scission (which decreases M_w) and grafting (which increases M_w).

Table 4-2: Summary of GPC results (n = 3).

Sample Name	M_n *kDa*	M_w *kDa*	PDI M_w/M_n
Neat PLA	122 ± 9	159 ± 8	1.3 ± 0.03
PLA-g-SAh10	80 ± 4	131 ± 4	1.6 ± 0.09
PLA-g-SAh25	81 ± 6	131 ± 2	1.6 ± 0.09
PLA-g-SAh50	85 ± 1	141 ± 2	1.7 ± 0.03
PLA-g-SAh75	102 ± 2	271 ± 19	2.7 ± 0.12

Similarly, the PDI constantly increased from 1.3 ± 0.03 for neat PLA to 2.7 ± 0.12 for PLA-g-SAh75. The source for this variation can be due to both to grafting reactions and undesirable chain scission reactions. However, the GPC results may be slightly skewed by the fact that our analysis assumed that the chains were relatively linear after grafting. If branching occurred, the measured results could be expected to under-report the molecular weight given that the branching of SAh in PLA increases the molecular weight and density of polymer chains while decreasing their radius of gyration. This would then lead to the report of lower molecular weights as GPC is based on the size of polymer chains [294]. Studies of viscosity may be able to confirm the effect of branching on the molecular weight and PDI of the grafted polymer.

4.3.2 Polymer Structure

The product of the polymer grafting reaction between PLA and SAh was analyzed using ATR-FTIR. Figure 4-2a shows the FTIR curves for solvent cast films of neat PLA, neat MAh (powder form, as received by the provider), and PLA-g-SAh50 samples. Figure 4-2b depicts the ATR-FTIR spectra from 3200 cm^{-1} to 2700 cm^{-1} of all grafted polymers, including neat PLA and neat MAh. Neat PLA showed characteristic ATR-FTIR peaks at 1751 cm^{-1}, 1182 cm^{-1}, 1126 cm^{-1}, 1081 cm^{-1}-1035 cm^{-1}, and 872 cm^{-1}-954 cm^{-1}, corresponding to C=O stretching, C–O–C asymmetric stretching, C–OH side group vibrations, –CH stretching, and C–C vibrations, respectively [295, 296]. In the ATR-FTIR spectra of neat MAh and PLA-g-SAh50, the peaks at 3120 cm^{-1} (also displayed in Figure 4-2b) and 1781 cm^{-1} correspond to the C=O asymmetric stretching, and at 1859 cm^{-1} and 1746 cm^{-1} correspond to the C=O symmetric stretching of cyclic anhydride [281, 297–300]. The presence of these asymmetric and symmetric C=O stretching bands suggest the presence of SAh in the PLA-g-SAh50 and other grafted polymer films. Similar to this work, Detyothin *et al.* monitored these symmetric and asymmetric stretches of the C=O bonds – part of the cyclic anhydride ring – to show that SAh molecules were grafted onto PLA back bone using free radical melt grafting [289]. In addition, the grafting of SAh to PLA, by the bond cleavage of the C=C bond to C-C in MAh, to form SAh, and the formation of a free radicals in the C-H group of PLA, could be monitored by analysing the C=C (830 cm^{-1} and 694 cm^{-1}) and C-H (2850 cm^{-1}) bond stretches [297, 300]. In Figure 4-2a, the drop in the C=C bending bond peaks at 830 cm^{-1} and 694 cm^{-1}, Figure 4-2a, from neat MAh to PLA-g-SAh50 specimens suggest the process of bond cleavage of the C=C bond in MAh to C-C in SAh upon the presence of free radical from the C-H bond or from the AIBN free radical initiator. In addition, in Figure 4-2b, the decrease in the peaks in the proximity of the 2850 cm^{-1} band — corresponding to sp^3 C-H stretch — may suggest the formation of a free radicals in the C-H group of PLA [301, 302]. Similar to previous reports, the use of ATR-FTIR to monitor relevant bonds involved in the grafting of SAh into PLA can provide some evidence of these reaction [281, 297–300].

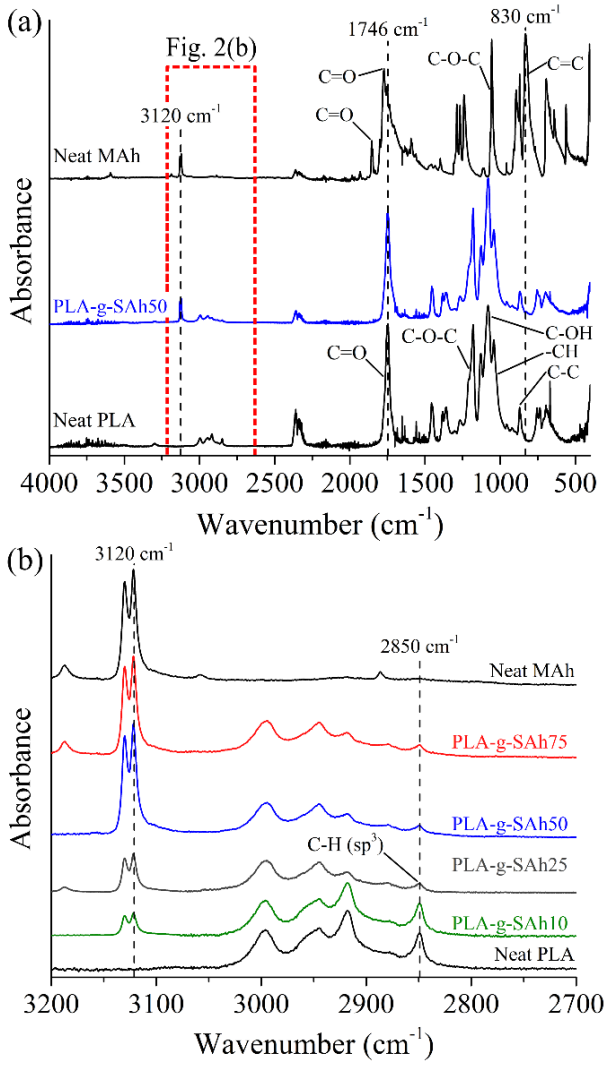

Figure 4-2: ATR-FTIR curves between (a) 4000 cm^{-1} and 400 cm^{-1}, and (b) from 3200 cm^{-1} to 2700 cm^{-1} of neat PLA, neat MAh, PLA-g-SAh50, and other graft polymer samples.

4.3.3 Thermal Properties and Degree of Grafting

The thermal properties and thermal stability of the PLA-g-SAh were evaluated by means of DSC and TGA. Table 4-3: Thermal properties from DSC of neat PLA and PLA-g-SAh (n = 3, P < 0.01). summarizes the glass transition temperature, T_g, melting temperature, T_m, and specific heat of fusion, ΔH_m, of the neat PLA and PLA-g-SAh samples. In addition, the DSC curves are presented in Figure 4-3, where vertical lines labeled as $T_{g,\,PLA}$ and $T_{m,\,PLA}$ mark the glass transition temperature and the peak of the endothermic melting process of neat PLA. In general, the ΔH_m, T_g, and T_m were found to decrease with the increase of initial MAh content. For instance, the T_g,

T_m, and ΔH_m decreased from to 31°C ± 2°C, 140°C ± 3°C, and 29.8 J/g ± 0.5 J/g for neat PLA to 28°C ± 1°C (*P = 0.04)*, 116°C ± 2°C (*P* = 0.05), and 19.2 J/g ± 0.7 J/g (*P* = 0.001) for the PLA-g-SAh50 samples, respectively. As seen in Figure 4-3, the decrease in the thermal properties was more significant for PLA-SAh grafts with higher initial MAh content. The decrease in the polymer Mw and increase in PDI (section *4.3.1 Molecular Weight*) provided evidence of chain branching and chain scission during the polymer grafting reaction between PLA and SAh. This branching and scission could be responsible of the reduction of T_g. In addition, the increase in the PDI may lead to the formation of irregular structures and amorphous regions in the polymer, further decreasing the temperature and energy required for the melting of the graft-polymer, *i.e.* T_m, and ΔH_m [284, 285, 288, 290, 303]. The results presented in this work align with what has been reported by others [285, 290]. For instance, Ma *et al.* [290] investigated the effects of different concentrations of MAh in a poly(lactic acid) (PLA)-g-maleic anhydride (MA)-co-styrene (St) copolymer that was synthetized by free radical polymerization using dicumyl peroxide (DCP) as an initiator. In their work, they reported that after copolymerization the melting point of neat PLA went from 179°C to 176°C for a 4.5 wt% MAh and 0.5 wt% DCP set of samples [290]. As suggested by the results in this work, and as reported by Ma *et al.* [290], the free radical polymerization between PLA and MAh lead to a decrease of T_g, T_m, and ΔH_m of PLA.

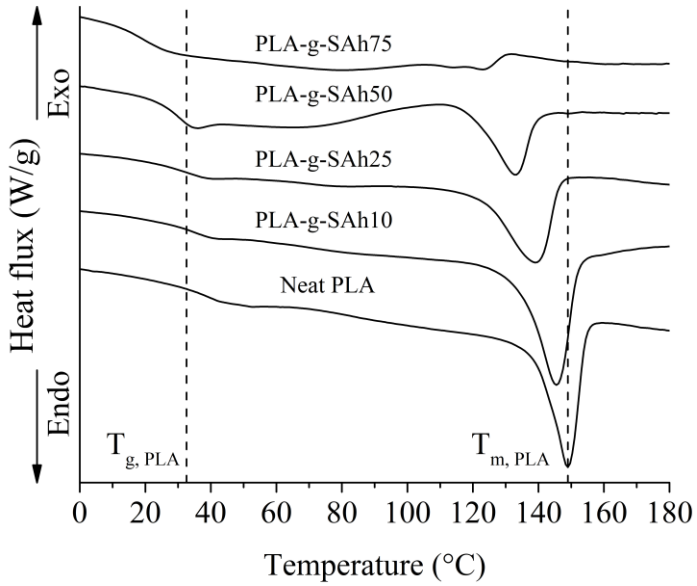

Figure 4-3: DSC curves of neat PLA and PLA-g-SAh with different initial contents of MAh. Vertical lines labeled as T_g and T_m mark the glass transition and melting peak temperatures of neat PLA.

Table 4-3: Thermal properties from DSC of neat PLA and PLA-g-SAh ($n = 3$, $P < 0.01$).

Sample Name	T_g (°C)	T_m (°C)	ΔH_m (J/g)
Neat PLA	31 ± 2	140 ± 3	29.8 ± 0.5
PLA-g-SAh10	32 ± 1	133 ± 2	21.8 ± 0.4
PLA-g-SAh25	30 ± 2	121 ± 3	20.6 ± 0.6
PLA-g-SAh50	28 ± 1	116 ± 2	19.2 ± 0.7
PLA-g-SAh75	21 ± 2	108 ± 3	2 ± 0.8
MAh	-	53	138

The thermal stability of the graft-polymer was characterized using TGA technique, and defined as the onset temperature during volatilization of the specimens. Figure 4-4 shows representative curves of sample weight against temperature (Figure 4-4a), and summarizes the thermal stability properties of all compositions (Figure 4-4b). Neat PLA was found to be thermally stable at temperatures as high as 352°C (T_d). In contrast, the degradation temperature, T_d, of neat MAh samples was found to be 120°C. The TGA results show that the thermal stability of the graft-polymers decreased with the addition of initial MAh into the polymer solution. This degradation process was found to take place in two stages. An initial reduction of mass was found at temperatures between that of the degradation of neat MAh (120°C) and that of neat PLA (352°C). This is likely due to neat (unreacted) MAh molecules that became volatile at a lower temperature than neat PLA and PLA-g-SAh. Upon further heating, the degradation of neat PLA and PLA-g-SAh occurred. Given that this stage is more representative of the actual thermal stability of the grafted polymer, Figure 4-4b, summarizes the onset temperature at which this second process starts. As it has been reported previously, the thermal degradation of neat PLA is associated with hydrolysis of ester groups and accelerated by the end groups (–COOH) [303, 304]. While PLA-g-SAh graft-polymers, can be expected to share the degradation mechanism of neat PLA[303], the onset of thermal degradation at lower temperatures for samples with MAh of 75 wt% may additionally be attributed in part to a wider distribution of the chain size, as evidenced by the higher PDI values for these materials (section *4.3.1 Molecular Weight*). In addition, Figure 4-4b shows the degradation temperature of the PLA-MAh50 and PLA-3AIBN specimens descried above (section *4.2.4 Thermal Characterization*). No significant difference between neat PLA and PLA-

3AIBN was found, suggesting that the processing method alone does not lead to the degradation of PLA. The degradation of PLA-MAh is discussed in more detail below.

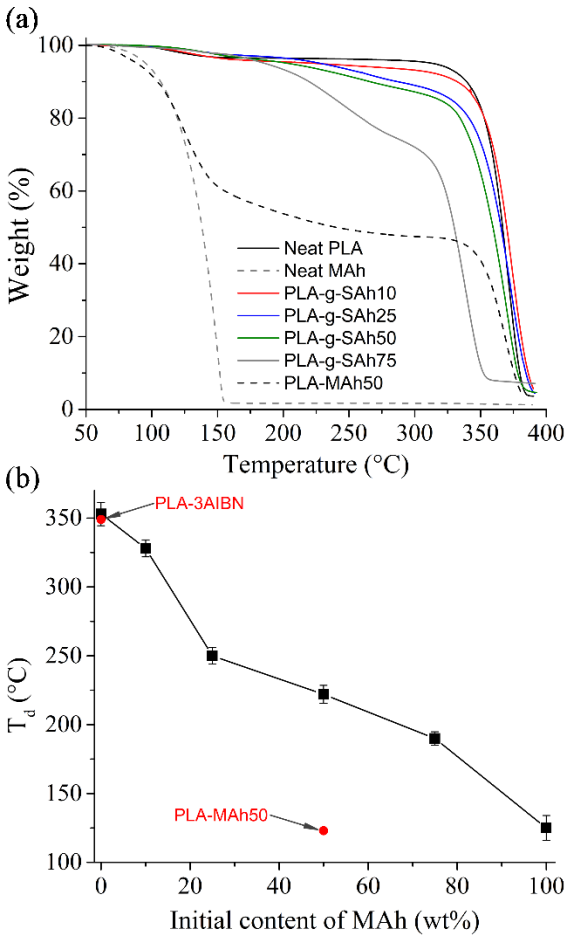

Figure 4-4: TGA (a) curves of neat PLA, neat MAh, a film comprised of a 50/50 blend of PLA and MAh without initiator (PLA-MAh50), and grafted polymers (n = 3), and (b) degradation temperature of PLA-g-SAh with different initial contents of MAh. Reference samples (PLA with initiator without MAh and PLA-MAh50) are denoted in red.

While the graft-polymerization of PLA and MAh by means of free radical polymerization has been reported by Hwang *et al.* [285], Detyothin *et al.* [288, 289], Ma *et al.* [290], Du *et al.* [291], Csikós *et al.* [292], Birnin-Yauri *et al.* [293], and others, the vast majority of these works use melt-based methods for the blending of polymers and creation of free radicals required for the formation of PLA-g-SAh. Given that these melt-based techniques are done at temperatures from 160°C to 190°C, it is likely that they lead to the partial or complete degradation of MAh. While these high temperatures are required for the melting and blend of PLA, they are higher than the

degradation temperature of MAh, here reported to be 120°C. In contrast in our work we report a procedure for the grafting of PLA and SAh that is based in a solution method that is executed at a temperature of 100°C, which is well below the degradation temperature of MAh.

The degree of grafting of SAh in the PLA polymer chains was estimated based on the results of the TGA, and makes use of the fact that – as shown in Figure 4-4a – the T_d of neat MAh (120°C) is much lower than that of neat PLA (352°C). For each sample, the drop in mass during heating from room temperature to T_d of the grafted polymer was assumed to correspond to volatilization of unreacted MAh. The mass of grafted SAh was then assumed to be the difference between the initial fraction of MAh added and the fraction of mass volatilized below 120°C. The main assumptions in this analysis are: *i)* All MAh initially added to the solution is incorporated into the cast polymer films; *ii)* All unreacted MAh is evaporated below T_d of the grafted polymer, and *iii)* PLA itself is not degraded below the T_d of the grafted polymer.

The ^{1}H-NMR spectra, Figure 4-5, were used to estimate the degree of grafting on SAh into PLA. The spectra for neat PLA shows the representative signals at 1.2-1.5 and 5.0-5.2 ppm corresponded to -CH_3 and -H respectively. Neat MAh shows a signal at around 7 ppm, corresponding to –H. After grafting, the signal for the succinic anhydride (SAh) group was found in the region of 2-2.2 ppm corresponding to the –CH_2 in the free group in the grafted succinic anhydride [285, 305]. The estimation of the degree of grafting by comparing the area of the peaks associated to MAh and SAh.

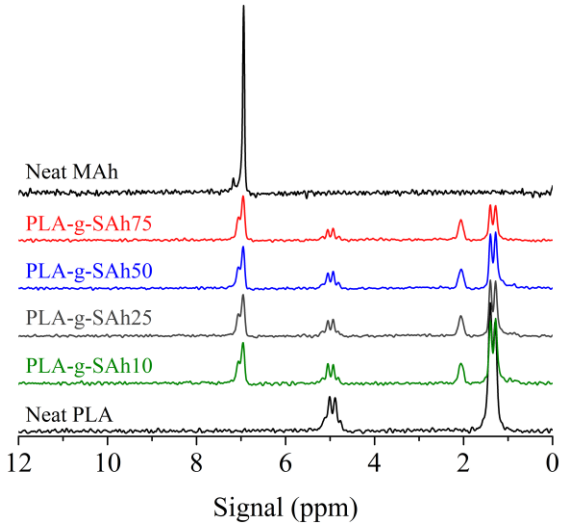

Figure 4-5: ^{1}H-NMR spectra of neat PLA, neat MAh, and other graft polymer samples

All grafted samples undergo higher losses in mass below 352°C than neat PLA: this thermal degradation is attributed to the degradation of unreacted MAh. To evaluate this assumption, samples of 50 wt% MAh (PLA-MAh50) were also characterized with TGA. The thermal degradation process of the PLA-MAh50 composition (solvent blend of PLA and MAh without free radical initiator) occurred in two stages, Figure 4-4a. Initially, there was a rapid drop in 50 wt% at around 120°C, likely to be linked to the thermal degradation of neat MAh. Subsequently, the remaining 50 wt% of the samples degraded near the thermal degradation temperature of PLA. This process differs from the thermal degradation of the PLA-g-SAh50 specimens, where the initial drop of mass was 22 wt% and the remaining 78 wt% degraded at around 225°C. The estimation of the degree of grafting assumes that the initial drop in mass (22 wt%) is linked to the degradation of unreacted MAh and that the remaining 28 wt% from the initial content of MAh (50 wt%) was grafted onto the PLA backbone. Following this rationale, the degree of grafting was estimated to be 28 wt% ± 2 wt% for the PLA-g-SAh50 composition. Figure 4-6 shows the estimated degree of grafting in terms of the initial content of MAh in the solution. In general, the increase in initial concentration of MAh led to a linear increase in the degree of grafting in PLA. The efficiency of grafting, calculated as the ratio between the grafting degree and initial content of MAh, was found to be 56.6% ± 3.6% for all initial contents of MAh. ^{1}H-NMR spectroscopy was used to validate these results. The efficiency was found to be 46.73% ± 1.1%. The results found in both methods, Figure 4-6, suggest an agreement between TGA and ^{1}H-NMR methods, particularly for low initial contents of MAh. Similar results have been reported by Ma *et al.* [290]. In their work, the degree of grafting and grafting efficiency were estimated for different concentrations of MAh in a poly(lactic acid) (PLA)-g-maleic anhydride (MAh)-co-styrene (St) copolymer, synthetized by free radical polymerization through extrusion process and using dicumyl peroxide (DCP) as an initiator. In their work, the relation between initial MAh and grafted SAh was found to be linear, i.e. the increase in initial content of SAh led to a linear increase in grafted SAh, similar to that one displayed in Figure 4-6. Moreover, their work reported a grafting efficiently of about 25%. The higher grafting efficiency found in the current work could be related to the extended time of reaction used (1 hour), and lower processing temperature, which, as discussed above, may reduce the degradation of MAh during the grafting process. This finding suggest that the methods presented in this work have potential to provide higher grafting degree than those by melt-mixing methods. This may be particular beneficial in applications where high grafting degree of SAh is

needed, in particular those where SAh works as compatibilizer in polymer blends [288, 289] and composites [303], or as responsive element [191].

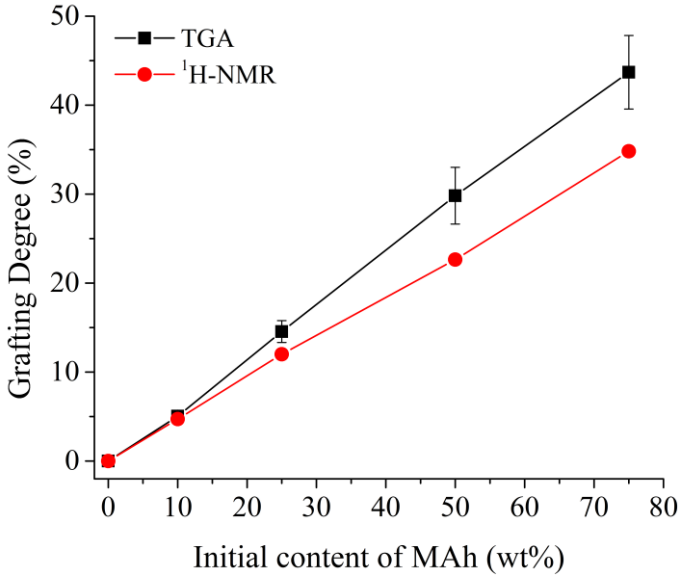

Figure 4-6: Grafting degree of grafting by TGA (n =3) and ^{1}H-NMR of succinic anhydride on PLA as function of the initial content of maleic anhydride concentration in solution.

4.3.4 Amine Response: Polymer Structure

The reaction between SAh in the PLA-g-SAh and methylamine was characterized by using ATR-FTIR. The comparison of FTIR spectra between 1400 cm^{-1} and 980 cm^{-1} of PLA-g-SAh50 samples before and after methylamine exposure is presented in Figure 4-7. The spectra before exposure shows the C–O–C asymmetric stretching, C–OH side group vibrations, –CH stretching of PLA in the 1182 cm-1, 1126 cm^{-1}, 1081 cm^{-1}, 1035 cm^{-1} bands as previously shown in Figure 4-2 (section *4.3.2 Polymer Structure*). In addition to the PLA peaks, the spectrum (Figure 4-7), shows the presence of C–N stretching vibration of aliphatic amines in the 1290-1150 cm^{-1} region for the PLA-g-SAh films that were exposed to methylamine; this supports the reaction of SAh and methylamine proposed in Figure 4-1 [306].

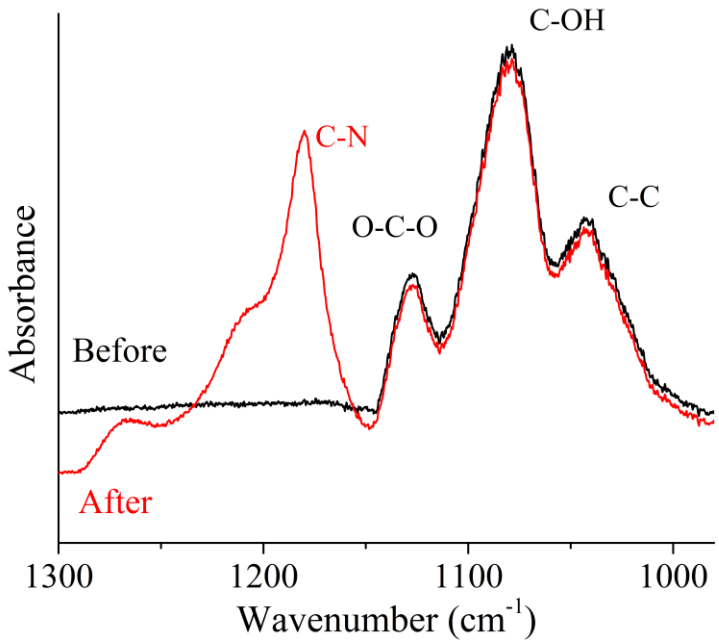

Figure 4-7: FTIR curves between 1300 cm-1 and 980 cm-1 PLA-g-SAh50 samples before and after exposure to methylamine vapor from a 400 ppm solution

XPS scans were done in PLA-g-SAh50 samples in order to trace the presence of amine, e.g. -NH_2, groups on the surface of the polymer films after exposure to methylamide vapours. As expected, carbon (C_{1S}) and oxygen (O_{1S}) were detected before and after exposure as they are the main constituents in the PLA-g-SAh polymer. However, in the samples exposed to methylamine, nitrogen (N) groups were detected. The XPS survey scan curves and their deconvolution for C_{1S} before and after exposure to amines are shown in Figure 4-8a and Figure 4-8b, respectively. In addition, the scan peak for N_{1S} before and after exposure and its deconvolution after amine exposure are shown in Figure 4-8c and Figure 4-8d. As reported previously, the C_{1S} spectrum can be deconvolved into two peak components at 285.8 eV and 283.6 eV before exposure (Figure 4-8a), which correspond to the carbon atoms of C-O and C-C groups, respectively. Similarly, the C_{1S} spectrum following exposure can be deconvolved into peaks at 286.9 eV and 283.6 eV, which correspond to C-N-C and C-C groups [307, 308]. In addition to these two peaks in Figure 4-8b, those corresponding to C=O and C-O (288.3 eV and 285.8 eV) may be present but cannot be distinguished. The N_{1S} spectra, Figure 4-8d, can be deconvolved into two components at 401.2 eV and 399.5 eV, which correspond to the nitrogen atoms of C-N-C and N-H/N-H_2 groups, respectively [307–309]. As shown in Figure 4-8c, there was not presence of this peak prior

exposure to amines. The C-N-C peak present in both the C_{1S} and N_{1S}, as well as the FTIR results discussed above, suggest that there is a reaction between the SAh group in the PLA-g-SAh and methylamine.

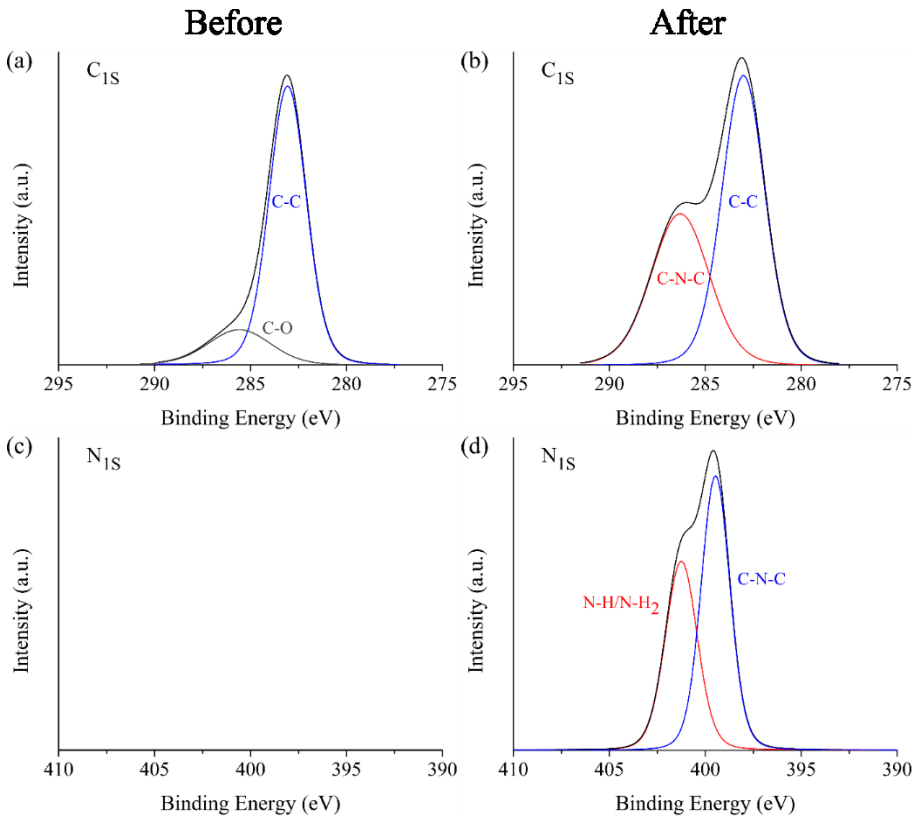

Figure 4-8: XPS curves for (a, b) C_{1S} and (c, d) N_{1S} before and after exposure to vapours of 400 ppm methylamine solution

4.3.5 Amine Response: Thermal Properties

The thermal properties of the PLA-g-SAh polymer films were evaluated by DSC. Figure 4-9 displays the DSC curves for the graft-polymers, both before (dotted lines) and after (solid lines) exposure to methylamine. In addition, Table 4-4 summarizes the thermal properties from these curves. As described and argued in section *4.3.3 Thermal Properties and Degree of Grafting*, as the initial MAh content to graft the PLA-g-SAh polymer increases, there is a decrease in ΔH_m, T_g, and T_m due to the chain scission that occurs during the grafting reaction between PLA and MAh. However, the exposure to methylamine was found to lead to changes in thermal properties of the graft-polymers. In general, the ring opening reaction lead to an increase in ΔH_m , T_g and T_m in the

graft-polymers when compared with the thermal properties before amine exposure. This increase was found to be more significant with increasing in MAh content. For instance, the PLA-g-SAh10 composition did not present a significant increase in thermal properties, while the PLA-g-SAh75 has an increase of T_g from 21°C ± 2°C to 30°C ± 3°C ($P = 0.01$), of T_m from 108°C ± 3°C to 121°C ± 1°C ($P = 0.002$), and of ΔH_m from 2 J/g ± 0.8 J/g to 20.6 J/g ± 0.9 J/g (P 0). Little data has been reported in the past about changes in thermal properties before and after amine ring opening of SAh. Based on the results described here, we suggest that this change could be led by alterations in inter- and intra- molecular interactions in the graft-polymer. In particular, the ring opening amidation reaction of SAh to form PLA-g-succinamic acid, Figure 4-1b, and subsequent reaction with the amine group in methylamine can cause higher inter molecular interactions as a section of the polymer (SAh) opens up which can be responsible of an increase in heat and temperature required for endothermic processes such as glass transition and melting [280, 310, 311]. In addition, and as reported by Kesim *et al.* [280, 311], the creation of new available OH groups can cause more intermolecular H-bonded interactions, decreasing mobility of PLA-g-SAh chains which contributes to that increase in thermal properties [310]. In addition, the study of thermal properties due to similar structural changes, e.g. the transition from linear to cyclic structures and vice versa, were studied by Sugai *et al.* [312]. In their work, the structural and thermal properties of photo-cleavable linear and cyclic poly(L-lactide) (PLLA) and poly(D-lactide) (PDLA) were studied. They reported that the transformation from a cyclic to a linear molecular structure led to an increase from 128°C to 142°C. This difference could be due to the higher level of physical entanglement and intermolecular interactions between polymer chains.

Table 4-4: Thermal properties from DSC of neat PLA and PLA-g-SAh before and after exposure to methylamine ($n = 3$).

Sample Name	Before			After		
	T_g (°C)	T_m (°C)	ΔH_m (J/g)	T_g (°C)	T_m (°C)	ΔH_m (J/g)
PLA-g-SAh10	32 ± 1	133 ± 2	21.8 ± 0.4	31 ± 3	142 ± 2	24.8 ± 0.4
PLA-g-SAh25	30 ± 2	121 ± 3	20.6 ± 0.6	32 ± 2	135 ± 1	26.9 ± 0.6
PLA-g-SAh50	28 ± 1	116 ± 2	19.2 ± 0.7	31 ± 1	126 ± 2	23.8 ± 0.5
PLA-g-SAh75	21 ± 2	108 ± 3	2 ± 0.8	30 ± 3	121 ± 1	20.6 ± 0.9

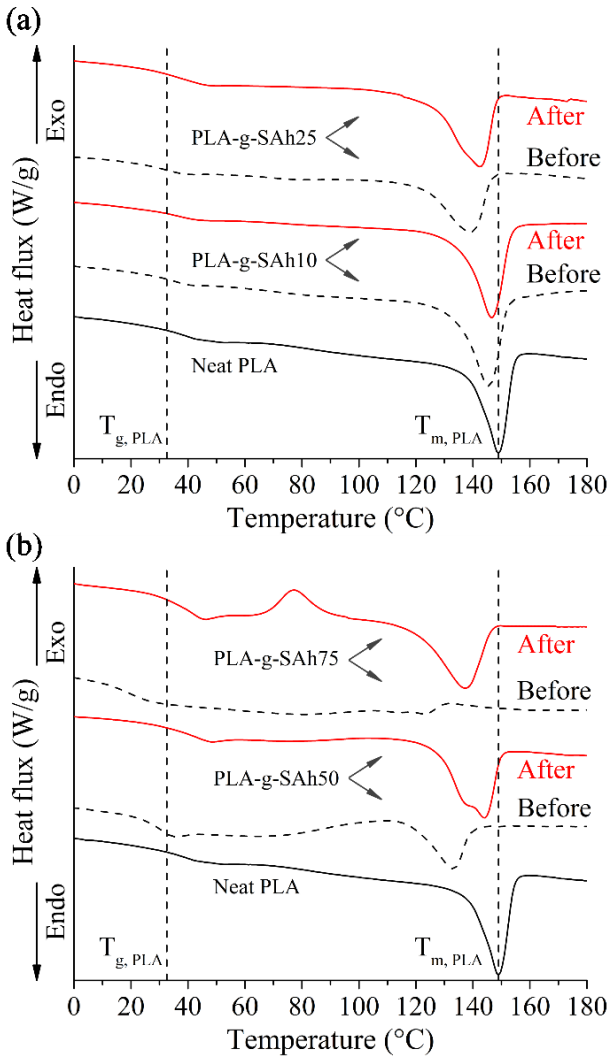

Figure 4-9: DSC curves of neat PLA and PLA-g-SAh with different initial contents of MAh before and after exposure to methylamine. Vertical lines labeled as T_g and T_m mark the glass transition and melting peak temperatures of neat PLA.

To further investigate the selectivity and mechanism of the response, various control samples were also characterized. A set of samples was exposed to water vapor (without methylamine), no change in the thermal properties was found. This suggests that, as illustrated in Figure 4-1b, water would not go through a similar reaction as that between the methylamine and SAh group in the PLA-g-SAh polymer converts the succinic anhydride (SAh) into the corresponding PLA-g-succinamic acid. In addition, to generate a blank set of samples for the reaction between SAh and methylamine into succinamic acid (succinic acid-methylamine), samples of pure PLA were exposed to both 400 ppm methylamine and water for as long 8 hours. Similarly, this did not show

evidence of structural changes in PLA, perhaps because there was not SAh present to react with methylamine. In our future work, we will vary the concentration of amine in the solution to determine the limit of detection.

4.4 Comparison with Literature

When compared with other polymers that respond to amines vapour proposed in the last 3 years, the grafted polymers presented in this work showed some advantages and disadvantages. Some details of these responsive polymer are summarized in Table 4-5. While these materials have been shown to respond to amines using different mechanisms, they require the use of additional instruments and equipment such as UV lamps in He *et al.* [137], QCMs in Das *et al.* [313], and 4-point probe equipment in Khan *et al.* [314]. Based on the characterization done in this work, the response of change in polymer structure and thermal properties have the potential to engineer sensing elements that respond to the presence of amines by changing in color (as the ring opening reaction of SAh can protonate a pH responsive dye) which are of much interest due to their simplicity, similar to those presented by Jin *et al.* [29]. In contrast with recent reports, this work presents a simple solution based method for the grating of SAh onto PLA polymers chains. This method allows for a high efficiency of grafting and the potential to tailor the responsive properties of the grafted polymer with the change in initial concertation of MAh.

In contrast with the work presented by Jin *et al.* [29] and Khan *et al.* [314], the ring opening amidation reaction presented in our work is not reversible; the reverse reaction can only occur in the presence of heat or an acid. The resulting responsive material can therefore not be used for real-time monitoring of amine concentration. This irreversible behavior is, however, desirable in some applications, analogous to temperature-time indicators (TTIs) where exposure to the stimulus leads to a gradual change in property – often color – of the sensor. A record of exposure to the stimulus is therefore preserved, even once the stimulus is removed.

Table 4-5: Relevant responsive polymers that react to amines (from 2017 to 2019)

Material	Amines	Mechanism	Response	Ref.
Nitrated polythiophene (NPTh)	Ethylenediamine, putrescine, cadaverine, spermidine, phenethylamine, histamine	The biogenic amine (BA) easily diffuses into the polymer film and forms charge transfer complexes with NPTh. These NPThδ+-BAδ− complexes lead to the change in color of the film.	A fast change in color from light brown to a highly deep dark brown	[29]
Alkaline earth metal–organic coordination polymer	Methylamine, dimethylamine, trimethylamine	Amines combine with unsaturated carboxylic groups in the polymer. The carboxylic group can no longer vibrate, increasing the rigidity and educe the loss of non-radiation energy of the ligand, causing the increase of the fluorescence emission intensity	On/Off change in fluorescence with initial and final peaks at 525 nm and 612 nm	[137]
Polyaniline-titanium(IV) sulphosalicylophosphate composite	Methylamine, ethylamine	The lone pair of nitrogen of amine interacts with the imine nitrogen of Pani, decreasing the intensity of positive charge which decreases the conductivity	Reversible change in resistivity measured with 4-point probe	[314]
Schiff base 3(aminopropyl)triethoxysilane (APTES)	Methylamine, ethylamine, diethylamine,	Small molecules of amines are trapped in molecular pores introduced by the	Polymer-coated quartz crystal microbalance (QCM) substrate absorbs the amines, increasing	[313]

	triethylamine, tertbutylamine ammonia	bulky group of Schiff base attached to polysiloxane. They are stabilized by H-bonds and dipole-dipole inter- action	the mass of the film and the mass	
EuCl3 with 4,4′-biphenyldicarboxylic acid (H2BPDC)	Methylamine, dimethylamine, trimethylamine	Fluorescence quenching by the amines	Drop in fluorescent emission at 413, 578, 592, 614 (main peak), 650 and 704 nm when excited by UV light of 311 nm	[315]
PLA-g-SAh	Methylamine	Amidation of SAh in PLA-g-SAh with methylamine. Lone electron pair of the amine conducts a nucleophilic attack on the C=O π bond of SAh to start a ring opening reaction.	Increase in melting point and donation of protons during ring opening of SAh. Potential in color change indicators and electrochemical sensing.	This work

4.5 Conclusions

In this study, we presented a solution-based method to graft PLA with SAh with a high degree of efficiency, and demonstrated the response of PLA-g-SAh to amines. Most previous work on PLA-g-SAh has focused on using melt-mixing; one advantage of our technique is that it takes place well below the degradation temperature of MAh/SAh. In addition, we achieved a higher efficiency of grafting than achieved previously by melt mixing (e.g Ma *et al.* [290] and Hwang *et al.* [285]); this allowed for a high degree of grafting overall. The structural and thermal properties of the graft-polymers were studied. The increase in branching in the PLA chains, as consequence of grafting, led to a decrease in melting point and crystallinity of the polymer (as compared with neat PLA). Following grafting, PLA-g-SAh films were exposed to the vapor of a 400 pm amine solution. This concentration was selected as it is indicative of spoilage in fresh fish products [24]. While other studies have reported the reaction between SAh-grafted polymers (such as PMVE-co-MAh [316]) and amines, the study of the effect of the degree of grafting on the reaction with amines has not been explored in the past. Our materials exhibited significant changes in thermal properties after exposure to the amine vapor, as the methylamine-caused ring opening of SAh increased physical interactions and OH-bonded interactions of the polymer which increased its thermal properties. Due to the structural changes that occur within the grafted polymer upon exposure to the amine vapor, this work presents potential opportunities for the development of real-time amine sensing elements that are simple to use, biodegradable, and simple to produce at a large scale. In our future work we will leverage the reaction that occurs between the amine vapor and SAh groups to engineer colorimetric sensors.

5. *Colorimetric Indicators for Volatile Amines Based on Responsive Poly (lactic acid) (PLA) and Succinic Anhydride graft-polymer*[3]

ABSTRACT: Smart materials that can undergo changes in color upon the detection of amines has the potential to provide information of the freshness of fish and meat. In this work, we study the use of poly (lactic acid)-g-succinic anhydride (PLA-g-SAh) polymer – coupled with pH sensitive dyes – as amine-responsive materials for color change indicators. In this system, the reaction between SAh and amines protonates the dye and leads to an irreversible change in color in the indicators. The resulting change in color was recorded and monitored with standardized photos and UV-Vis spectroscopy. Initially, indicators of different degrees of SAh (from 5 wt% to 45 wt%) grafted onto PLA were exposed to the vapours from a 400 ppm amine solution. Samples with the higher degrees of grafting underwent the most visible changes in color. A more detailed study of the effect of temperature and amine concentration was done in indicators with 30 wt% SAh. The limits of detection, half-time and kinetics of the response are also presented. Higher temperatures and concentrations were found increase the degree of the color change while decreasing the half-time of response of the indicators. This work shows potential opportunities for the development of simple real-time amine indicator.

[3] A version of this chapter will be submitted for consideration of a peer-reviewd journal as Adrián Lopera-Valle, Anastasia Elias, "*Amine Responsive Poly(lactic acid) (PLA) and Succinic Anhydride (SAh) Graft-Polymer: Synthesis and Characterization*" Refer to the preface of this thesis for more information.

5.1 Introduction

Smart materials – which undergo visible and gradual changes in color as response to a particular stimulus – can be effective tools to monitor the storage conditions and freshness of food. For instance, time-temperature indicators have been developed to track the refrigeration history of goods, providing information about their cumulative exposure to temperatures that could compromise their freshness [72]. While storage conditions including temperature, humidity, and exposure to oxygen are good indirect indications of food quality [26], it is also desirable to monitor *direct* indicators of food quality such as chemicals released during food ripening (e.g. ethylene oxide [6]) and spoilage. In the case of fish and meat, biogenic amines – including ammonia, putrescine, dimethylamine, trimethylamine, putrescine, cadaverine, dopamine, histamine and methylamine [23–25] – are known by-products of natural degradation. For instance, the concentration of amines present in an enclosed package of game Atlantic fish (e.g. red drum) has been shown to increase from 130 ppm to 350 ppm at 4°C in the span of 12 days of storage (as food freshness decreases) [24, 261]. Therefore, the design and testing of simple devices that can respond to amines are desirable for monitoring food freshness and safety, particularly in fresh fish and meat, as amines have been shown to increase in concentration with time as food freshness decreases [24, 261].

The detection and quantification of amines in vapour, gas or solution have been done with a variety of methods including electrochemical sensors [264, 265], electrical-based sensors [266], optical detection methods [23, 267], and high performance liquid chromatography [262, 263]. While effective, most of these methods require a power supply and/or lab-scale analytic equipment and trained personnel. A possible way to overcome these drawbacks is by implementing simple elements based on smart materials that undergoes a specific and sensitive reaction to amines. For instance, He *et al.* proposed the use of an alkaline earth metal–organic coordination polymer for the detection of methylamine, dimethylamine, and trimethylamine [137]. In the response of this polymer, amines bond with unsaturated carboxylic groups in the polymer and restrict their vibrations, thereby increasing the rigidity of the polymer. This reduces the loss of non-radiation energy of the ligand, causing the increase of the fluorescence emission intensity, leading to an on/off change in fluorescence with initial and final peaks at 525 nm and 612 nm.

A key element in engineering an amine-responsive smart material is the use of a molecule or functional group that undergoes a selective reaction with amines. Anhydrides such as maleic anhydride (MAh) and succinic anhydride (SAh) have been reported to react with amines. In the first step of this reaction, the lone electron pair of the amine conducts a nucleophilic attack on the C=O π bond of the anhydride to form a tetrahedral intermediate, while the second carbonyl becomes part of the leaving group on the other side of the anhydride ring [268–275]. Following this, the removal of a proton from the leaving group by the amine and the donation of an electron from the carboxylate group back to the C=O π bond, which is much less electrophilic than in an acid anhydride [268–273]. While the reaction between MAh or SAh and amines has been used as initial step for classical approaches to the synthesis of maleimide and succinimide, this process requires the dehydration of the intermediate acid, usually promoted by acids and/or temperature [274, 276, 277]. At room temperature, the most likely pathway is that the ring-opening reaction converts the anhydride into the corresponding dicarboxylic acid monoamide, maleamic acid or succinamic acid for MAh and SAh, respectively [268, 270, 274]. This reaction can result in physical and/or chemical changes that can be leveraged in smart materials. For examples, Fiddes *et al.* proposed to use carbon black(CB) /polyethylene-vinyl-acetate(PEVA)/maleic-anhydride (MAh) conductive polymer composites (CPCs) to passive radio frequency ID (RFID) tags sensors for the detection of biogenic amines present in the spoilage of meat [316]. In their work, MAh was used as the sensing element in the composite, by binding to primary amines to form a stable amide bonds and making the CPC more hygroscopic [279, 316].

In the previous chapter, this thesis demonstrated a solution-based method to graft high percentage of SAh onto a backbone of poly-lactic acid – a degradable bio-based material that is increasingly being utilized in food packaging –forming PLA-g-SA. NMR and TGA studies revealed that the efficiency of the graft reaction was ~52%, leading to a graft-polymer with up to 43.7% grafted SAh. This work then determined that upon exposure to the vapours from a 400 ppm methylamine solution the anhydrite-amine ring-opening reaction led to changes in the structural and thermal properties of the grafted-polymer [317]. For example, FTIR characterization before and after exposure to amines showed the presence of C-N stretching, and indicated that the ring reaction proceeded as described above, and as shown in Figure 5-1. Finally, the evaluation of the thermal events of glass transition and melting suggested that there was a change in the polymer structure and its inter/intra-molecular interactions. The results that were presented reflect the

potential that PLA-g-SAh – which produce H+ ions through the anhydride-amine reaction – could have as responsive element in electrochemical sensors, in responsive CPCs, or colorimetric indicators that respond to the presence of volatile amines [317].

In this study, we investigate the use of a PLA-g-SAh polymer, coupled with a pH sensitive dye, as an amine-responsive sensing material that undergoes an irreversible change in color upon exposure to small concentrations of amines in vapor (Figure 5-1). Initially, the effect of the composition of the grafted polymer, i.e. the degree of grafting of SAh in PLA, on the change in color of the indicators was characterized. In order to monitor and prove the responsive behavior of SAh in the graft-polymers, samples were exposed to the vapours from a 400 ppm methylamine solution in deionized water under room conditions. Following this, a further characterization of the indicators was done under different condition of amine concentration and temperature. The change in color was evaluated by means of UV-Vis spectroscopy performed before and after exposure to amines. The potential of utilizing these polymer-based color change indicators in intelligent packaging that can monitor the freshness of food based on the response of polymers to amines is discussed.

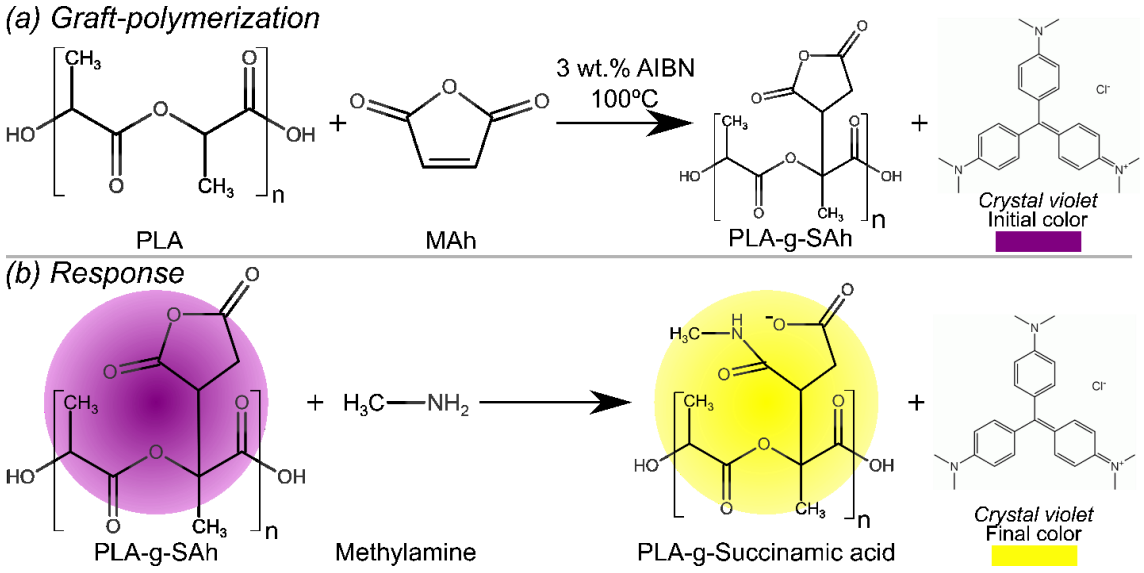

Figure 5-1: Proposed free radical graft-polymerization reaction between PLA and MAh, and the color change response of PLA-g-SAh and methylamine to form PLA-g-Succinamic acid

5.2 Experimental Methods

5.2.1 Polymer synthesis

The method used to synthesize the succinic acid-grafted PLA was described in the previous chapter [317]. Poly(lactic acid) (PLA, 4042D, NatureWorks LCC, Minnetonka, MN, USA), comprised of 92% L-lactide and 8% D-lactide units, pellets were dried in an oven at 70°C for at least 8 hours in other to remove absorbed water from the environment. Following drying, a 40 mg/ml PLA solution in toluene (No. 244511, Sigma-Aldrich, St. Louis, MO, USA) was prepared in an air-cooled reflux setup at 100°C for 1.5 hours. The graft-polymers were synthetized by adding maleic anhydrite (MAh, No. 63200, Sigma-Aldrich, St. Louis, MO, USA) and 3 wt% azobisisobutyronitrile (AIBN, No. 441090, Sigma-Aldrich, St. Louis, MO, USA), as free radical initiator (Figure 5-1). The solution was kept at 100°C for one hour in order to ensure the complete decomposition of the free radical initiator. Based on the characterization work presented in the previous chapter [317], Table 5-1 lists the composition of the blends of PLA and MAh used in the synthesis of the materials, as well as the fraction of SAh that actually grafted onto PLA and the resulting molecular weight.

Table 5-1: Sample composition

Polymer blend	PLA wt%	MAh wt%	SAh wt%	Mw [317] kDa
Neat PLA	100	0	0	122
PLA-g-SAh5	87	10	5.1	80
PLA-g-SAh15	72	25	14.6	81
PLA-g-SAh30	47	50	29.8	85
PLA-g-SAh45	22	75	43.7	102

5.2.2 Fabrication of color change indicators

To produce color-changing indicators, a pH sensitive dye, crystal violet (pH range 0.1-2.0, No. 69710, Sigma-Aldrich, St. Louis, MO, USA), was mixed into the polymer solutions described in Table 5-1 at concentration of 0.2 mg/ml. The dye-containing polymer solution was sprayed using a commercial air-brush (No. 8574428, Princess Auto, Winnipeg, Manitoba, Canada)

attached to a building air line at 40 psi of nominal pressure. Filter paper (>11μm particle retention, diameter 55 mm circles, No. 1001055 Whatman™ Qualitative Filter Paper, GE Healthcare, Chicago, IL, USA) was used as substrate, and mounted with masking tape on a flat vertical surface placed 15 cm from the nozzle of the air-brush. After 3 to 4 passes, the filter papers were uniformly covered by the dye-containing polymer solution. The sprayed papers were dried overnight under ambient conditions to eliminate the solvent.

Additional samples of PLA-g-SAh30 were prepared for further characterization of these indicators to test the effect of temperature and amine concentration. To maximize the contrast of the visible color change, a second dye was added. In this new formulation, both crystal violet (pH range 0.1-2.0, No. 69710, Sigma-Aldrich, St. Louis, MO, USA) and thymol blue (pH range 1.2-2.8, No. 114545, Sigma-Aldrich, St. Louis, MO, USA) mixed into the polymer solution at concentrations of 0.2 mg/ml and 0.01 mg/ml, respectively. Similarly, the dye-containing polymer solution was sprayed using a commercial air-brush onto filter paper substrates following the methods described above.

5.2.3 Scanning electron microscopy

The morphology of both as-received filter paper (hereafter referred to as bare) and PLA-g-SAh coated filter papers was evaluated using a field emission scanning electron microscope (SEM) (Zeiss Sigma 300 VP-FESEM, Zeiss, Cambridge, UK). A sputter coater (EM SCD 005, Leica-Baltec Instrument, Balzers, Liechtenstein) with a carbon evaporation accessory was used to deposit a thin carbon coating onto the surface of the paper samples to prevent them from charging in the SEM. Images of the papers were captured using secondary electron (SE) mode.

5.2.4 Effect of SAh content on sensor response

As an initial assessment of the performance of the color change indicators, the effect of different initial MAh concentrations, listed in Table 5-1, on the color change response of the indicators was investigated. The color indicators were placed inside a cylindrical glass container (25 cm diameter × 8 cm tall) with 500 ml of 400 ppm amine solution in water at 21°C for 8 hours. The samples were then placed on a stainless steel platform inside the glass container such that they were suspended about 20 mm above the level of the amine solution. Color change measurements

were carried out on a spectrophotometer UV-VIS (Hitachi U-3900H, Hitachi Ltd, Tokyo, Japan) in absorbance mode, and measured from 710 nm to 380 nm, at a scanning rate of 120 nm/min. The collected UV-VIS spectra were plotted and compared.

In addition, pictures of the color change indicators were taken before and after exposure to methylamine vapour with a 3968 × 2976 pixels camera, set at an ISO of 1600, shutter of 1/640 sec, exposure compensation of 0, and white balance for indoor white light, at a distance of 10 cm. These parameters were kept constant in order to reliably visualize the changes in the color of the indicators due to their exposure to methylamine.

5.2.5 Effect of amine concentration and temperature

The response of the PLA-g-SAh30 color change indicators to vapors of amines was characterized by means of UV-VIS spectroscopy at various time steps during exposure to methylamine vapour. The color change indicators were placed inside a cylindrical glass container (25 cm diameter × 8 cm tall) with 300 ml of amine solution at 5°C, 14°C, and 21°C for 24 hours. Amine solutions of 50 ppm, 150 ppm, 300 ppm, and 600 ppm were used. The temperature of the solution was controlled by placing this glass container inside a larger 34 cm × 38 cm × 15 cm plastic container with DI water that circulated through a refrigerated/heated recirculating bath (Model 911, PolyScience Ltd, Niles, IL, USA). Samples were removed from these conditions at desired time-points (from 0 to 24 hours), halting the color change, photographed and characterized using a spectrophotometer. Measurements were carried out on a spectrophotometer UV-VIS (Hitachi U-3900H, Hitachi Ltd, Tokyo, Japan) in absorbance mode, and measured from 710 nm and 380 nm, at a scanning rate of 120 nm/min.

The collected UV-VIS spectra generally present a peak at maximum absorbance within the wavelength range measured, associated to the concentration of protons in the polymer comprising the indicator (Figure 5-2). With the change in color of the paper-based indicators, the wavelength at which the maximum absorbance (λ_{max}) occurs shifts. Therefore, the wavelength of λ_{max} can be plotted as a function of time in order to track the color change response of the indicators. Following this, a sigmoidal regression, Figure 5-2, was used to model the relationship between λ_{max} and time for the different test conditions described above in this section, as follows,

$$\lambda_{max}(t) = \frac{\lambda_0 - \lambda_f}{1 + \left(\frac{t}{t_{1/2}}\right)^p} + \lambda_f \qquad \text{Eq. 8}$$

where λ_0 and λ_f are the initial and final wavelengths of the maximum absorbance (which would represent the initial and final colors of the indicators), $t_{1/2}$ is the midpoint of response of the indicators (time required to reach the midpoint between λ_0 and λ_f), and p is the power of the sigmoidal regression. The regression coefficient, r^2, was found to be above 0.95 for all cases.

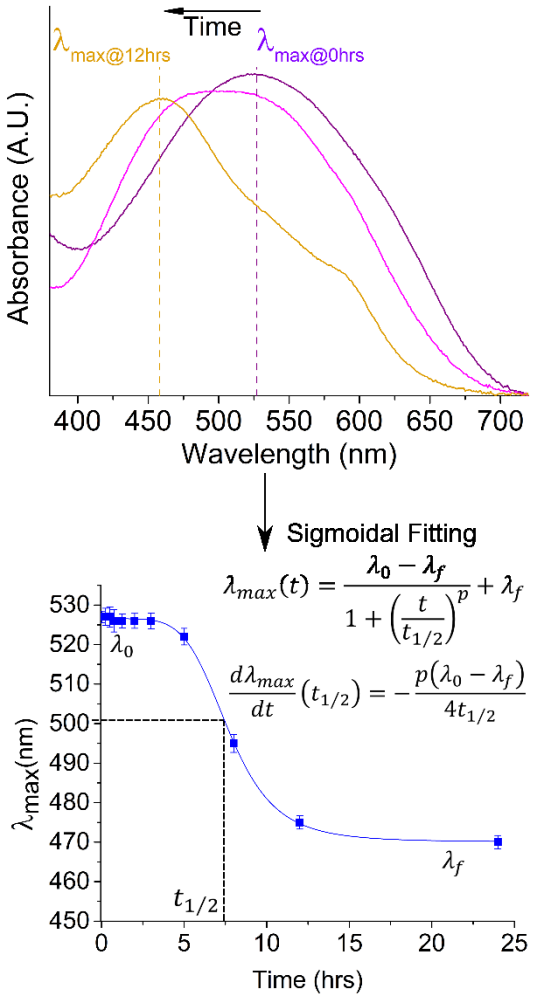

Figure 5-2: Data analysis for sensor characterization

In addition, the derivative of λ_{max}, Eq. 8, with respect to time can be further solved and evaluated for $t = t_{1/2}$ in order to find the rate of change of color with respect to time at the midpoint of the transition between λ_0 and λ_f. This leads to Eq. 9 as follows,

$$\kappa = \frac{d\lambda_{max}}{dt}\left(t_{1/2}\right) = -\frac{p(\lambda_0 - \lambda_f)}{4t_{1/2}} \qquad \text{Eq. 9}$$

The values of λ_f, $t_{1/2}$, and κ were used to characterize the magnitude of the response, time of response, and sensitivity of the color change indicators presented in this work.

5.3 Results and Discussion

5.3.1 Scanning electron microscopy

Low and high magnification SEM images, shown in Figure 5-3, were used to characterize and compare the morphology of the bare and PLA-g-SAh-coated papers. Figure 5-3a and Figure 5-3b depict bare papers (at low and high magnification, respectively), while Figure 5-3c and Figure 5-3d depict coated papers (also at two different magnifications). The bare papers appear to be comprised of randomly oriented cellulose fibers that form voids distributed in a homogeneous fashion. These voids are natural of filter papers and are meant to allow fluids pass through the filter while trapping larger matter. On the other hand, the coated paper presented a significant decrease in visible voids as the PLA-g-SAh appears to be deposited over them. In uncoated samples, (Figure 5-3b) there is a network-like structure created by voids and randomly oriented fibres. After spray coating (Figure 5-3d), the majority of these voids and fibres were covered with a thin PLA-g-SAh graft-polymer film. The SEM images in Figure 5-3 suggest that the polymer was effectively deposited in the filter papers. These morphology features were consistent throughout the different contents of SAh listed in Table 5-1.

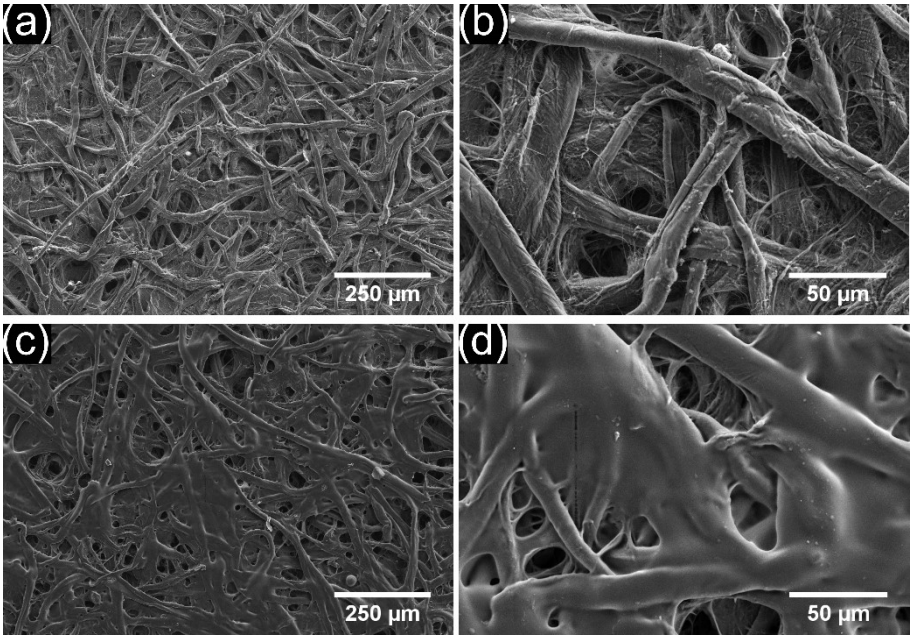

Figure 5-3: a) Low and b) high magnification SEM image of a bare paper filter; c) low and d) high magnification SEM image of a PLA-g-SAh coated filter paper

5.3.2 Effect of SAh content on sensor response

Color change indicators were prepared by mixing crystal violet pH dye with succinic anhydride-grafted PLA (Table 5-1) dissolved in toluene at 0.2 mg/ml and spray coating the resulting mixtures onto filter paper. To determine which grafted polymer would undergo the most visible change in color upon exposure to amines, these indicators were then exposed to the vapours of a methylamine solutions of 400 ppm. With pH of 6.8 ± 0.2 (n = 5), this solution falls in the pH range of amines associated with fish spoilage (pH 6 to 7.5 [318]). The response of the color change indicators was characterized both by photographs taken under standardized settings and using UV-Vis spectrometry in absorbance mode (measurements taken on 5 random location around the center region of the samples). The resulting UV-Vis spectra therefore correspond to the complementary color of the indicator. The peak absorbance for the neat PLA indicators before exposure to methylamine was 548 nm ± 3 nm (n = 15, appearing violet in color), and around 590 nm ± 8 nm (n = 60, appearing violet-blue in color) for those of PLA-g-SAh samples. The larger standard deviation of the PLA-g-SAh samples reflects the fact that the exact color is dependent on the amount of SAh grafted to the PLA backbone. For instance, as can be seen in Figure 5-4, the PLA-g-SAh5 samples had an initial main peak of 589 nm ± 4 nm (n = 15, appearing blue-violet to blue)

while that one for the PLA-g-SAh45 samples was 613 nm ± 2 nm (n = 15, appearing blue). This shows that initial and final color of the indicators are directly affected by the concentration of SAh in the polymer, where more violet samples are indicative of a lower pH, while a bluer color indicates a higher pH within the color change scale of crystal violet. This change suggests that the increase in SAh in the graft-polymerization reaction increased the pH of the polymer deposited on the paper substrates.

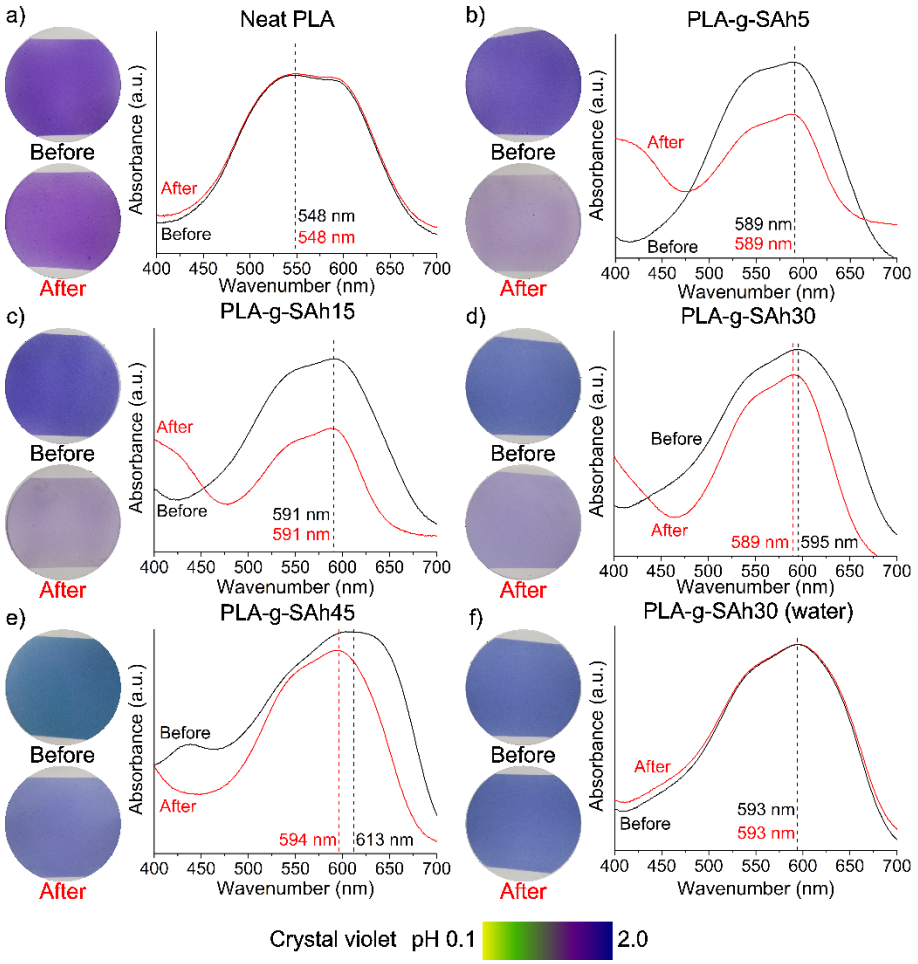

Figure 5-4: Adsorption UV-Vis spectra and images of color change indicators before and after their exposure to methylamine (n = 5)

After exposure to amines, the indicators presented a change in color that — similar to the initial color of the indicators — was dependent on the content of SAh. For instance, the UV-Vis spectra of the PLA-g-SAh5 and PLA-g-SAh15 set of samples did not present a significant change in color. Moreover, the UV-Vis spectra showed a drop in the intensity of the absorbance peak at

589 nm with an increase in the absorbance at around 400 nm. This drop in intensity was easily observable in the photos (Figure 5-4b and Figure 5-4c), and measured to be 19% ± 0.8% (at λ = 589 nm, *n* = 15) for PLA-g-SAh5 and 28% ± 0.7% (at λ = 591 nm, *n* = 15) for PLA-g-SAh15. Despite the lack of shift in λ, the measured drop in intensity was visible by naked eye. This could constitute a response to the exposure to amine vapours.

On the other hand, the indicators produced using PLA-g-SAh30 and PLA-g-SAh45 underwent a change in both the intensity of color and the color itself, as shown in Figure 5-4d and Figure 5-4e. The absorbance peak of the PLA-g-SAh30 indicators shifted from 595 nm ± 2 nm (*n* = 15) to 589 nm ± 3 nm (*n* = 15) after exposure to amines, and an 11% ± 1.0% (at λ = 595 nm, *n* = 15) drop in intensity was observed. In addition, the PLA-g-SAh45 indicators underwent a change in intensity and color, with the maximum absorbance peak starting at 613 nm ± 3 nm (appearing blue, *n* = 15) and decreasing to 594 nm ± 4 nm (appearing violet, *n* = 15), while the peak intensity decreased roughly 8% ± 0.6% (at λ = 594 nm, *n* = 15). Following the color scale of crystal violet, the degree of protonation of the dye (and the corresponding pH of the polymer coatings) increased as a result of the formation of succinamic acid upon the reaction of methylamine with succinic acid (SAc-methylamine). These indicators changed in color as consequence of the change in the protonation of the dye in the graft-polymer coating when SAh reacted with the amine group in methylamine to form succinamic acid. The larger relative shift in peak (and change in color) occurs for the samples with a higher fractional composition of SAh on the polymer backbone, as these are the functional groups that react with methylamine and consequently, as depicted in Figure 5-1, protonate the crystal violet dye in higher degree.

To further investigate the mechanism and the selectivity of the response, various control samples were also characterized. Samples of PLA-g-SAh30 were exposed to water vapor (without methylamine), and little to no change in color was observed (Figure 5-4f). In addition to those shown in Figure 5-4, a set of samples was sprayed with only dye (no polymer was deposited) and exposed to methylamine vapor from a 400 ppm solution as control experiment. No change in color was observed after exposure (shown in Figure 5-5a), indicating that the observed color change does not result simply from the vapor interacting directly with the dye. This is expected given that its pH of the solution (6.8 ± 0.2, *n* = 5) is well beyond the color change range of crystal violet (pH range 0.1-2.0) which explains why no change in color was observed in this control [319]. Finally,

as a blank set of samples for the reaction between SAh and methylamine, samples of neat PLA were exposed to both 400 ppm methylamine and water for as long 8 hours. No change in color was observed after exposure (shown in Figure 5-5b). The results of these control experiments indicate that the grafted polymer reaction with methylamide plays a fundamental role in the color change response of the indicators (shown in Figure 5-4), caused by the protonation of the dye [319].

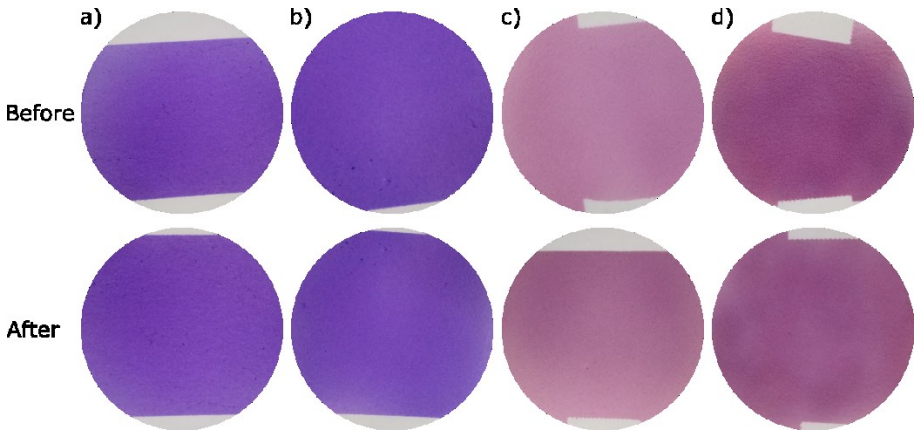

Figure 5-5: Blank samples of a) papers sprayed with only dye (no polymer was deposited) and exposed to methylamine vapor from a 400 ppm solution as control experiment; b) neat PLA exposed to water vapour; c) PLA-g-SAh30 indicators exposed to water vapour and d) to the vapours from a 300 ppm solution of methanol

Finally, this color change tests allowed us to conclude that as the PLA-g-SAh30 (Figure 5-4d) and PLA-g-SAh45 (Figure 5-4e) compositions presented a more visible and intense change in color as their higher concentration of SAh could allow for a higher protonation of the crystal violet molecules (Figure 5-1).

Given the more visible (and measured by UV-Vis) change in color and also in thermal stability (reported in the previous chapter as Lopera-Valle *et al.* [317]), the PLA-g-SAh30 composition was chosen to characterize the effects of temperature and amine concentration on the response of color change indicators.

5.3.3 Color change performance – concentration and temperature

A detailed characterization of the performance of the PLA-g-SAh30 indicators under different conditions of temperature and amine solution concentration was conducted. Aiming to increase the contrast of the visible color change that occurred when crystal violet was used as a dye, thymol blue was added as second dye. The final color of the indicators after 24 hrs of exposure to different conditions of temperature and amine concentration was captured with standardized photos and characterized with UV-Vis, and displayed in Figure 5-6. Figure 5-6a shows photos of the indicators after 24 hrs of exposure to 50 ppm, 150 ppm, 300 ppm, and 600 ppm solutions of methylamine at 5°C, 14°C, and 22°C, while Figure 5-6b shows the UV-Vis spectra for indicators at 22°C and different amine concentrations. The initial color of all indicators was an intense purple, similar to that of PLA-g-SAh30 in Figure 5-4d. As shown in Figure 5-6a, some of the indicators presented some purple color regions after exposure to methylamine (and the consequent color change). These regions may be locations of the indicator where the polymer was not homogenously sprayed onto the filter papers as this fabrication process was done by hand and limited control on the deposition rate are likely to happen. In the future, using a robotic arm or a 3-axis frame for the deposition of the polymer solution onto papers could allow to fabricate more homogenously coated papers.

The change in color that occurred upon exposure to amines was observed to be affected by both temperature and concentration. At a fixed temperature (Figure 5-6c), the largest color changes were observed for the solutions with highest concentration. For instance, at a constant temperature of 22°C, the wavenumber of the peak absorption, λ_f, for specimens exposed to 50 ppm amine solution for 24 hrs did not change from the initial color, 523 nm ± 2 nm (n = 15, appearing violet). As the concentration of amines increased to 150 ppm, 300 ppm, and 600 ppm, the peak of maximum absorbance decreased to 470 nm ± 2 nm (n = 15, appearing red-orange), 460 nm ± 3 nm (n = 15, appearing orange), and 460 nm ± 2 nm (n = 15, appearing yellow), respectively. Similarly, at a fixed concentration (Figure 5-6d), color changes were more drastic at higher temperatures than lower ones.

The effects of temperature and concentration are likely linked by both an increase in the kinetic of reaction of SAh and methylamine, and a decrease in the vapour pressure of the methylamine in water as the temperature increases. This would then translate into a higher

concentration of methylamine vapour in the air around the color change indicators, leading to a higher conversion of SAh into succinamic acid (SAc-methylamine).

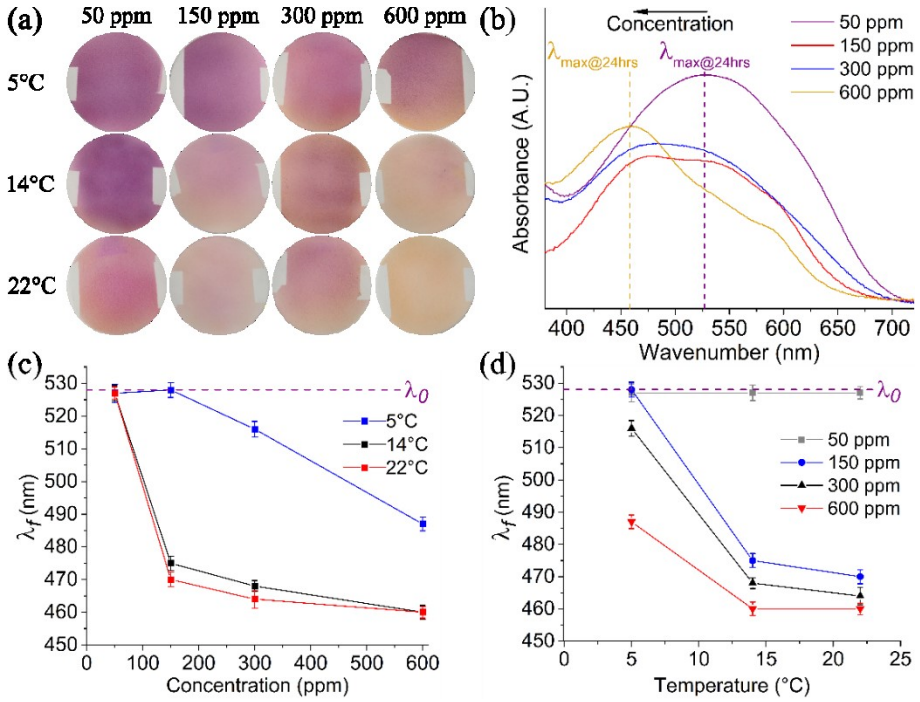

Figure 5-6: Characterization of PLA-g-SAh30 indicators after 24 hrs of exposure to different methylamine concentrations and temperatures. (a) Color of sensors exposed to methylamine concentrations and temperatures indicated, (b) UV-Vis spectra for samples at 22°C and different amine concentrations, and effect of (c) temperature and (d) concentration on the color of the color indicators based on UV-Vis absorbance after 24 hrs of exposure to methylamine.

The monitoring of the color change with UV-Vis measurements suggests that the color change indicators, when exposed to methylamine in this set up, require a minimum concentration, known as low limit of detection, and a minimum temperature, perhaps closely related to a thermal barrier, to show a significant change in color. The results illustrated in Figure 5-6d suggest that the limit of detection lays between 150 ppm and 300 ppm for all temperatures tested in this study. For instance, no significant change in color was measured for any temperature at 50 ppm concentration, and no change was observed below 150 ppm when the solution was kept at 14°C. This means that the limit of detection at 5°C is between 150 ppm and 300 ppm, while that of systems at 14°C and 22°C is between 50 ppm and 150 ppm. In the case of the effect of temperature, Figure 5-6c, the results of λ_f in terms of concentration for different temperature shows that that temperatures

between 5°C and 14°C would lead to the response of the sensors at any concentration above 50 ppm.

Selectivity tests were done in this group of indicators. A set sample of PLA-g-SAh30 indicators were exposed to water vapour and to the vapours from a 300 ppm solution of methanol for as long as 8 hours. No apparent color change was observed in any of the tests (shown in Figure 5-5c and Figure 5-5d).

5.3.4 Color transition and sensor characterization – kinetics

The transition from the initial to final color of the indicators was captured in photos and measured by UV-Vis (measurements taken on 5 random location around the center region of the samples) at various time steps. As an example of this process, particularly of the effect of concentration, Figure 5-7 shows photos of two sets of color change indicators exposed to 600 ppm (Figure 5-7a) and 50 ppm (Figure 5-7b) at 22°C after 12 hrs of exposure to methylamine. Given that no significant change in color was observed past 12 hrs, this time was concluded to be enough for the indicators to reach steady state. The pictures clearly show that higher concentration of methylamine, at 600 ppm led to a noticeable change in color in less than 2 hrs, and that the color ceased to change further beyond 3 hours of exposure. On the other hand, at the lower concentration of 50 ppm, a significant change of color did not occur even after 12 hrs. This visual characterization suggests that the increase in concentration, and in temperature are direct determinants of the time required for the indicators so display a noticeable change in color as consequence to the exposure to amines.

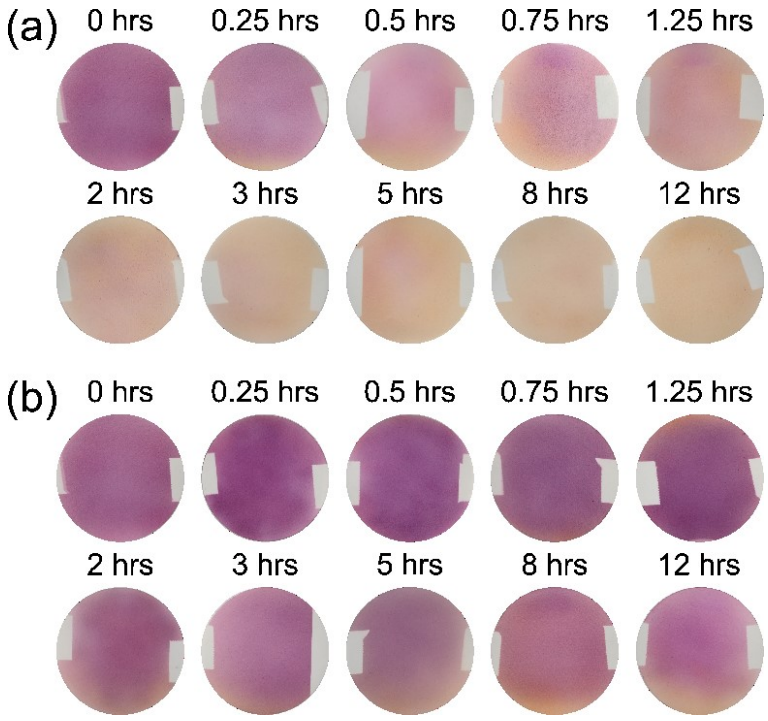

Figure 5-7: Color change of colorimetric sensor exposed to (a) 600 ppm, and (b) 50 ppm at 22°C

The kinetic of the color change of the indicators shown in Figure 5-7 was monitored with UV-Vis over a 24 hr period. Figure 5-8 shows the changes in the peak wavelength based on UV-Vis spectra for different temperatures and concentrations. Figure 5-8a shows an example of the time evolution UV-Vis spectra during the exposure time. Figure 5-8b, Figure 5-8c and Figure 5-8d display the time traces of the peak wavelength for 5°C, 14°C, and 22°C, respectively, at different methylamine concentrations. The time traces of the color of the indicators seems to be consistent for the different temperatures and concentrations.

A sigmoidal numerical fitting of the results presented in Figure 5-8b to Figure 5-8c into Eq. 8 was used to model the kinetics of color change. The advantage of doing this lays in the possibility of characterizing the process of color change in terms of concentration and temperature. While the initial color of indicators was consistent for all the conditions, the final peak wavelength and the time required for this change to occur were different for all conditions. In Eq. 8, this time is represented by the response half-time, $t_{1/2}$: the time required for the color to transition from λ_0 to λ_f, . Table 5-2 summarizes the half response time of the indicators under the conditions tested. Similar to the final color of the indicators, $t_{1/2}$, was affected by temperature and concentration.

Given that change in color required a minimum concentration and temperature to take place, some of the tested conditions did not lead to a change in color and there was no half-time of response to be reported. For the concentrations reported, the increase in temperature was found to decrease, $t_{1/2}$. For instance, the half-times of the indicators exposed to 300 ppm solution of amines at 5°C and 22°C were roughly 9.8 hrs and 2.6 hrs respectively. This represents a 70% decrease in half-time. In parallel, the increasing the concentration of amine in the vapour led to a decrease in $t_{1/2}$. The half time for samples at 14°C and 150 ppm was 12.9 hrs, while that one of tests at 600 ppm was 2.6 hrs. These results suggest that increase in temperature and concentration decrease the time required for the indicators to produce a visible change in color.

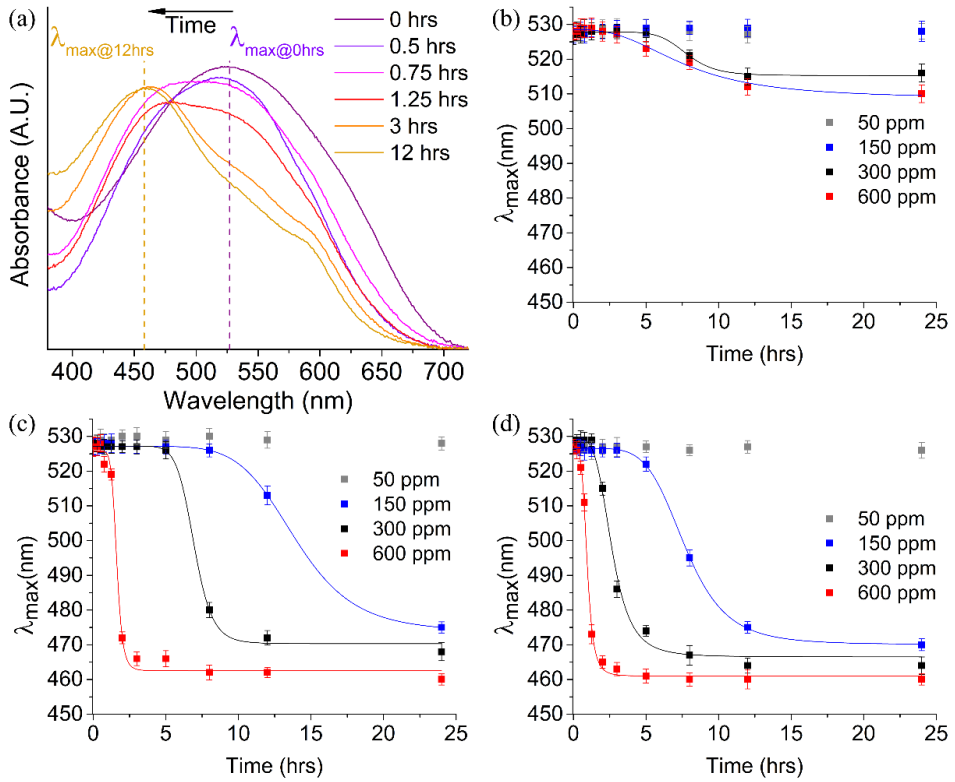

Figure 5-8: Response of PLA-g-SAh30 indicators as a function of time. (a) Uv-Vis spectra time series for the response of colorimetric sensors exposed to 300 ppm solution at 22°C. Wavelength of the maximum absorbance peak versus time (hrs) for samples exposed to different methylamine concentrations as measured at (b) 5°C, (c) 14°C, and (d) 22°C.

Table 5-2: Half-time (hrs) of response of the indicators under different conditions of concentration and temperature

	Temperature (°C)		
Concentration (ppm)	5	14	22
50	--	--	--
150	--	12.9	7.7
300	9.8	6.9	2.6
600	7.6	1.6	0.9

The rate of color change was studied by evaluating the derivative of the color change fitted models at the half time of the color change, Eq. 9. Figure 5-9 displays the rate of color change, κ, in terms of temperature, Figure 5-9a, and concentration, Figure 5-9b, for different concentrations and temperatures respectively. An increase in temperature and concentration led to an increase in *κ*. For instance, indicators exposed to vapours from 300 ppm at solutions 22°C presented a κ of 25 nm/hr while an increase in concentration to 600 ppm led to a κ of 80 nm/hr. These results are correlated with lower half-times of response as higher temperature and concentration would lead to faster and more significant changes in color, shown in Figure 5-8. The rate of color change in terms of temperature for different concentrations, Figure 5-9b, suggests that the rate of color change was the same for those samples exposed to 14°C and 22°C as *κ* in terms of concentration. This is also displayed in Figure 5-9a, where for all concentrations, the temperature had little to no effect on the rate of color change for tests at 14°C and 22°C.

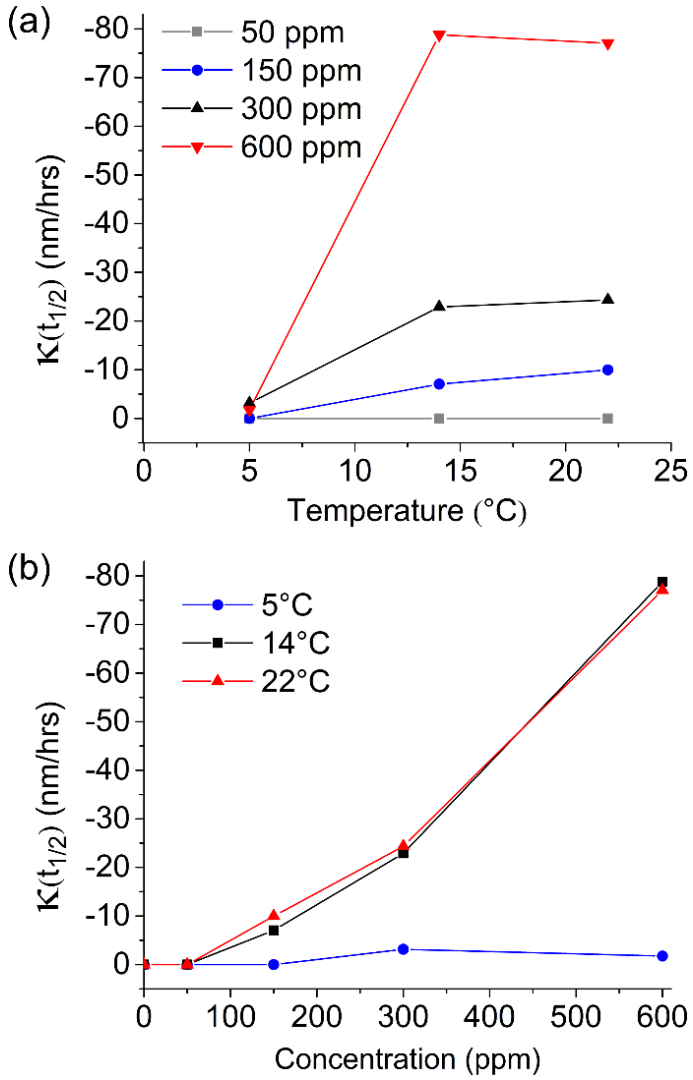

Figure 5-9: Effect of (a) temperature and (b) concentration on the rate of color change at half-time of response.

In summary, the PLA-g-SAh30 color change indicators tested in this work underwent a noticeable change in color when exposed to the vapours from methylamine solutions at concentrations above 150 ppm and at temperatures above 5°C. Exposing the sensors to vapours at higher temperature and concentration led to higher concentration of methylamine to react with SAh in the grafted polymer, leading to a higher degree of protonation of the dye and a stronger change in color. In addition, at the lowest temperature of 5°C – similar to the temperature used in food refrigeration – only concentrations of above 150 ppm of methylamine led to a change in color of the indicators.

5.4 Comparison with literature

When compared with some of the color-based indicators for amines and food freshness proposed in the last 3 years, the indicators proposed in this work showed some particular advantages and disadvantages. Some of the details of these color-change amine sensors are summarized in Table 5-3. For instance, Iswarya *et al.* [320], Yin *et al.* [321], and Ismail *et al.* [322] proposed the use of metal ions and stabilized nanoparticles to trace the presence of amines, e.g. dopamine, melamine, and ammonia. The changes in particles size and yield (in the case of metal ion for the formation of particles) [321], and the interaction between particles (for stable nanoparticles that change in distribution) [320] were used as response to the presence of amines. While they presented a limit of detection as low as 10 ppm, the complex nature for characterization, control, and disposal of metal nanoparticles (silver, Ag, and gold, Au, in these cases) make their implementation less favourable when compared to the air-sprayed PLA-g-SAh proposed in this work [320–322]. In addition, other recent studies, like those by Domínguez-Aragón *et al.* [318] and Urmila *et al.* [323], have proposed to directly measure the pH of the meat samples by means of color change dyes and indicators [318, 323]. In the case of Urmila *et al.* [323], they proposed and tested the use of complex data processing for the calibration and analysis of an array of pH dyes that allowed good selectivity of analytes associated with chicken freshness. One limitation of the indicators the current work is in terms of selectivity: SAh reacts with amines in general rather than with methylamine in specific. Further work is required to understand how this applies to real samples.

Table 5-3: Recent color change indicators for amines relevant to this work (from 2015 to 2018)

Sensor	Amines	Mechanism	Application	Ref.
Array of metalloporphyrins and pH indicators	Spoilage volatile organic compounds (SVOC)	Metalloporphyrin dyes respond to most of the SVOCs during chicken spoilage. pH indictors also respond to hydrogen sulphide and the organic acids. The color changes are process by a multivariate calibration algorithm to asses spoilage	Chicken freshness	[323]
Amino acids L-histidine capped metal nanoparticles	Dopamine	The presence of dopamine lead to the increase in size and yield of nanoparticles (Au, Ag, and Au/Ag)	Recognition of neurological disorders	[320]
H2O2 + Au ions	Melamine	Formation of Au nanoparticles (red) from the reduction of Au ion by H2O2. The presence of melamine, slows down the formation and size of Au nanoparticles (blue)	Infant formula adulteration	[321]
Poly(ortho-phenylenediamine-co-aniline) copolymer	Trimethylamine Dimethylamine Ammonia	The pH of the amines was reflected by the aniline component in the copolymer	Tilapia freshness	[318]
Fruit extracted silver nanoparticles	Ammonia	Initially orange, the Ag colloids form an Ag (NH3)2+ coordination complex when in contact with ammonia. This increases the surface charge of Ag NPs which results isolated and more hydrophilic particles with a blue color	Detection of carcinogenic compounds	[322]
PLA-g-SAh + crystal violet + thymol blue	Methylamine	SAh in PLA-g-SAh reacts with methylamine. This reaction changes the protonation of a pH dye in the polymer, producing a change in color in crystal violet	Methylamine in fish spoilage	This work

5.5 Conclusions

In this study, the feasibility of using PLA-g-SAh (synthetized by a solution-based method) for the fabrication of color change indicators for amines was investigated. The previous chapter proposed and assessed a method for the high degree grafting of succinic anhydride into PLA chains [317]. The current study leveraged this reaction to produce color change indicators by protonating a pH sensitive dye. These indicators were then tested under different condition of temperature and concentration of amines in solution. The characterization of the indicators studied in this work showed that a minimum temperature, between 5°C and 14°C, and concentration, between 150 ppm and 300 ppm in the amine solution. Given that the safe temperatures for the storage of fish has been defined between below 4°C, while concentrations of amines, depending on the combination of amines present, that are considered safe for human consumption have been defined to be below 500 to 1000 ppm [324], these indicators can potentially be used to monitor the conditions present in packaged fish. The polymer backbone used in this work – PLA – is a biopolymer that is increasingly being incorporated into packaging materials; our sensor is designed for integration with such packaging. This work presents potential opportunities for the development of real-time amine indicators that are simple to use, biodegradable, and simple to produce at a large scale. Moreover, further tailoring of the indicators response can be achieved by exposing various compositions of grafted polymer to different conditions of temperature and amine concentration.

6. Final remarks

Conclusions

This thesis focused on the conceptualization, development, and study of two new applications for responsive polymers and composite materials in the fabrication of intelligent packaging systems. After a brief review of applications of responsive polymers on different types of intelligent packaging, this thesis focused on the characterization and testing of a HEMA-PEGDA-silver conductive polymer composites (CPCs) for the fabrication of humidity sensing elements. The effects of the composition and fabrication methods on the sensing properties of these materials were evaluated and compared. The study of these sensing elements demonstrated their potential for the monitoring of storage conditions of produce sensitive to humidity. Following this, the attention of this thesis shifted to the design and testing of a responsive PLA-g-SAh polymer that selectively responded to amines – by-product of fish spoilage –by undergoing changes in the polymer chain structure and thermal properties. Finally, the reaction between amines and PLA-g-SAh was leveraged to fabricate color change indicators that responded to different concentrations of amines. This was achieved by blending a pH sensitive dye with the polymer in solution and spraying it onto commercial filter paper. The study of these polymers and of their response to by-products of fish spoilage, shines light on the development of simple, inexpensive and efficient indictors for the large scale production of fish and meat.

Chapter 3 of this thesis focused on a conductive polymer composite (CPC) material that can respond to changes in humidity by changing its electrical properties. This CPC was comprised of a blend of HEMA-PEGDA and silver (Ag). One of the novelties of this work was in the fabrication of humidity sensors with materials that exhibited low electrical resistivity and high response to

changes in RH when compared with similar CPCs from the literature. This work significantly contributed to the understanding of the effect of geometry on the sensing properties of CPC-based sensors. Here, the sensing properties of films and fine lines direct deposition methods were compared and discussed. In addition, the work presented in Chapter 3 is a novel platform for the development of low-resistance sensing elements based on CPCs that respond to particular stimuli (e.g. humidity, VOC) by undergoing large swelling of the polymer matrix. These type of systems are shown to have the potential to be integrated into low-power and portable devices into food packaging systems.

Chapter 4 presented a method for the synthesis of a responsive polymer that underwent changes in structural and thermal properties upon exposure to amines. To achieve this, succinic anhydride was used as responsive functional group and grafted onto PLA. A novel solution-based method to graft PLA with SAh with a high degree of efficiency and comprehensive evidence of the response of PLA-g-SAh to amines were presented. The high degree of grafting and efficiency of grafting of SAh into PLA chains is a significant contribution of this work, as it uses processing temperatures that avoid thermal degradation of SAh. The response of SAh to amines has been reported in the past, moreover, the study of changes in structural and thermal properties following this response was not widely studied prior this study.

Following the synthesis and characterization of the PLA-g-SAh, Chapter 5 discussed the feasibility of using PLA-g-SAh for the fabrication of color change indicators for amines. In this chapter, this reaction was leveraged to produce color change indicators by protonating a pH sensitive dye. The method of fabrication and the testing conditions of these simple indicators was a novelty of this work. The indicators were tested under different condition of temperature and concentration of amines in solution. These conditions were considered such that they fit the safe

temperatures for the storage of fish, while concentrations of amines, depending on the combination of amines present, that are considered safe for human consumption have been defined to be below 500 to 1000 ppm. This thesis demonstrated that these indicators can potentially be used to monitor the conditions present in packaged fish.

The main contributions and novelties of this work are the development of protocols and procedures for the characterization and application of materials and methods with the potential to be applied on other systems for packaging of food and other products. The ideas of leveraging the response properties of polymers for new applications are often a challenge that requires a rigorous study of materials. This thesis presented a set of methods to evaluate the response of polymers to particular elements, for the fabrication of sensing elements and of indicators for safe storage and freshness of food. While other sensors and indicators in food storage or other applications can differ in the requirements targeted for humidity sensing and amine monitoring, the methods presented in this thesis can be used in the sensing of other analytes such as ethylene gas or other organic volatile compounds in produce.

The materials studied in this thesis were found to have the potential to be used in intelligent packaging that can allow the monitoring of storage conditions and freshness of food. These materials can be used to engineer devices and elements that provide dynamic feedback to the consumer on the actual conditions of a product. This information can be a tool to reduce food waste by informing consumers about the quality and safety of food, and has the potential to be extended to applications of intelligent packaging in pharmaceuticals, electronics, medicine, and others.

Future work

The different studies in this thesis open the opportunity to answer new questions about some of the materials and methods here discussed.

The study of the effects of geometry and processing on the sensing properties of low-resistivity CPCs opens the door to manufacture and characterize RFID components. For instance, sensing elements in the integrated circuit or the antenna can be fabricated with CPCs that change in resistivity as consequence of changes in relative humidity, leading to changes in the response from the RFID. Techniques such as inkjet and direct write printing can be used to pattern responsive elements within RFIDs.

In addition, future work may include experiments that can determine the selectivity of these the CPCs here studied. The response to changes in other stimuli such as temperature and pressure should be also evaluated. While this study focused on polymer matrices which swell in response to water, the composition of the matrix could be tailored to enable sensing of other analytes such as volatile organic compounds.

Based on the study of the response of PLA-g-SAh to amines, new responsive polymer composites as sensing elements in sensors for amines can be engineered. Using PLA-g-SAh as matrix and conducting elements such as silver particles, this CPC would potentially react to amines by increasing hygroscopicity, swelling more water after the SAh groups in the grafted polymer react with amine groups. As studied in Chapter 3, this swelling would then lead to an increase in electrical resistivity, producing a signal for the increase in concentration of amines.

Finally, the study of color change indicators for methylamine opens up the opportunity to test their response to other volatile amines associated with fish and meat freshness. In addition to

this, it would be valuable to conduct tests with samples of commercial fish and meat. These tests would make the use of color change indicators for monitoring fish and meat freshness more robust.

References

1. FAO Global Food Losses and Food Waste: Extent, Causes and Prevention, Rome, 2011.
2. Nikkel, L., Maguire, M., Gooch, M., Bucknell, D., LaPlain, D., Dent, B., Whitehead, P., Felfel, A. The avoidable crisis of Food Waste: The Roadmap, Ontario, Canada, 2019.
3. FAO Food Wastage Footprint: Full Cost Accounting, 2014.
4. Hoekstra, A. Y.; Mekonnen, M. M. The water footprint of humanity, *Proc. Natl. Acad. Sci.*, **2012**, *vol. 109, no. 9*, pp. 3232–3237. DOI: 10.1073/pnas.1109936109.
5. Arvanitoyannis, I. S.; Stratakos, A. C. Application of Modified Atmosphere Packaging and Active/Smart Technologies to Red Meat and Poultry: A Review, *Food Bioprocess Technol.*, **2012**, *vol. 5, no. 5*, pp. 1423–1446. DOI: 10.1007/s11947-012-0803-z.
6. Poyatos-Racionero, E.; Ros-Lis, J. V.; Vivancos, J. L.; Martínez-Máñez, R. Recent advances on intelligent packaging as tools to reduce food waste, *J. Clean. Prod.*, **2018**, *vol. 172*, pp. 3398–3409. DOI: 10.1016/j.jclepro.2017.11.075.
7. Lee, S. J.; Rahman, A. T. M. M. *Intelligent Packaging for Food Products*. Elsevier Ltd, 2013.
8. Zou, Y.; Wan, H.; Zhang, X.; Ha, D.; Wang, P. Electronic Nose and Electronic Tongue, in *Bioinspired Smell and Taste Sensors*, P. Wang, Q. Liu, C. Wu, and K. J. Hsia, Eds. Dordrecht: Springer Netherlands, 2015, pp. 19–44.
9. Kerry, J. P.; O'Grady, M. N.; Hogan, S. A. Past, current and potential utilisation of active and intelligent packaging systems for meat and muscle-based products: A review, *Meat Sci.*, **2006**, *vol. 74, no. 1*, pp. 113–130. DOI: 10.1016/j.meatsci.2006.04.024.
10. Jeong, B.; Gutowska, A. Lessons from nature: stimuli-responsive polymers and their biomedical applications, *Trends Biotechnol.*, **2002**, *vol. 20, no. 7*, pp. 305–311. DOI: 10.1016/S0167-7799(02)01962-5.
11. Bajpai, A. K.; Shukla, S. K.; Bhanu, S.; Kankane, S. Responsive polymers in controlled drug delivery, *Prog. Polym. Sci.*, **2008**, *vol. 33, no. 11*, pp. 1088–1118. DOI: 10.1016/j.progpolymsci.2008.07.005.
12. Balint, R.; Cassidy, N. J.; Cartmell, S. H. Conductive polymers: Towards a smart biomaterial for tissue engineering, *Acta Biomater.*, **2014**, *vol. 10, no. 6*, pp. 2341–2353. DOI: 10.1016/j.actbio.2014.02.015.
13. Hu, J.; Liu, S. Responsive Polymers for Detection and Sensing Applications: Current Status and Future Developments, *Macromolecules*, **2010**, *vol. 43, no. 20*, pp. 8315–8330. DOI:

10.1021/ma1005815.

14. Berg, L.; Lentz, C. P. Effect of Relative Humidity, Temperature, and Length of Storage on Decay and Quality of Potatoes and Onions, *J. Food Sci.*, **1973**, *vol. 38, no. 1*, pp. 81–83. DOI: 10.1111/j.1365-2621.1973.tb02781.x.

15. Lee, S. J.; Si, J.; Yun, H. S.; Ko, G. The Effect of Temperature and Relative Humidity on the Survival of Foodborne Viruses during Food Storage, *Appl. Environ. Microbiol.* , **2015**. DOI: 10.1128/AEM.04093-14.

16. Suma, A.; Sreenivasan, K.; Singh, A. K.; Radhamani, J. Role of relative humidity in processing and storage of seeds and assessment of variability in storage behaviour in brassica spp. and Eruca sativa, *Sci. World J.*, **2013**, *vol. 2013*. DOI: 10.1155/2013/504141.

17. Zhuang, Z.; Qi, D.; Zhao, C.; Na, H. A novel highly sensitive humidity sensor derived from sulfonated poly(ether ether ketone) with metal salts-ion substitution, *Sensors Actuators B Chem.*, **2016**, *vol. 236*, pp. 701–711. DOI: 10.1016/j.snb.2016.06.063.

18. Hamouche, H.; Makhlouf, S.; Chaouchi, A.; Laghrouche, M. Humidity Sensor Based on Keratin bio Polymer Film, *Sensors Actuators A Phys.*, **2018**, *vol. 282*, pp. 132–141. DOI: 10.1016/j.sna.2018.09.025.

19. Fei, T.; Dai, J.; Jiang, K.; Zhao, H.; Zhang, T. Stable cross-linked amphiphilic polymers from a one-pot reaction for application in humidity sensors, *Sensors Actuators B Chem.*, **2016**, *vol. 227*, pp. 649–654. DOI: 10.1016/j.snb.2016.01.038.

20. Lin, Q.; Li, Y.; Yang, M. Highly sensitive and ultrafast response surface acoustic wave humidity sensor based on electrospun polyaniline/poly(vinyl butyral) nanofibers, *Anal. Chim. Acta*, **2012**, *vol. 748*, pp. 73–80. DOI: 10.1016/j.aca.2012.08.041.

21. Trigo-López, M.; Muñoz, A.; Ibeas, S.; García, F. C.; Serna, F.; García, J. M. Solid sensory polymer kit for the easy and rapid determination of the concentration of water in organic solvents and ambient humidity, *Sensors Actuators B Chem.*, **2014**, *vol. 191*, pp. 233–238. DOI: 10.1016/j.snb.2013.09.099.

22. Luo, H. *et al.* Shape memory-enhanced water sensing of conductive polymer composites, *Mater. Lett.*, **2015**, *vol. 161*, pp. 189–192. DOI: 10.1016/j.matlet.2015.08.105.

23. Banimuslem, H. *et al.* Dye-modified carbon nanotubes for the optical detection of amines vapours, *Sensors Actuators B Chem.*, **2015**, *vol. 207*, pp. 224–234. DOI: 10.1016/j.snb.2014.10.046.

24. Rodríguez-Méndez, M. L.; Gay, M.; Apetrei, C.; De Saja, J. A. Biogenic amines and fish freshness assessment using a multisensor system based on voltammetric electrodes. Comparison between CPE

and screen-printed electrodes, *Electrochim. Acta*, **2009**, *vol. 54, no. 27*, pp. 7033–7041. DOI: 10.1016/j.electacta.2009.07.024.

25. Lázaro, C. A. *et al.* Biogenic amines as bacterial quality indicators in different poultry meat species, *LWT - Food Sci. Technol.*, **2015**, *vol. 60, no. 1*, pp. 15–21. DOI: 10.1016/j.lwt.2014.09.025.

26. Lopera-Valle, A.; Elias, A. Low-resistance silver microparticle-HEMA-PEGDA composites for humidity sensing, *Smart Mater. Struct.*, **2018**, *vol. 27, no. 10*, pp. 1–16. DOI: 10.1088/1361-665X/aad355.

27. Khot, L. R.; Panigrahi, S.; Lin, D. Development and evaluation of piezoelectric-polymer thin film sensors for low concentration detection of volatile organic compounds related to food safety applications, *Sensors Actuators B Chem.*, **2011**, *vol. 153, no. 1*, pp. 1–10. DOI: 10.1016/j.snb.2010.05.043.

28. Pavase, T. R. *et al.* Recent advances of conjugated polymer (CP) nanocomposite-based chemical sensors and their applications in food spoilage detection: A comprehensive review, *Sensors Actuators B Chem.*, **2018**, *vol. 273*, pp. 1113–1138. DOI: 10.1016/J.SNB.2018.06.118.

29. Jin, Y.-J.; Kwak, G. Detection of biogenic amines using a nitrated conjugated polymer, *Sensors Actuators B Chem.*, **2018**, *vol. 271*, pp. 183–188. DOI: 10.1016/J.SNB.2018.05.091.

30. Häußler, L.; Wienhold, U.; Albrecht, V.; Zschoche, S. Simultaneous TA and MS analysis of alternating styrene-maleic anhydride and styrene-maleimide copolymers, *Thermochim. Acta*, **1996**, *vol. 277, no. 1–2*, pp. 17–27. DOI: 10.1016/0040-6031(95)02518-9.

31. Schaefer, D.; Cheung, W. M. Smart Packaging: Opportunities and Challenges, *Procedia CIRP*, **2018**, *vol. 72*, pp. 1022–1027. DOI: 10.1016/j.procir.2018.03.240.

32. Yam, K. L.; Takhistov, P. T.; Miltz, J. Intelligent Packaging: Concepts and Applications, *J. Food Sci.*, **2005**, *vol. 70, no. 1*, pp. R1–R10. DOI: 10.1111/j.1365-2621.2005.tb09052.x.

33. Steenis, N. D.; van Herpen, E.; van der Lans, I. A.; Ligthart, T. N.; van Trijp, H. C. M. Consumer response to packaging design: The role of packaging materials and graphics in sustainability perceptions and product evaluations, *J. Clean. Prod.*, **2017**, *vol. 162*, pp. 286–298. DOI: 10.1016/j.jclepro.2017.06.036.

34. Bolumar, T.; Andersen, M. L.; Orlien, V. Antioxidant active packaging for chicken meat processed by high pressure treatment, *Food Chem.*, **2011**, *vol. 129, no. 4*, pp. 1406–1412. DOI: 10.1016/j.foodchem.2011.05.082.

35. Li, W.; Li, L.; Cao, Y.; Lan, T.; Chen, H.; Qin, Y. Effects of PLA Film Incorporated with ZnO Nanoparticle on the Quality Attributes of Fresh-Cut Apple, *Nanomaterials*, **2017**, *vol. 7, no. 8*, p.

207. DOI: 10.3390/nano7080207.

36. Lin, Z.; Decker, E. A.; Goddard, J. M. Preparation of metal chelating active packaging materials by laminated photografting, *J. Coatings Technol. Res.*, **2016**, *vol. 13, no. 2*, pp. 395–404. DOI: 10.1007/s11998-015-9767-z.

37. Johnson, D. R.; Tian, F.; Roman, M. J.; Decker, E. A.; Goddard, J. M. Development of Iron-Chelating Poly(ethylene terephthalate) Packaging for Inhibiting Lipid Oxidation in Oil-in-Water Emulsions, *J. Agric. Food Chem.*, **2015**, *vol. 63, no. 20*, pp. 5055–5060. DOI: 10.1021/acs.jafc.5b00796.

38. Ahn, B. J.; Gaikwad, K. K.; Lee, Y. S. Characterization and properties of LDPE film with gallic-acid-based oxygen scavenging system useful as a functional packaging material, *J. Appl. Polym. Sci.*, **2016**, *vol. 133, no. 43*. DOI: 10.1002/app.44138.

39. Kaewklin, P.; Siripatrawan, U.; Suwanagul, A.; Lee, Y. S. Active packaging from chitosan-titanium dioxide nanocomposite film for prolonging storage life of tomato fruit, *Int. J. Biol. Macromol.*, **2018**, *vol. 112*, pp. 523–529. DOI: 10.1016/j.ijbiomac.2018.01.124.

40. Vilela, C. *et al.* A concise guide to active agents for active food packaging, *Trends Food Sci. Technol.*, **2018**, *vol. 80*, pp. 212–222. DOI: 10.1016/j.tifs.2018.08.006.

41. Vanderroost, M.; Ragaert, P.; Devlieghere, F.; De Meulenaer, B. Intelligent food packaging: The next generation, *Trends Food Sci. Technol.*, **2014**, *vol. 39, no. 1*, pp. 47–62. DOI: 10.1016/j.tifs.2014.06.009.

42. Kuswandi, B.; Wicaksono, Y.; Jayus; Abdullah, A.; Heng, L. Y.; Ahmad, M. Smart packaging: sensors for monitoring of food quality and safety, *Sens. Instrum. Food Qual. Saf.*, **2011**, *vol. 5, no. 3–4*, pp. 137–146. DOI: 10.1007/s11694-011-9120-x.

43. Brockgreitens, J.; Abbas, A. Responsive Food Packaging: Recent Progress and Technological Prospects, *Compr. Rev. Food Sci. Food Saf.*, **2016**, *vol. 15, no. 1*, pp. 3–15. DOI: 10.1111/1541-4337.12174.

44. Donsì, F.; Annunziata, M.; Sessa, M.; Ferrari, G. Nanoencapsulation of essential oils to enhance their antimicrobial activity in foods, *LWT - Food Sci. Technol.*, **2011**, *vol. 44, no. 9*, pp. 1908–1914. DOI: 10.1016/j.lwt.2011.03.003.

45. Fathi, M.; Mozafari, M. R.; Mohebbi, M. Nanoencapsulation of food ingredients using lipid based delivery systems, *Trends Food Sci. Technol.*, **2012**, *vol. 23, no. 1*, pp. 13–27. DOI: 10.1016/j.tifs.2011.08.003.

46. Müller, P.; Schmid, M. Intelligent Packaging in the Food Sector: A Brief Overview, *Foods*, **2019**,

vol. 8, no. 1, p. 16. DOI: 10.3390/foods8010016.

47. Kuckling, D.; Doering, A.; Krahl, F.; Arndt, K.-F. Stimuli-Responsive Polymer Systems, in *Polymer Science: A Comprehensive Reference*, Elsevier, 2012, pp. 377–413.

48. Schmaljohann, D. Thermo- and pH-responsive polymers in drug delivery, *Adv. Drug Deliv. Rev.*, **2006**, *vol. 58, no. 15*, pp. 1655–1670. DOI: 10.1016/J.ADDR.2006.09.020.

49. Roy, D.; Brooks, W. L. A.; Sumerlin, B. S. New directions in thermoresponsive polymers, *Chem. Soc. Rev.*, **2013**, *vol. 42, no. 17*, p. 7214. DOI: 10.1039/c3cs35499g.

50. Ward, M. A.; Georgiou, T. K. Thermoresponsive Polymers for Biomedical Applications, *Polymers (Basel).*, **2011**, *vol. 3, no. 3*, pp. 1215–1242. DOI: 10.3390/polym3031215.

51. Schacher, F. H.; Rupar, P. A.; Manners, I. Functional Block Copolymers: Nanostructured Materials with Emerging Applications, *Angew. Chemie Int. Ed.*, **2012**, *vol. 51, no. 32*, pp. 7898–7921. DOI: 10.1002/anie.201200310.

52. Capek, I. Nature and properties of ionomer assemblies. II, *Adv. Colloid Interface Sci.*, **2005**, *vol. 118, no. 1–3*, pp. 73–112. DOI: 10.1016/j.cis.2005.06.005.

53. Stuart, M. A. C. *et al.* Emerging applications of stimuli-responsive polymer materials, *Nat. Mater.*, **2010**, *vol. 9, no. 2*, pp. 101–113. DOI: 10.1038/nmat2614.

54. Seyfoori, A.; Seyyed Ebrahimi, S. A.; Yousefi, A.; Akbari, M. Efficient targeted cancer cell detection, isolation and enumeration using immuno-nano/hybrid magnetic microgels, *Biomater. Sci.*, **2019**. DOI: 10.1039/C9BM00552H.

55. Tomatsu, I.; Peng, K.; Kros, A. Photoresponsive hydrogels for biomedical applications, *Adv. Drug Deliv. Rev.*, **2011**, *vol. 63, no. 14–15*, pp. 1257–1266. DOI: 10.1016/j.addr.2011.06.009.

56. Sun, X.-Z.; Wang, X.; Wu, J.-Z.; Li, S.-D. Development of thermosensitive microgel-loaded cotton fabric for controlled drug release, *Appl. Surf. Sci.*, **2017**, *vol. 403*, pp. 509–518. DOI: 10.1016/j.apsusc.2017.01.198.

57. Tavakoli, J.; Tang, Y. Hydrogel Based Sensors for Biomedical Applications: An Updated Review, *Polymers (Basel).*, **2017**, *vol. 9, no. 12*, p. 364. DOI: 10.3390/polym9080364.

58. Biji, K. B.; Ravishankar, C. N.; Mohan, C. O.; Srinivasa Gopal, T. K. Smart packaging systems for food applications: a review, *J. Food Sci. Technol.*, **2015**, *vol. 52, no. 10*, pp. 6125–6135. DOI: 10.1007/s13197-015-1766-7.

59. Nguyen, H. Q.; Ta, B. Q.; Hoivik, N.; Halvorsen, E.; Aasmundtveit, K. E. Carbon nanotube based gas sensor for expiration detection of perishable food, in *2013 13th IEEE International Conference on Nanotechnology (IEEE-NANO 2013)*, 2013, pp. 675–678.

60. Medeiros, E. S.; Gregório, R.; Martinez, R. A.; Mattoso, L. H. C. A Taste Sensor Array Based on Polyaniline Nanofibers for Orange Juice Quality Assessment, *Sens. Lett.*, **2009**, *vol. 7, no. 1*, pp. 24–30. DOI: 10.1166/sl.2009.1005.

61. Matindoust, S.; Farzi, A.; Baghaei Nejad, M.; Shahrokh Abadi, M. H.; Zou, Z.; Zheng, L.-R. Ammonia gas sensor based on flexible polyaniline films for rapid detection of spoilage in protein-rich foods, *J. Mater. Sci. Mater. Electron.*, **2017**, *vol. 28, no. 11*, pp. 7760–7768. DOI: 10.1007/s10854-017-6471-z.

62. Tripathi, A.; Misra, K. P.; Shukla, R. K. Enhancement in ammonia sensitivity with fast response by doping Al 2 O 3 in polyaniline, *J. Appl. Polym. Sci.*, **2013**, *vol. 130, no. 3*, pp. 1941–1948. DOI: 10.1002/app.39379.

63. Liu, M.-C.; Dai, C.-L.; Chan, C.-H.; Wu, C.-C. Manufacture of a Polyaniline Nanofiber Ammonia Sensor Integrated with a Readout Circuit Using the CMOS-MEMS Technique, *Sensors*, **2009**, *vol. 9, no. 2*, pp. 869–880. DOI: 10.3390/s90200869.

64. Huang, X. *et al.* Reduced graphene oxide–polyaniline hybrid: Preparation, characterization and its applications for ammonia gas sensing, *J. Mater. Chem.*, **2012**, *vol. 22, no. 42*, p. 22488. DOI: 10.1039/c2jm34340a.

65. López-Rubio, A.; Lagarón, J. M.; Ocio, M. J. Active Polymer Packaging of Non-Meat Food Products, in *Smart Packaging Technologies for Fast Moving Consumer Goods*, Chichester, UK: John Wiley & Sons, Ltd, 2008, pp. 19–32.

66. Smolander, M. Freshness Indicators for Food Packaging, in *Smart Packaging Technologies for Fast Moving Consumer Goods*, Chichester, UK: John Wiley & Sons, Ltd, 2008, pp. 111–127.

67. Lloyd, K.; Mirosa, M.; Birch, J. Active and Intelligent Packaging, in *Encyclopedia of Food Chemistry*, *vol. 3*, Elsevier, 2019, pp. 177–182.

68. Pennanen, K. *et al.* European Consumers' Perceptions of Time-Temperature Indicators in Food Packaging, *Packag. Technol. Sci.*, **2015**, *vol. 28, no. 4*, pp. 303–323. DOI: 10.1002/pts.2105.

69. Realini, C. E.; Marcos, B. Active and intelligent packaging systems for a modern society, *Meat Sci.*, **2014**, *vol. 98, no. 3*, pp. 404–419. DOI: 10.1016/j.meatsci.2014.06.031.

70. Galagan, Y.; Su, W.-F. Fadable ink for time–temperature control of food freshness: Novel new time–temperature indicator, *Food Res. Int.*, **2008**, *vol. 41, no. 6*, pp. 653–657. DOI: 10.1016/j.foodres.2008.04.012.

71. Lu, L.; Zheng, W.; Lv, Z.; Tang, Y. Development and Application of Time-temperature Indicators Used on Food during the Cold Chain Logistics, *Packag. Technol. Sci.*, **2013**, *vol. 26*, pp. 80–90.

DOI: 10.1002/pts.2009.

72. Anbukarasu, P.; Sauvageau, D.; Elias, A. L. Time-Temperature Indicator Based on Enzymatic Degradation of Dye-Loaded Polyhydroxybutyrate, *Biotechnol. J.*, **2017**, *vol. 12, no. 9*, pp. 1–9. DOI: 10.1002/biot.201700050.

73. Tamplin, M. L. Integrating predictive models and sensors to manage food stability in supply chains, *Food Microbiol.*, **2018**, *vol. 75*, pp. 90–94. DOI: 10.1016/j.fm.2017.12.001.

74. Fang, Z.; Zhao, Y.; Warner, R. D.; Johnson, S. K. Active and intelligent packaging in meat industry, *Trends Food Sci. Technol.*, **2017**, *vol. 61, no. 2*, pp. 60–71. DOI: 10.1016/j.tifs.2017.01.002.

75. Kalpana, S.; Priyadarshini, S. R.; Maria Leena, M.; Moses, J. A.; Anandharamakrishnan, C. Intelligent Packaging: Trends and Applications in Food Systems, *Trends Food Sci. Technol.*, **2019**. DOI: 10.1016/j.tifs.2019.09.008.

76. Ganji, F.; Abdekhodaie, M. J. Chitosan–g-PLGA copolymer as a thermosensitive membrane, *Carbohydr. Polym.*, **2010**, *vol. 80, no. 3*, pp. 740–746. DOI: 10.1016/j.carbpol.2009.12.021.

77. Gil, E.; Hudson, S. Stimuli-reponsive polymers and their bioconjugates, *Prog. Polym. Sci.*, **2004**, *vol. 29, no. 12*, pp. 1173–1222. DOI: 10.1016/j.progpolymsci.2004.08.003.

78. Zamanlui, S.; Amirabad, L. M.; Soleimani, M.; Faghihi, S. Influence of hydrodynamic pressure on chondrogenic differentiation of human bone marrow mesenchymal stem cells cultured in perfusion system, *Biologicals*, **2018**, *vol. 56*, pp. 1–8. DOI: 10.1016/j.biologicals.2018.04.004.

79. Tavagnacco, L.; Zaccarelli, E.; Chiessi, E. On the molecular origin of the cooperative coil-to-globule transition of poly(N -isopropylacrylamide) in water, *Phys. Chem. Chem. Phys.*, **2018**, *vol. 20, no. 15*, pp. 9997–10010. DOI: 10.1039/C8CP00537K.

80. Yang, J. M.; Yang, S. J.; Lin, H. T.; Wu, T.-H.; Chen, H.-J. Chitosan containing PU/Poly(NIPAAm) thermosensitive membrane for wound dressing, *Mater. Sci. Eng. C*, **2008**, *vol. 28, no. 1*, pp. 150–156. DOI: 10.1016/j.msec.2007.01.011.

81. Hong, S. Y. *et al.* High-Sensitivity, Skin-Attachable, and Stretchable Array of Thermo-Responsive Suspended Gate Field-Effect Transistors with Thermochromic Display, *Adv. Funct. Mater.*, **2019**, *vol. 29, no. 6*, p. 1807679. DOI: 10.1002/adfm.201807679.

82. Lavrenova, A.; Balkenende, D. W. R.; Sagara, Y.; Schrettl, S.; Simon, Y. C.; Weder, C. Mechano- and Thermoresponsive Photoluminescent Supramolecular Polymer, *J. Am. Chem. Soc.*, **2017**, *vol. 139, no. 12*, pp. 4302–4305. DOI: 10.1021/jacs.7b00342.

83. Hoffman, A. S. *et al.* Really smart bioconjugates of smart polymers and receptor proteins, *J. Biomed. Mater. Res.*, **2000**, *vol. 52, no. 4*, pp. 577–586. DOI: 10.1002/1097-4636(20001215)52:4<577::AID-

JBM1>3.0.CO;2-5.

84. Liu, C.; Qin, H.; Mather, P. T. Review of progress in shape-memory polymers, *J. Mater. Chem.*, **2007**, *vol. 17, no. 16*, p. 1543. DOI: 10.1039/b615954k.

85. Xie, T. Tunable polymer multi-shape memory effect, *Nature*, **2010**, *vol. 464, no. 7286*, pp. 267–270. DOI: 10.1038/nature08863.

86. Mauritz, K. A.; Moore, R. B. State of Understanding of Nafion, *Chem. Rev.*, **2004**, *vol. 104, no. 10*, pp. 4535–4586. DOI: 10.1021/cr0207123.

87. Page, K. A.; Cable, K. M.; Moore, R. B. Molecular Origins of the Thermal Transitions and Dynamic Mechanical Relaxations in Perfluorosulfonate Ionomers, *Macromolecules*, **2005**, *vol. 38, no. 15*, pp. 6472–6484. DOI: 10.1021/ma0503559.

88. Kim, Y. H.; Wool, R. P. A theory of healing at a polymer-polymer interface, *Macromolecules*, **1983**, *vol. 16, no. 7*, pp. 1115–1120. DOI: 10.1021/ma00241a013.

89. Wojtecki, R. J.; Meador, M. A.; Rowan, S. J. Using the dynamic bond to access macroscopically responsive structurally dynamic polymers, *Nat. Mater.*, **2011**, *vol. 10, no. 1*, pp. 14–27. DOI: 10.1038/nmat2891.

90. Ghosh, B.; Urban, M. W. Self-Repairing Oxetane-Substituted Chitosan Polyurethane Networks, *Science (80-.).*, **2009**, *vol. 323, no. 5920*, pp. 1458–1460. DOI: 10.1126/science.1167391.

91. Blaiszik, B. J.; Kramer, S. L. B.; Olugebefola, S. C.; Moore, J. S.; Sottos, N. R.; White, S. R. Self-Healing Polymers and Composites, *Annu. Rev. Mater. Res.*, **2010**, *vol. 40, no. 1*, pp. 179–211. DOI: 10.1146/annurev-matsci-070909-104532.

92. Kunzelman, J.; Crenshaw, B. R.; Kinami, M.; Weder, C. Self-Assembly and Dispersion of Chromogenic Molecules: A Versatile and General Approach for Self-Assessing Polymers, *Macromol. Rapid Commun.*, **2006**, *vol. 27, no. 23*, pp. 1981–1987. DOI: 10.1002/marc.200600642.

93. Seeboth, A.; Lötzsch, D.; Ruhmann, R.; Muehling, O. Thermochromic Polymers—Function by Design, *Chem. Rev.*, **2014**, *vol. 114, no. 5*, pp. 3037–3068. DOI: 10.1021/cr400462e.

94. Zarrintaj, P. *et al.* Thermo-sensitive polymers in medicine: A review, *Eur. Polym. J.*, **2019**, *vol. 117*, pp. 402–423. DOI: 10.1016/j.eurpolymj.2019.05.024.

95. Fuciños, C.; Fuciños, P.; Míguez, M.; Katime, I.; Pastrana, L. M.; Rúa, M. L. Temperature- and pH-Sensitive Nanohydrogels of Poly(N-Isopropylacrylamide) for Food Packaging Applications: Modelling the Swelling-Collapse Behaviour, *PLoS One*, **2014**, *vol. 9, no. 2*, p. e87190. DOI: 10.1371/journal.pone.0087190.

96. Vu, C. H. T.; Won, K. Novel water-resistant UV-activated oxygen indicator for intelligent food

packaging, *Food Chem.*, **2013**, *vol. 140, no. 1–2*, pp. 52–56. DOI: 10.1016/j.foodchem.2013.02.056.

97. Mills, A.; Lawrie, K.; Bardin, J.; Apedaile, A.; Skinner, G. A.; O'Rourke, C. An O 2 smart plastic film for packaging, *Analyst*, **2012**, *vol. 137, no. 1*, pp. 106–112. DOI: 10.1039/C1AN15774D.

98. Li, Y.; Yang, M. J.; She, Y. Humidity sensitive properties of crosslinked and quaternized poly(4-vinylpyridine-co-butyl methacrylate), *Sensors Actuators B Chem.*, **2005**, *vol. 107, no. 1*, pp. 252–257. DOI: 10.1016/j.snb.2004.10.008.

99. Lee, S.; Park, J.-W. Reversible humidity-driven tuning of the light scattering properties of PS:PEG-based porous polymer films: Understanding derived from the cross-sensitivity of a luminescent oxygen sensor, *Sensors Actuators B Chem.*, **2019**, *vol. 298*, p. 126883. DOI: 10.1016/j.snb.2019.126883.

100. Kerry, J. P. New Packaging Technologies, Materials and Formats for Fast-Moving Consumer Products, in *Innovations in Food Packaging*, *2nd ed.*, J. A. Han, Ed. London, UK: Elsevier Ltd., 2014, pp. 549–584.

101. Hogan, S. A.; Kerry, J. P. Smart Packaging of Meat and Poultry Products, in *Smart Packaging Technologies for Fast Moving Consumer Goods*, Chichester, UK: John Wiley & Sons, Ltd, 2008, pp. 33–59.

102. Choi, I.; Lee, J. Y.; Lacroix, M.; Han, J. Intelligent pH indicator film composed of agar/potato starch and anthocyanin extracts from purple sweet potato, *Food Chem.*, **2017**, *vol. 218*, pp. 122–128. DOI: 10.1016/j.foodchem.2016.09.050.

103. Philippova, O. E.; Hourdet, D.; Audebert, R.; Khokhlov, A. R. pH-Responsive Gels of Hydrophobically Modified Poly(acrylic acid), *Macromolecules*, **1997**, *vol. 30, no. 26*, pp. 8278–8285. DOI: 10.1021/ma970957v.

104. Drozdov, A. D.; Christiansen, J. deClaville; Sanporean, C.-G. Inhomogeneous swelling of pH-responsive gels, *Int. J. Solids Struct.*, **2016**, *vol. 87*, pp. 11–25. DOI: 10.1016/j.ijsolstr.2016.02.037.

105. Tonge, S. .; Tighe, B. . Responsive hydrophobically associating polymers: a review of structure and properties, *Adv. Drug Deliv. Rev.*, **2001**, *vol. 53, no. 1*, pp. 109–122. DOI: 10.1016/S0169-409X(01)00223-X.

106. Connal, L. A.; Li, Q.; Quinn, J. F.; Tjipto, E.; Caruso, F.; Qiao, G. G. pH-Responsive Poly(acrylic acid) Core Cross-Linked Star Polymers: Morphology Transitions in Solution and Multilayer Thin Films, *Macromolecules*, **2008**, *vol. 41, no. 7*, pp. 2620–2626. DOI: 10.1021/ma7019557.

107. He, E.; Yue, C. Y.; Tam, K. C. Association Behavior of Star-Shaped pH-Responsive Block Copolymer: Four-Arm Poly(ethylene oxide)- b -Poly(methacrylic acid) in Aqueous Medium,

Langmuir, **2009**, *vol. 25, no. 9*, pp. 4892–4899. DOI: 10.1021/la804056p.

108. Lee, A. S.; Bütün, V.; Vamvakaki, M.; Armes, S. P.; Pople, J. A.; Gast, A. P. Structure of pH-Dependent Block Copolymer Micelles: Charge and Ionic Strength Dependence, *Macromolecules*, **2002**, *vol. 35, no. 22*, pp. 8540–8551. DOI: 10.1021/ma0114842.

109. Chen, J.-K.; Chang, C.-J. Fabrications and Applications of Stimulus-Responsive Polymer Films and Patterns on Surfaces: A Review, *Materials (Basel).*, **2014**, *vol. 7, no. 2*, pp. 805–875. DOI: 10.3390/ma7020805.

110. Tang, H.; Zhao, W.; Yu, J.; Li, Y.; Zhao, C. Recent Development of pH-Responsive Polymers for Cancer Nanomedicine, *Molecules*, **2018**, *vol. 24, no. 1*, p. 4. DOI: 10.3390/molecules24010004.

111. Park, S. Y.; Bae, Y. H. Novel pH-sensitive polymers containing sulfonamide groups, *Macromol. Rapid Commun.*, **1999**, *vol. 20, no. 5*, pp. 269–273. DOI: 10.1002/(SICI)1521-3927(19990501)20:5<269::AID-MARC269>3.0.CO;2-3.

112. Nakamura, M.; Sanji, T.; Tanaka, M. Fluorometric sensing of biogenic amines with aggregation-induced emission-active tetraphenylethenes, *Chem. - A Eur. J.*, **2011**, *vol. 17, no. 19*, pp. 5344–5349. DOI: 10.1002/chem.201003285.

113. Boscher, N. D. *et al.* Optical sensing responses of CrIIICl(TPP)(H2O)-based coatings obtained by an atmospheric pressure plasma method – Application to the detection of volatile amines, *Sensors Actuators B Chem.*, **2014**, *vol. 191*, pp. 553–560. DOI: 10.1016/j.snb.2013.10.044.

114. Pacquit, A.; Lau, K.; McLaughlin, H.; Frisby, J.; Quilty, B.; Diamond, D. Development of a volatile amine sensor for the monitoring of fish spoilage, *Talanta*, **2006**, *vol. 69, no. 2*, pp. 515–520. DOI: 10.1016/j.talanta.2005.10.046.

115. Pacquit, A. *et al.* Development of a smart packaging for the monitoring of fish spoilage, *Food Chem.*, **2007**, *vol. 102, no. 2*, pp. 466–470. DOI: 10.1016/j.foodchem.2006.05.052.

116. Zhong, X. *et al.* Rapid and ultrasensitive detection of biogenic amines with colorimetric sensor array, *Sensors Actuators, B Chem.*, **2018**, *vol. 274, no. October 2017*, pp. 464–471. DOI: 10.1016/j.snb.2018.07.129.

117. Kuswandi, B.; Jayus; Restyana, A.; Abdullah, A.; Heng, L. Y.; Ahmad, M. A novel colorimetric food package label for fish spoilage based on polyaniline film, *Food Control*, **2012**, *vol. 25, no. 1*, pp. 184–189. DOI: 10.1016/j.foodcont.2011.10.008.

118. Kuswandi, B.; Jayus; Oktaviana, R.; Abdullah, A.; Heng, L. Y. A Novel On-Package Sticker Sensor Based on Methyl Red for Real-Time Monitoring of Broiler Chicken Cut Freshness, *Packag. Technol. Sci.*, **2014**, *vol. 27, no. 1*, pp. 69–81. DOI: 10.1002/pts.2016.

119. Kuswandi, B.; Jayus; Larasati, T. S.; Abdullah, A.; Heng, L. Y. Real-Time Monitoring of Shrimp Spoilage Using On-Package Sticker Sensor Based on Natural Dye of Curcumin, *Food Anal. Methods*, **2012**, *vol. 5, no. 4*, pp. 881–889. DOI: 10.1007/s12161-011-9326-x.

120. Ma, Q.; Liang, T.; Cao, L.; Wang, L. Intelligent poly (vinyl alcohol)-chitosan nanoparticles-mulberry extracts films capable of monitoring pH variations, *Int. J. Biol. Macromol.*, **2018**, *vol. 108*, pp. 576–584. DOI: 10.1016/j.ijbiomac.2017.12.049.

121. Moreira, J. B.; Terra, A. L. M.; Costa, J. A. V.; Morais, M. G. de Development of pH indicator from PLA/PEO ultrafine fibers containing pigment of microalgae origin, *Int. J. Biol. Macromol.*, **2018**, *vol. 118*, pp. 1855–1862. DOI: 10.1016/j.ijbiomac.2018.07.028.

122. Wu, C. *et al.* Preparation of an intelligent film based on chitosan/oxidized chitin nanocrystals incorporating black rice bran anthocyanins for seafood spoilage monitoring, *Carbohydr. Polym.*, **2019**, *vol. 222*, p. 115006. DOI: 10.1016/j.carbpol.2019.115006.

123. Liang, T.; Wang, L. A pH-Sensing Film from Tamarind Seed Polysaccharide with Litmus Lichen Extract as an Indicator, *Polymers (Basel).*, **2017**, *vol. 10, no. 1*, p. 13. DOI: 10.3390/polym10010013.

124. Kurek, M.; Garofulić, I. E.; Bakić, M. T.; Ščetar, M.; Uzelac, V. D.; Galić, K. Development and evaluation of a novel antioxidant and pH indicator film based on chitosan and food waste sources of antioxidants, *Food Hydrocoll.*, **2018**, *vol. 84*, pp. 238–246. DOI: 10.1016/j.foodhyd.2018.05.050.

125. Jung, J.; Puligundla, P.; Ko, S. Proof-of-concept study of chitosan-based carbon dioxide indicator for food packaging applications, *Food Chem.*, **2012**, *vol. 135, no. 4*, pp. 2170–2174. DOI: 10.1016/j.foodchem.2012.07.090.

126. Lee, K.; Ko, S. Proof-of-concept study of a whey protein isolate based carbon dioxide indicator to measure the shelf-life of packaged foods, *Food Sci. Biotechnol.*, **2014**, *vol. 23, no. 1*, pp. 115–120. DOI: 10.1007/s10068-014-0015-6.

127. Saliu, F.; Della Pergola, R. Carbon dioxide colorimetric indicators for food packaging application: Applicability of anthocyanin and poly-lysine mixtures, *Sensors Actuators B Chem.*, **2018**, *vol. 258*, pp. 1117–1124. DOI: 10.1016/j.snb.2017.12.007.

128. Wang, Y. *et al.* CO2-responsive Polymeric Fluorescent Sensor with Ultrafast Response, *Chinese J. Polym. Sci.*, **2018**, *vol. 36, no. 12*, pp. 1321–1327. DOI: 10.1007/s10118-018-2167-y.

129. Sun, H.; Chen, X.; Han, X.; Liu, H. Dual Thermoresponsive Aggregation of Schizophrenic PDMAEMA- b -PSBMA Copolymer with an Unrepeatable pH Response and a Recycled CO 2 /N 2 Response, *Langmuir*, **2017**, *vol. 33, no. 10*, pp. 2646–2654. DOI: 10.1021/acs.langmuir.7b00065.

130. Chen, S.; Yu, H.; Zhao, C.; Hu, R.; Zhu, J.; Li, L. Indolo[3,2 -b]carbazole derivative as a fluorescent probe for fluoride ion and carbon dioxide detections, *Sensors Actuators B Chem.*, **2017**, *vol. 250*, pp. 591–600. DOI: 10.1016/j.snb.2017.05.012.

131. Ma, Y.; Promthaveepong, K.; Li, N. CO 2 -Responsive Polymer-Functionalized Au Nanoparticles for CO 2 Sensor, *Anal. Chem.*, **2016**, *vol. 88, no. 16*, pp. 8289–8293. DOI: 10.1021/acs.analchem.6b02133.

132. Li, Y. Humidity sensors using in situ synthesized sodium polystyrenesulfonate/ZnO nanocomposites, *Talanta*, **2004**, *vol. 62, no. 4*, pp. 707–712. DOI: 10.1016/j.talanta.2003.09.011.

133. Geng, L.; Zhao, Y.; Huang, X.; Wang, S.; Zhang, S.; Wu, S. Characterization and gas sensitivity study of polyaniline/SnO2 hybrid material prepared by hydrothermal route, *Sensors Actuators B Chem.*, **2007**, *vol. 120, no. 2*, pp. 568–572. DOI: 10.1016/J.SNB.2006.03.009.

134. Dong, L. *et al.* Highly sensitive vapor detection of amines with fluorescent conjugated polymer: A novel lasing turn-on sensory mechanism, *Sensors Actuators B Chem.*, **2013**, *vol. 180*, pp. 28–34. DOI: 10.1016/j.snb.2011.11.046.

135. Pablos, J. L. *et al.* Polymer chemosensors as solid films and coated fibres for extreme acidity colorimetric sensing, *J. Mater. Chem. A*, **2015**, *vol. 3, no. 6*, pp. 2833–2843. DOI: 10.1039/C4TA06009A.

136. Wang, X.; Si, Y.; Wang, J.; Ding, B.; Yu, J.; Al-Deyab, S. S. A facile and highly sensitive colorimetric sensor for the detection of formaldehyde based on electro-spinning/netting nano-fiber/nets, *Sensors Actuators B Chem.*, **2012**, *vol. 163, no. 1*, pp. 186–193. DOI: 10.1016/j.snb.2012.01.033.

137. He, D.-F. *et al.* An UV equipped box for photoactivation with a fluorescent coordination polymer for recognizing amine gases by “turn-color” in air, *Sensors Actuators B Chem.*, **2017**, *vol. 247*, pp. 238–244. DOI: 10.1016/J.SNB.2017.02.178.

138. Azzouz, A.; Vikrant, K.; Kim, K.-H.; Ballesteros, E.; Rhadfi, T.; Malik, A. K. Advances in colorimetric and optical sensing for gaseous volatile organic compounds, *TrAC Trends Anal. Chem.*, **2019**, *vol. 118*, pp. 502–516. DOI: 10.1016/j.trac.2019.06.017.

139. Sanjuán, A. M.; Reglero Ruiz, J. A.; García, F. C.; García, J. M. Recent developments in sensing devices based on polymeric systems, *React. Funct. Polym.*, **2018**, *vol. 133*, pp. 103–125. DOI: 10.1016/j.reactfunctpolym.2018.10.007.

140. iPolycond Consortium *Introduction to Conductive Polymer Composites*, *First ed.* Shrewsbury, UK: Smithers Rapra Technology, 2011.

141. Pang, H.; Xu, L.; Yan, D.-X. X.; Li, Z.-M. M. Conductive polymer composites with segregated structures, *Prog. Polym. Sci.*, **2014**, *vol. 39, no. 11*, pp. 1908–1933. DOI: 10.1016/j.progpolymsci.2014.07.007.

142. Kong, I. *Polymers with Nano-Encapsulated Functional Polymers*. Elsevier Inc., 2016.

143. Mohd Radzuan, N. A.; Sulong, A. B.; Sahari, J. A review of electrical conductivity models for conductive polymer composite, *Int. J. Hydrogen Energy*, **2016**. DOI: 10.1016/j.ijhydene.2016.03.045.

144. Feller, J. F.; Castro, M.; Kumar, B. Polymer–carbon nanotube conductive nanocomposites for sensing, in *Polymercarbon nanotube composites Preparation properties and applications*, Woodhead Publishing Limited, 2011, pp. 760–803.

145. Lux, F. Models proposed to explain the electrical conductivity of mixtures made of conductive and insulating materials, *J. Mater. Sci.*, **1993**, *vol. 28, no. 2*, pp. 285–301. DOI: 10.1007/BF00357799.

146. Ruschau, G. R.; Yoshikawa, S.; Newnham, R. E. Resistivities of conductive composites, *J. Appl. Phys.*, **1992**, *vol. 72, no. 3*, pp. 953–959. DOI: 10.1063/1.352350.

147. Stru¨Mpler, R.; Glatz-Reichenbach, J. FEATURE ARTICLE Conducting Polymer Composites, *J. Electroceramics*, **1999**, *vol. 3, no. 4*, pp. 329–346. DOI: 10.1023/a:1009909812823.

148. Zavickis, J.; Linarts, A.; Knite, M. The downshift of the electrical percolation threshold in polyisoprene-nanostructured carbon composites, *Energetika*, **2011**, *vol. 57, no. 1*. DOI: 10.6001/energetika.v57i1.2043.

149. Celzard, A.; McRae, E.; Marêché, J. F.; Furdin, G.; Sundqvist, B. Conduction mechanisms in some graphite–polymer composites: Effects of temperature and hydrostatic pressure, *J. Appl. Phys.*, **1998**, *vol. 83, no. 3*, pp. 1410–1419. DOI: 10.1063/1.366904.

150. Nilsson, F. *et al.* Simulating the effective electric conductivity of polymer composites with high aspect ratio fillers, *Compos. Sci. Technol.*, **2016**, *vol. 132*, pp. 16–23. DOI: 10.1016/j.compscitech.2016.06.008.

151. Cesano, F. *et al.* Relationship between morphology and electrical properties in PP/MWCNT composites: Processing-induced anisotropic percolation threshold, *Mater. Chem. Phys.*, **2016**, *vol. 180*, pp. 284–290. DOI: 10.1016/j.matchemphys.2016.06.009.

152. Grossiord, N. *et al.* High-conductivity polymer nanocomposites obtained by tailoring the characteristics of carbon nanotube fillers, *Adv. Funct. Mater.*, **2008**, *vol. 18, no. 20*, pp. 3226–3234. DOI: 10.1002/adfm.200800528.

153. Kim, D.; Kim, Y.; Choi, K.; Grunlan, J.; Yu, C. Improved Thermoelectric Behavior of, *ACS Nano*,

2010, *vol. 4, no. 1*, pp. 513–523. .

154. Mierczynska, A. *et al.* Effects of expandable graphite and modified ammonium polyphosphate on the flame-retardant and mechanical properties of wood flour-polypropylene composites, *Polym. Polym. Compos.*, **2013**, *vol. 21, no. 7*, pp. 449–456. DOI: 10.1002/app.

155. Al-Saleh, M. H.; Gelves, G. A.; Sundararaj, U. Copper nanowire/polystyrene nanocomposites: Lower percolation threshold and higher EMI shielding, *Compos. Part A Appl. Sci. Manuf.*, **2011**, *vol. 42, no. 1*, pp. 92–97. DOI: 10.1016/j.compositesa.2010.10.003.

156. Lu, J. *et al.* Chemo-sensitivity of latex-based films containing segregated networks of carbon nanotubes, *Sensors Actuators B Chem.*, **2011**, *vol. 155, no. 1*, pp. 28–36. DOI: 10.1016/j.snb.2010.11.017.

157. Kumar, B.; Park, Y. T.; Castro, M.; Grunlan, J. C.; Feller, J. F. Fine control of carbon nanotubes–polyelectrolyte sensors sensitivity by electrostatic layer by layer assembly (eLbL) for the detection of volatile organic compounds (VOC), *Talanta*, **2012**, *vol. 88*, pp. 396–402. DOI: 10.1016/j.talanta.2011.11.006.

158. Liu, Q.; Tai, H.; Yuan, Z.; Zhou, Y.; Su, Y.; Jiang, Y. A High-Performances Flexible Temperature Sensor Composed of Polyethyleneimine/Reduced Graphene Oxide Bilayer for Real-Time Monitoring, *Adv. Mater. Technol.*, **2019**, *vol. 4, no. 3*, p. 1800594. DOI: 10.1002/admt.201800594.

159. Huang, Y. *et al.* High-resolution flexible temperature sensor based graphite-filled polyethylene oxide and polyvinylidene fluoride composites for body temperature monitoring, *Sensors Actuators A Phys.*, **2018**, *vol. 278*, pp. 1–10. DOI: 10.1016/j.sna.2018.05.024.

160. Nassira, H. *et al.* Gelatin-Graphene Nanocomposites with Ultralow Electrical Percolation Threshold, *Adv. Mater.*, **2016**, *vol. 28, no. 32*, pp. 6914–6920. DOI: 10.1002/adma.201601115.

161. Qi, H.; Liu, J.; Pionteck, J.; Potschke, P.; Mader, E. Carbon nanotube-cellulose composite aerogels for vapour sensing, *Sensors Actuators, B Chem.*, **2015**, *vol. 213*, pp. 20–26. DOI: 10.1016/j.snb.2015.02.067.

162. Knite, M.; Ozols, K.; Zavickis, J.; Tupureina, V.; Klemenoks, I.; Orlovs, R. Elastomer – Carbon Nanotube Composites as Prospective Multifunctional Sensing Materials, *J. Nanosci. Nanotechnol.*, **2009**, *vol. 9, no. 6*, pp. 3587–3592. DOI: 10.1166/jnn.2009.NS34.

163. Levin, Z. S.; Robert, C.; Feller, J. F.; Castro, M.; Grunlan, J. C. Flexible latex—polyaniline segregated network composite coating capable of measuring large strain on epoxy, *Smart Mater. Struct.*, **2013**, *vol. 22, no. 1*, p. 15008. .

164. Nakano, H.; Shimizu, K.; Takahashi, S.; Kono, A.; Ougizawa, T.; Horibe, H. Resistivity–

temperature characteristics of filler-dispersed polymer composites, *Polymer (Guildf).*, **2012**, *vol. 53, no. 26*, pp. 6112–6117. DOI: 10.1016/j.polymer.2012.10.046.

165. Zha, J.-W. W.; Li, W.-K. K.; Liao, R.-J. J.; Bai, J. B.; Dang, Z.-M. M. High performance hybrid carbon fillers/binary–polymer nanocomposites with remarkably enhanced positive temperature coefficient effect of resistance, *J. Mater. Chem. A*, **2013**, *vol. 1, no. 3*, pp. 843–851. DOI: 10.1039/C2TA00429A.

166. Király, A.; Ronkay, F. Temperature dependence of electrical properties in conductive polymer composites, *Polym. Test.*, **2015**, *vol. 43*, pp. 154–162. DOI: 10.1016/j.polymertesting.2015.03.011.

167. Wei, X.-P.; Luo, Y.-L.; Xu, F.; Chen, Y.-S. Sensitive conductive polymer composites based on polylactic acid filled with multiwalled carbon nanotubes for chemical vapor sensing, *Synth. Met.*, **2016**, *vol. 215*, pp. 216–222. DOI: 10.1016/j.synthmet.2016.02.023.

168. Lee, C.-Y.; Lee, G.-B. Humidity Sensors: A Review, *Sens. Lett.*, **2005**, *vol. 3, no. 1*, pp. 1–15. DOI: 10.1166/sl.2005.001.

169. Chen, Z.; Lu, C. Humidity Sensors: A Review of Materials and Mechanisms, *Sens. Lett.*, **2005**, *vol. 3, no. 4*, pp. 274–295. DOI: 10.1166/sl.2005.045.

170. Singh, P.; Shekhar Kushwaha, C.; Shukla, S. K.; Dubey, G. C. Synthesis and humidity sensing property of α-Fe 2 O 3 and polyaniline composite, *Mater. Today Proc.*, **2018**, *vol. 5, no. 3*, pp. 9118–9125. DOI: 10.1016/j.matpr.2017.10.030.

171. Kafy, A.; Akther, A.; Shishir, M. I. R.; Kim, H. C.; Yun, Y.; Kim, J. Cellulose nanocrystal/graphene oxide composite film as humidity sensor, *Sensors Actuators A Phys.*, **2016**, *vol. 247*, pp. 221–226. DOI: 10.1016/j.sna.2016.05.045.

172. K. Shukla, S.; Bharadvaja, A.; K. Parashar, G.; P. Mishra, A.; C. Dubey, G.; Tiwari, A. Fabrication Of Ultra-sensitive Optical Fiber Based Humidity Sensor Using TiO2 thin Film, *Adv. Mater. Lett.*, **2012**, *vol. 3, no. 5*, pp. 365–370. DOI: 10.5185/amlett.2012.5350.

173. Lee, J.; Cho, D.; Jeong, Y. A resistive-type sensor based on flexible multi-walled carbon nanotubes and polyacrylic acid composite films, *Solid. State. Electron.*, **2013**, *vol. 87*, pp. 80–84. DOI: 10.1016/j.sse.2013.05.001.

174. Buenger, D.; Topuz, F.; Groll, J. Hydrogels in sensing applications, *Prog. Polym. Sci.*, **2012**, *vol. 37, no. 12*, pp. 1678–1719. DOI: 10.1016/j.progpolymsci.2012.09.001.

175. Baird, J. A.; Olayo-Valles, R.; Rinaldi, C.; Taylor, L. S. Effect of Molecular Weight, Temperature, and Additives on the Moisture Sorption Properties of Polyethylene Glycol, *J. Pharm. Sci.*, **2010**, *vol. 99, no. 1*, pp. 154–168. DOI: 10.1002/jps.21808.

176. Groll, J. *et al.* Biofunctionalized, Ultrathin Coatings of Cross-Linked Star-Shaped Poly(ethylene oxide) Allow Reversible Folding of Immobilized Proteins, *J. Am. Chem. Soc.*, **2004**, *vol. 126, no. 13*, pp. 4234–4239. DOI: 10.1021/ja0318028.

177. Lee, S. *et al.* Fabrication of high-quality single-crystal Cu thin films using radio-frequency sputtering., *Sci. Rep.*, **2014**, *vol. 4*, p. 6230. DOI: 10.1038/srep06230.

178. Sun, G.; Chu, C. C. Synthesis, characterization of biodegradable dextran-allyl isocyanate-ethylamine/polyethylene glycol-diacrylate hydrogels and their in vitro release of albumin, *Carbohydr. Polym.*, **2006**, *vol. 65, no. 3*, pp. 273–287. DOI: 10.1016/j.carbpol.2006.01.015.

179. Lee, H.; Chung, S.; Kim, M.-G.; Lee, L. P.; Lee, J. Y. Near-Infrared-Light-Assisted Photothermal Polymerization for Transdermal Hydrogelation and Cell Delivery., *Adv. Healthc. Mater.*, **2016**, *vol. 5, no. 13*, pp. 1638–45. DOI: 10.1002/adhm.201600048.

180. Lee, S. H.; Lee, W. G.; Chung, B. G.; Park, J. H.; Khademhosseini, A. Rapid Formation of Acrylated Microstructures by Microwave-Induced Thermal Crosslinking, *Macromol. Rapid Commun.*, **2009**, *vol. 30, no. 16*, pp. 1382–1386. DOI: 10.1002/marc.200900199.

181. Kim, K. M.; Poliquit, B. Z.; Lee, Y.-G.; Won, J.; Ko, J. M.; Cho, W. Il Enhanced separator properties by thermal curing of poly(ethylene glycol)diacrylate-based gel polymer electrolytes for lithium-ion batteries, *Electrochim. Acta*, **2014**, *vol. 120*, pp. 159–166. DOI: 10.1016/j.electacta.2013.12.077.

182. Pardeshi, C. V.; Belgamwar, V. S. Controlled synthesis of N,N,N-trimethyl chitosan for modulated bioadhesion and nasal membrane permeability, *Int. J. Biol. Macromol.*, **2016**, *vol. 82*, pp. 933–944. DOI: 10.1016/j.ijbiomac.2015.11.012.

183. Andreani, T. *et al.* Effect of mucoadhesive polymers on the in vitro performance of insulin-loaded silica nanoparticles: Interactions with mucin and biomembrane models, *Eur. J. Pharm. Biopharm.*, **2015**, *vol. 93*, pp. 118–126. DOI: 10.1016/j.ejpb.2015.03.027.

184. Eshel-Green, T.; Eliyahu, S.; Avidan-Shlomovich, S.; Bianco-Peled, H. PEGDA hydrogels as a replacement for animal tissues in mucoadhesion testing, *Int. J. Pharm.*, **2016**, *vol. 506, no. 1*, pp. 25–34. DOI: 10.1016/j.ijpharm.2016.04.019.

185. Lee, N. Y.; Jung, Y. K.; Park, H. G. On-chip colorimetric biosensor based on polydiacetylene (PDA) embedded in photopolymerized poly(ethylene glycol) diacrylate (PEG-DA) hydrogel, *Biochem. Eng. J.*, **2006**, *vol. 29, no. 1*, pp. 103–108. DOI: 10.1016/j.bej.2005.02.025.

186. Havens, N.; Trihn, P.; Kim, D.; Luna, M.; Wanekaya, A. K.; Mugweru, A. Redox polymer covalently modified multiwalled carbon nanotube based sensors for sensitive acetaminophen and ascorbic acid detection, *Electrochim. Acta*, **2010**, *vol. 55, no. 6*, pp. 2186–2190. DOI:

10.1016/j.electacta.2009.11.054.

187. Kumar, B.; Castro, M.; Feller, J. F. Poly(lactic acid)-multi-wall carbon nanotube conductive biopolymer nanocomposite vapour sensors, *Sensors Actuators, B Chem.*, **2012**, *vol. 161, no. 1*, pp. 621–628. DOI: 10.1016/j.snb.2011.10.077.

188. Su, P. G.; Chiu, S. R.; Lin, Y. Te Flexibility and electrical and humidity-sensing properties of N-substituted pyrrole derivatives and composite films of Au nanoparticles/N-substituted pyrrole derivatives, *Sensors Actuators, B Chem.*, **2016**, *vol. 224*, pp. 833–840. DOI: 10.1016/j.snb.2015.10.077.

189. Rastogi, P. K.; Ganesan, V.; Krishnamoorthi, S. A promising electrochemical sensing platform based on a silver nanoparticles decorated copolymer for sensitive nitrite determination, *J. Mater. Chem. A*, **2014**, *vol. 2*, pp. 933–943. DOI: 10.1039/c3ta13794e.

190. Ghosale, A.; Shankar, R.; Ganesan, V.; Shrivas, K. Direct-Writing of Paper Based Conductive Track using Silver Nano-ink for Electroanalytical Application, *Electrochim. Acta*, **2016**, *vol. 209*, pp. 511–520. DOI: 10.1016/j.electacta.2016.05.109.

191. Fiddes, L. K.; Chang, J.; Yan, N. Electrochemical detection of biogenic amines during food spoilage using an integrated sensing RFID tag, *Sensors Actuators, B Chem.*, **2014**, *vol. 202*, pp. 1298–1304. DOI: 10.1016/j.snb.2014.05.106.

192. Skinner, G. A. 11 – Smart labelling of foods and beverages, in *Advances in Food and Beverage Labelling*, 2015, pp. 191–205.

193. Nopwinyuwong, A.; Trevanich, S.; Suppakul, P. Development of a novel colorimetric indicator label for monitoring freshness of intermediate-moisture dessert spoilage, *Talanta*, **2010**, *vol. 81, no. 3*, pp. 1126–1132. DOI: 10.1016/j.talanta.2010.02.008.

194. Lorwongtragool, P.; Wisitsoraat, A.; Kerdcharoen, T. An electronic nose for amine detection based on polymer/SWNT-COOH nanocomposites, *INEC 2010 - 2010 3rd Int. Nanoelectron. Conf. Proc.*, **2010**, *no. c*, pp. 73–74. DOI: 10.1109/INEC.2010.5424531.

195. Bibi, F.; Guillaume, C.; Gontard, N.; Sorli, B. A review: RFID technology having sensing aptitudes for food industry and their contribution to tracking and monitoring of food products, *Trends Food Sci. Technol.*, **2017**, *vol. 62*, pp. 91–103. DOI: 10.1016/j.tifs.2017.01.013.

196. Zhu, R.; Desroches, M.; Yoon, B.; Swager, T. M. Wireless Oxygen Sensors Enabled by Fe(II)-Polymer Wrapped Carbon Nanotubes, *ACS Sensors*, **2017**, *vol. 2, no. 7*, pp. 1044–1050. DOI: 10.1021/acssensors.7b00327.

197. Quintero, A. V. *et al.* Smart RFID label with a printed multisensor platform for environmental

monitoring, *Flex. Print. Electron.*, **2016**, *vol. 1, no. 2*, p. 025003. DOI: 10.1088/2058-8585/1/2/025003.

198. Eom, K.-H.; Hyun, K.-H.; Lin, S.; Kim, J.-W. The Meat Freshness Monitoring System Using the Smart RFID Tag, *Int. J. Distrib. Sens. Networks*, **2014**, *vol. 10, no. 7*, p. 591812. DOI: 10.1155/2014/591812.

199. Oprea, A.; Barsan, N.; Weimar, U.; Bauersfeld, M.-L.; Ebling, D.; Wollenstein, J. Capacitive Humidity Sensors on Flexible RFID Labels, in *TRANSDUCERS 2007 - 2007 International Solid-State Sensors, Actuators and Microsystems Conference*, 2007, pp. 2039–2042.

200. Salmerón, J. F. *et al.* Printed single-chip UHF passive radio frequency identification tags with sensing capability, *Sensors Actuators A Phys.*, **2014**, *vol. 220*, pp. 281–289. DOI: 10.1016/j.sna.2014.10.023.

201. Shukla, S. K. *et al.* Nano-like magnesium oxide films and its significance in optical fiber humidity sensor, *Sensors Actuators B Chem.*, **2004**, *vol. 98, no. 1*, pp. 5–11. DOI: 10.1016/j.snb.2003.05.001.

202. Rittersma, Z. M.; Zaagman, W. J.; Zetstra, M.; Benecke, W. A monitoring instrument with capacitive porous silicon humidity sensors, *Smart Mater. Struct.*, **2000**, *vol. 9, no. 3*, p. 351. .

203. Dabhade, R. .; Bodas, D. S.; Gangal, S. . Plasma-treated polymer as humidity sensing material—a feasibility study, *Sensors Actuators B Chem.*, **2004**, *vol. 98, no. 1*, pp. 37–40. DOI: 10.1016/j.snb.2003.08.020.

204. Rittersma, Z. M. Recent achievements in miniaturised humidity sensors—a review of transduction techniques, *Sensors Actuators A Phys.*, **2002**, *vol. 96, no. 2*, pp. 196–210. DOI: 10.1016/S0924-4247(01)00788-9.

205. Sakai, Y.; Matsuguchi, M.; Yonesato, N. Humidity sensor based on alkali salts of poly(2-acrylamido-2-methylpropane sulfonic acid), *Electrochim. Acta*, **2001**, *vol. 46, no. 10*, pp. 1509–1514. DOI: 10.1016/S0013-4686(00)00746-5.

206. Xu, S.; Yu, W.; Yao, X.; Zhang, Q.; Fu, Q. Nanocellulose-assisted dispersion of graphene to fabricate poly(vinyl alcohol)/graphene nanocomposite for humidity sensing, *Compos. Sci. Technol.*, **2016**, *vol. 131*, pp. 67–76. DOI: 10.1016/j.compscitech.2016.05.014.

207. Ru, J. *et al.* A moisture and electric coupling stimulated ionic polymer-metal composite actuator with controllable deformation behavior, *Smart Mater. Struct.*, **2018**, *vol. 27, no. 2*, p. 02LT01. .

208. Ru, J.; Wang, Y.; Chang, L.; Chen, H.; Li, D. Preparation and characterization of water-soluble carbon nanotube reinforced Nafion membranes and so-based ionic polymer metal composite actuators, *Smart Mater. Struct.*, **2016**, *vol. 25, no. 9*, p. 95006. .

209. Peng, X. *et al.* A flexible humidity sensor based on KC–MWCNTs composites, *Appl. Surf. Sci.*, **2016**, *vol. 387*, pp. 149–154. DOI: 10.1016/j.apsusc.2016.05.108.

210. Park, M.-S.; Lim, T.-H.; Jeon, Y.-M.; Kim, J.-G.; Joo, S.-W.; Gong, M.-S. Humidity sensitive properties of copoly(TEAMPS/VP)/silver nanocomposite films, *Sensors Actuators B Chem.*, **2008**, *vol. 133, no. 1*, pp. 166–173. DOI: 10.1016/j.snb.2008.02.008.

211. Pandiyarajan, C. K.; Prucker, O.; Ruhe, J. Humidity Driven Swelling of the Surface-Attached Poly(N-alkylacrylamide) Hydrogels, *Macromolecules*, **2016**, *vol. 49, no. 21*, pp. 8254–8264. DOI: 10.1021/acs.macromol.6b01379.

212. Porter, T. L.; Stewart, R.; Reed, J.; Morton, K. Models of Hydrogel Swelling with Applications to Hydration Sensing, *Sensors*, **2007**, *vol. 7, no. 9*, pp. 1980–1991. DOI: 10.3390/s7091980.

213. Gerlach, G.; Arndt, K.-F. Hydrogel Sensors and Actuators, *Springer Ser. Chem. Sensors Biosens.*, **2009**, *vol. 6*, pp. 1–15. DOI: 10.1007/b100321.

214. Ganji, F.; Vasheghani-Farahani, S.; Vasheghani-Farahani, E. Theoretical Description of Hydrogel Swelling: A Review, *Iran. Polym. J.*, **2010**, *vol. 19, no. 5*, pp. 375–398. DOI: 10.1007/s12303-009-0004-6.

215. Wu, D.; Zhang, X.; Chu, C.-C. Synthesis, characterization and drug release from three-arm poly(ε-caprolactone) maleic acid/poly(ethylene glycol) diacrylate hydrogels, *J. Biomater. Sci. Polym. Ed.*, **2003**, *vol. 14, no. 8*, pp. 37–41. DOI: 10.1163/156856203768366521.

216. Tan, G.; Wang, Y.; Li, J.; Zhang, S. Synthesis and Characterization of Injectable Photocrosslinking Poly (ethylene glycol) Diacrylate based Hydrogels , *Polym. Bull.*, **2008**, *vol. 61, no. 1*, pp. 91–98. DOI: 10.1007/s00289-008-0932-8.

217. González-Henríquez, C. M.; Pizarro, G. del C.; Sarabia-Vallejos, M. A.; Terraza, C. A.; López-Cabaña, Z. E. In situ-preparation and characterization of silver-HEMA/PEGDA hydrogel matrix nanocomposites: Silver inclusion studies into hydrogel matrix, *Arab. J. Chem.*, **2014**. DOI: 10.1016/j.arabjc.2014.11.012.

218. Figueiredo, A. *et al.* Biocompatible Bacterial Cellulose-Poly(2-hydroxyethyl methacrylate) Nanocomposite Films, *Biomed Res. Int.*, **2013**, *vol. 2013*, pp. 1–14. .

219. Foo, E.; Jaafar, M.; Aziz, A.; Sim, L. C. Properties of spin coated epoxy/silica thin film composites: Effect of nano- and micron-size fillers, *Compos. Part A Appl. Sci. Manuf.*, **2011**, *vol. 42, no. 10*, pp. 1432–1437. DOI: 10.1016/j.compositesa.2011.06.007.

220. Schmidt, R. H.; Kinloch, I. A.; Burgess, A. N.; Windle, A. H. The Effect of Aggregation on the Electrical Conductivity of Spin-Coated Polymer/Carbon Nanotube Composite Films, *Langmuir*,

2007, *vol. 23, no. 10*, pp. 5707–5712. DOI: 10.1021/la062794m.

221. Rivadeneyra, A.; Fernández-Salmerón, J.; Agudo-Acemel, M.; López-Villanueva, J. A.; Palma, A. J.; Capitan-Vallvey, L. F. A printed capacitive–resistive double sensor for toluene and moisture sensing, *Sensors Actuators B Chem.*, **2015**, *vol. 210*, pp. 542–549. DOI: 10.1016/j.snb.2015.01.036.

222. Inc., M. E. Material Product Data Sheet: Silver Conductor 6105, Chicago, USA, 2016.

223. Le Roux, J. D.; Paul, D. R. Preparation of composite membranes by a spin coating process, *J. Memb. Sci.*, **1992**, *vol. 74, no. 3*, pp. 233–252. DOI: 10.1016/0376-7388(92)80064-Q.

224. Moradi, M.-A. *et al.* Bimodal Latex Effect on Spin-Coated Thin Conductive Polymer–Single-Walled Carbon Nanotube Layers, *Langmuir*, **2015**, *vol. 31, no. 44*, pp. 11982–11988. DOI: 10.1021/acs.langmuir.5b02756.

225. Ghosh, S. S. *et al.* Why specific mixed solvent composition leads to appropriate film formation of composite during spin coating?, *Appl. Phys. Lett.*, **2013**, *vol. 102, no. 5*, pp. 1–6. DOI: 10.1063/1.4791696.

226. Ogi, T.; Modesto-Lopez, L. B.; Iskandar, F.; Okuyama, K. Fabrication of a large area monolayer of silica particles on a sapphire substrate by a spin coating method, *Colloids Surfaces A Physicochem. Eng. Asp.*, **2007**, *vol. 297, no. 1–3*, pp. 71–78. DOI: 10.1016/j.colsurfa.2006.10.027.

227. Standard, A. *ASTM D2584: Standard Test Method for Ignition Loss of Glass Strands and Fabrics*, *vol. 1, no. August*. 2005.

228. ASTM Standard *ASTM D3171: Standard Test Methods for Constituent Content of Composite Materials*, *no. May 2009*. 2010.

229. Kaw, A. *Mechanics of Composite Materials*. 2006.

230. Sigma-Aldrich Product Specification Sheet: Poly(ethylene glycol) diacrylate - average Mn 575, St. Louis, USA, 2017.

231. Sigma-Aldrich Product Specification Sheet: 2-Hydroxyethyl methacrylate, St. Louis, USA, 2017.

232. Brumby, A. *et al.* Silver, Silver Compounds, and Silver Alloys, in *Ullmann's Encyclopedia of Industrial Chemistry*, *6th ed.*, Hoboken, USA: John Wiley and Sons, Inc, 2008, p. 21.

233. Esmaeli, E.; Ganjian, M.; Rastegar, H.; Kolahdouz, M.; Kolahdouz, Z.; Zhang, G. Q. Humidity sensor based on the ionic polymer metal composite, *Sensors Actuators B Chem.*, **2017**, *vol. 247*, pp. 498–504. DOI: 10.1016/j.snb.2017.03.018.

234. Lowrie, W. *Fundamentals of Geophysics*, *2007th ed.* New York, NY, USA: Cambridge University Press, 2007.

235. Muster, T. H.; Prestidge, C. A.; Hayes, R. A. Water adsorption kinetics and contact angles of silica

particles, *Colloids Surfaces A Physicochem. Eng. Asp.*, **2001**, *vol. 176, no. 2–3*, pp. 253–266. DOI: 10.1016/S0927-7757(00)00600-2.

236. Sadeqi-Moqadam, M.; Riahi, S.; Bahramian, A. An investigation into the electrical behavior of oil/water/reservoir rock interfaces: The implication for improvement in wettability prediction, *Colloids Surfaces A Physicochem. Eng. Asp.*, **2016**, *vol. 490*, pp. 268–282. DOI: 10.1016/j.colsurfa.2015.11.040.

237. Agboola, O.; Sadiku, E. R.; Mokrani, T. Nanomembrane Materials Based on Polymer Blends, in *Design and Applications of Nanostructured Polymer Blends and Nanocomposite Systems*, Elsevier Inc., 2016, pp. 101–123.

238. Liu, T.; Ozisik, R.; Siegel, R. W. Phase separation and surface morphology of spin-coated films of polyetherimide/polycaprolactone immiscible polymer blends, *Thin Solid Films*, **2007**, *vol. 515, no. 5*, pp. 2965–2973. DOI: 10.1016/j.tsf.2006.08.049.

239. Li, X.; Han, Y.; An, L. Surface morphology control of immiscible polymer-blend thin films, *Polymer (Guildf).*, **2003**, *vol. 44, no. 26*, pp. 8155–8165. DOI: 10.1016/j.polymer.2003.10.012.

240. Münch, A.; Please, C. P.; Wagner, B. Spin coating of an evaporating polymer solution, *Phys. Fluids*, **2011**, *vol. 23, no. 10*, pp. 24–29. DOI: 10.1063/1.3643692.

241. Uchida, S.; Murakami, T.; Iwamura, T.; Ishige, R.; Ando, S. Enhanced thermal conductivity in immiscible polyimide blend composites with needle-shaped ZnO particles, *RSC Adv.*, **2017**, *vol. 7*, pp. 15492–15499. DOI: 10.1039/c7ra00760d.

242. Kokkinis, D.; Schaffner, M.; Studart, A. R. Multimaterial magnetically assisted 3D printing of composite materials, *Nat. Commun.*, **2015**, *vol. 6*, p. 8643. .

243. Compton, B. G.; Lewis, J. A. 3D-printing of lightweight cellular composites, *Adv. Mater.*, **2014**, *vol. 26, no. 34*, pp. 5930–5935. DOI: 10.1002/adma.201401804.

244. Li, W. *et al.* Flexible Circuits and Soft Actuators by Printing Assembly of Graphene, *ACS Appl. Mater. Interfaces*, **2016**, *vol. 8, no. 19*, pp. 12369–12376. DOI: 10.1021/acsami.6b04235.

245. Hirota, E.; Ute, K.; Uehara, M.; Kitayama, T.; Tanaka, M.; Mochizuki, A. Study on blood compatibility with poly(2-methoxyethylacrylate) - Relationship between surface structure, water structure, and platelet compatibility in 2-methoxyethylacrylate/2-hydroxyethylmethacrylate diblock copolymer, *J. Biomed. Mater. Res. - Part A*, **2006**, *vol. 76, no. 3*, pp. 540–550. DOI: 10.1002/jbm.a.30563.

246. Wu, Y. H.; Park, H. B.; Kai, T.; Freeman, B. D.; Kalika, D. S. Water uptake, transport and structure characterization in poly(ethylene glycol) diacrylate hydrogels, *J. Memb. Sci.*, **2010**, *vol. 347, no. 1–*

2, pp. 197–208. DOI: 10.1016/j.memsci.2009.10.025.

247. Caldorera-Moore, M. *et al.* Swelling behavior of nanoscale, shape- and size-specific, hydrogel particles fabricated using imprint lithography, *Soft Matter*, **2011**, *vol. 7, no. 6*, p. 2879. DOI: 10.1039/c0sm01185a.

248. Bayer, I. S.; Martiradonna, L.; Athanassiou, A. Nanostructured Lubricated Silver Flake/Polymer Composites Exhibiting Robust Superhydrophobicity, in *Advances in Contact Angle, Wettability and Adhesion*, *2013 (vol.*, Beverly, MA, USA: John Wiley & Sons, Inc., 2013, pp. 203–225.

249. Siddiqui, M. N.; Redhwi, H. H.; Tsagkalias, I.; Softas, C.; Ioannidou, M. D.; Achilias, D. S. Synthesis and characterization of poly(2-hydroxyethyl methacrylate)/silver hydrogel nanocomposites prepared via in situ radical polymerization, *Thermochim. Acta*, **2016**, *vol. 643*, pp. 53–64. DOI: 10.1016/j.tca.2016.09.017.

250. Morita, S. Hydrogen-bonds structure in poly(2-hydroxyethyl methacrylate) studied by temperature-dependent infrared spectroscopy, *Front. Chem.*, **2014**, *vol. 2*, p. 10. DOI: 10.3389/fchem.2014.00010.

251. Morita, S.; Kitagawa, K.; Ozaki, Y. Hydrogen-bond structures in poly(2-hydroxyethyl methacrylate): Infrared spectroscopy and quantum chemical calculations with model compounds, *Vib. Spectrosc.*, **2009**, *vol. 51, no. 1*, pp. 28–33. DOI: 10.1016/j.vibspec.2008.09.008.

252. Lee, W.-F.; Huang, Y.-C. Swelling and antibacterial properties for the superabsorbent hydrogels containing silver nanoparticles, *J. Appl. Polym. Sci.*, **2007**, *vol. 106, no. 3*, pp. 1992–1999. DOI: 10.1002/app.26906.

253. Chandra Babu, A.; Prabhakar, M. N.; Suresh Babu, A.; Mallikarjuna, B.; Subha, M. C. S.; Chowdoji Rao, K. Development and characterization of semi-IPN silver nanocomposite hydrogels for antibacterial applications, *Int. J. Carbohydr. Chem.*, **2013**, *vol. 2013*, pp. 1–8. DOI: 10.1155/2013/243695.

254. Zellander, A. *et al.* Characterization of Pore Structure in Biologically Functional Poly(2-Hydroxyethyl Methacrylate) - Poly(Ethylene Glycol) Diacrylate (PHEMA-PEGDA), *PLoS One*, **2014**, *vol. 9, no. 5*, p. e96709. DOI: 10.1371/journal.pone.0096709.

255. Forney, C. F. Optimizing the Storage Temperature and Humidity for Fresh Cranberries: A Reassessment of Chilling Sensitivity, *HortScience* , **2008**, *vol. 43, no. 2*, pp. 439–446. .

256. Ahmad, Z.; Zafar, Q.; Sulaiman, K.; Akram, R.; Karimov, K. S. A Humidity Sensing Organic-Inorganic Composite for Environmental Monitoring, *Sensors (Basel).*, **2013**, *vol. 13, no. 3*, pp. 3615–3624. DOI: 10.3390/s130303615.

257. Farahani, H.; Wagiran, R.; Hamidon, M. N. Humidity Sensors Principle, Mechanism, and Fabrication Technologies: A Comprehensive Review, *Sensors (Basel).*, **2014**, *vol. 14, no. 5*, pp. 7881–7939. DOI: 10.3390/s140507881.

258. Ahmadipour, M.; Ain, M. F.; Ahmad, Z. A. Effect of thickness on surface morphology, optical and humidity sensing properties of RF magnetron sputtered CCTO thin films, *Appl. Surf. Sci.*, **2016**, *vol. 385*, pp. 182–190. DOI: 10.1016/j.apsusc.2016.05.098.

259. Huang, B. L. and P. T. L. and G. Q. L. and S. H. Z. and M. Q. Effects of ceramic-film thickness on humidity sensitivity of Al/Ba 1- x La x Nb y Ti 1- y O 3 /SiO 2 /Si structure, *Smart Mater. Struct.*, **2002**, *vol. 11, no. 4*, p. 504. .

260. Tripathy, A.; Sharma, P.; Sahoo, N.; Pramanik, S.; Abu Osman, N. A. Moisture sensitive inimitable Armalcolite/PDMS flexible sensor: A new entry, *Sensors Actuators B Chem.*, **2018**, *vol. 262*, pp. 211–220. DOI: 10.1016/j.snb.2018.01.207.

261. Silbande, A. *et al.* Effect of vacuum and modified atmosphere packaging on the microbiological, chemical and sensory properties of tropical red drum (Sciaenops ocellatus) fillets stored at 4 °C, *Int. J. Food Microbiol.*, **2018**, *vol. 266*, pp. 31–41. DOI: 10.1016/j.ijfoodmicro.2017.10.015.

262. Mattarozzi, M.; Lambertini, F.; Suman, M.; Careri, M. Liquid chromatography–full scan-high resolution mass spectrometry-based method towards the comprehensive analysis of migration of primary aromatic amines from food packaging, *J. Chromatogr. A*, **2013**, *vol. 1320*, pp. 96–102. DOI: 10.1016/j.chroma.2013.10.063.

263. Casella, I. G.; Gatta, M.; Desimoni, E. Determination of histamine by high-pH anion-exchange chromatography with electrochemical detection, *Food Chem.*, **2001**, *vol. 73, no. 3*, pp. 367–372. DOI: 10.1016/S0308-8146(01)00117-0.

264. Kang, J.; Hussain, A. T.; Catt, M.; Trenell, M.; Haggett, B.; Yu, E. H. Electrochemical detection of non-esterified fatty acid by layer-by-layer assembled enzyme electrodes, *Sensors Actuators, B Chem.*, **2014**, *vol. 190*, pp. 535–541. DOI: 10.1016/j.snb.2013.09.011.

265. Tanguy, N. R.; Fiddes, L. K.; Yan, N. Enhanced Radio Frequency Biosensor for Food Quality Detection Using Functionalized Carbon Nanofillers, *ACS Appl. Mater. Interfaces*, **2015**, *vol. 7, no. 22*, pp. 11939–11947. DOI: 10.1021/acsami.5b01876.

266. Wang, B.; Zhou, X.; Wu, Y.; Chen, Z.; He, C. Lead phthalocyanine modified carbon nanotubes with enhanced NH3sensing performance, *Sensors Actuators, B Chem.*, **2012**, *vol. 171–172*, pp. 398–404. DOI: 10.1016/j.snb.2012.04.084.

267. Hassan, A.; Basova, T.; Yuksel, F.; Gümüş, G.; Gürek, A. G.; Ahsen, V. Study of the interaction

between simazine and metal-substituted phthalocyanines using spectral methods, *Sensors Actuators, B Chem.*, **2012**, *vol. 175*, pp. 73–77. DOI: 10.1016/j.snb.2011.12.029.

268. Hu, G. H.; Lindt, J. T. Amidification of poly(styrene-co-maleic anhydride) with amines in tetrahydrofuran solution: A kinetic study, *Polym. Bull.*, **1992**, *vol. 29, no. 3–4*, pp. 357–363. DOI: 10.1007/BF00944831.

269. Silberberg, M. *Chemestry*, *5 th ed.* New York, NY, USA: McGraw-Hill, 2008.

270. Johnson, D. W. New Applications for Poly(ethylene-alt-maleic anhydride), University of Durham, 2010.

271. Samyn, P.; Deconinck, M.; Schoukens, G.; Stanssens, D.; Vonck, L.; Van den Abbeele, H. Synthesis and characterization of imidized poly(styrene-maleic anhydride) nanoparticles in stable aqueous dispersion, *Polym. Adv. Technol.*, **2012**, *vol. 23, no. 3*, pp. 311–325. DOI: 10.1002/pat.1871.

272. Donati, I.; Gamini, A.; Vetere, A.; Campa, C.; Paoletti, S. Synthesis, Characterization, and Preliminary Biological Study of Glycoconjugates of Poly(styrene- co -maleic acid), *Biomacromolecules*, **2002**, *vol. 3, no. 4*, pp. 805–812. DOI: 10.1021/bm020018x.

273. Cécile, C.; Hsieh, Y.-L. Hydrophilic polystyrene/maleic anhydride ultrafine fibrous membranes, *J. Appl. Polym. Sci.*, **2010**, *vol. 115, no. 2*, pp. 723–730. DOI: 10.1002/app.31003.

274. Su, S.; Du, F.-S.; Li, Z.-C. Synthesis and pH-dependent hydrolysis profiles of mono- and dialkyl substituted maleamic acids, *Org. Biomol. Chem.*, **2017**, *vol. 15, no. 39*, pp. 8384–8392. DOI: 10.1039/C7OB02188G.

275. Kumar, A.; Bhardwaj, N. K.; Singh, S. P. Sizing performance of alkenyl succinic anhydride (ASA) emulsion stabilized by polyvinylamine macromolecules, *Colloids Surfaces A Physicochem. Eng. Asp.*, **2018**, *vol. 539, no. September 2017*, pp. 132–139. DOI: 10.1016/j.colsurfa.2017.12.014.

276. Salewska, N.; Milewska, M. J. Efficient Method for the Synthesis of Functionalized Basic Maleimides, *J. Heterocycl. Chem.*, **2014**, *vol. 51, no. 4*, pp. 999–1003. DOI: 10.1002/jhet.1651.

277. Liu, Y.; Fu, J.; Ren, D.; Song, Z.; Jin, F.; Huo, Z. Efficient Synthesis of Succinimide from Succinic Anhydride in Water over Unsupported Nanoporous Nickel Material, *ChemistrySelect*, **2018**, *vol. 3, no. 2*, pp. 724–728. DOI: 10.1002/slct.201703154.

278. Sun, H.; Kabb, C. P.; Sims, M. B.; Sumerlin, B. S. Architecture-transformable polymers: Reshaping the future of stimuli-responsive polymers, *Prog. Polym. Sci.*, **2019**, *vol. 89*, pp. 61–75. DOI: 10.1016/J.PROGPOLYMSCI.2018.09.006.

279. Liu, H. Y.; Cao, K.; Huang, Y.; Yao, Z.; Li, B. G.; Hu, G. H. Kinetics and simulation of the imidization of poly(styrene-co-maleic anhydride) with amines, *J. Appl. Polym. Sci.*, **2006**, *vol. 100,*

no. 4, pp. 2744–2749. DOI: 10.1002/app.23371.

280. Kesim, H.; Rzaev, Z. M. O.; Dinçer, S.; Pişkin, E. Functional bioengineering copolymers. II. Synthesis and characterization of amphiphilic poly(N-isopropyl acrylamide-co-maleic anhydride) and its macrobranched derivatives, *Polymer (Guildf).*, **2003**, *vol. 44, no. 10*, pp. 2897–2909. DOI: 10.1016/S0032-3861(03)00177-0.

281. Díaz, A.; del Valle, L.; Franco, L.; Sarasua, J. R.; Estrany, F.; Puiggalí, J. Anhydric maleic functionalization and polyethylene glycol grafting of lactide-co-trimethylene carbonate copolymers, *Mater. Sci. Eng. C*, **2014**, *vol. 42*, pp. 517–528. DOI: 10.1016/J.MSEC.2014.05.069.

282. Auras, R.; Harte, B.; Selke, S. An overview of polylactides as packaging materials, *Macromol. Biosci.*, **2004**, *vol. 4, no. 9*, pp. 835–864. DOI: 10.1002/mabi.200400043.

283. Lopera-Valle, A.; Caputo, J. V; Leão, R.; Sauvageau, D.; Luz, S. M.; Elias, A. Influence of Epoxidized Canola Oil (eCO) and Cellulose Nanocrystals (CNCs) on the Mechanical and Thermal Properties of Polyhydroxybutyrate (PHB)—Poly(lactic acid) (PLA) Blends, *Polymers (Basel).*, **2019**, *vol. 11, no. 6*, pp. 1–18. DOI: 10.3390/polym11060933.

284. Issaadi, K.; Habi, A.; Grohens, Y.; Pillin, I. Maleic anhydride-grafted poly(lactic acid) as a compatibilizer in poly(lactic acid)/graphene oxide nanocomposites, *Polym. Bull.*, **2016**, *vol. 73, no. 7*, pp. 2057–2071. DOI: 10.1007/s00289-015-1593-z.

285. Hwang, S. W. *et al.* Grafting of maleic anhydride on poly(L-lactic acid). Effects on physical and mechanical properties, *Polym. Test.*, **2012**, *vol. 31, no. 2*, pp. 333–344. DOI: 10.1016/j.polymertesting.2011.12.005.

286. Ernzen, J. R. *et al.* Structure and properties relationship of melt reacted polyamide 6/malenized soybean oil, *J. Appl. Polym. Sci.*, **2016**, *vol. 133, no. 8*, pp. 1–10. DOI: 10.1002/app.43050.

287. Maharana, T.; Pattanaik, S.; Routaray, A.; Nath, N.; Sutar, A. K. Synthesis and characterization of poly(lactic acid) based graft copolymers, *React. Funct. Polym.*, **2015**, *vol. 93*, pp. 47–67. DOI: 10.1016/J.REACTFUNCTPOLYM.2015.05.006.

288. Detyothin, S.; Selke, S. E. M.; Narayan, R.; Rubino, M.; Auras, R. A. Effects of molecular weight and grafted maleic anhydride of functionalized polylactic acid used in reactive compatibilized binary and ternary blends of polylactic acid and thermoplastic cassava starch, *J. Appl. Polym. Sci.*, **2015**, *vol. 132, no. 28*, pp. 1–15. DOI: 10.1002/app.42230.

289. Detyothin, S.; Selke, S. E. M.; Narayan, R.; Rubino, M.; Auras, R. Reactive functionalization of poly(lactic acid), PLA: Effects of the reactive modifier, initiator and processing conditions on the final grafted maleic anhydride content and molecular weight of PLA, *Polym. Degrad. Stab.*, **2013**,

vol. 98, no. 12, pp. 2697–2708. DOI: 10.1016/j.polymdegradstab.2013.10.001.

290. Ma, P.; Jiang, L.; Ye, T.; Dong, W.; Chen, M. Melt free-radical grafting of maleic anhydride onto biodegradable poly(lactic acid) by using styrene as a comonomer, *Polymers (Basel).*, **2014**, *vol. 6, no. 5*, pp. 1528–1543. DOI: 10.3390/polym6051528.

291. Du, J.; Wang, Y.; Xie, X.; Xu, M.; Song, Y. Styrene-assisted maleic anhydride grafted poly(lactic acid) as an effective compatibilizer for wood flour/poly(lactic acid) bio-composites, *Polymers (Basel).*, **2017**, *vol. 9, no. 11*, pp. 1–12. DOI: 10.3390/polym9110623.

292. Csikós, Á.; Faludi, G.; Domján, A.; Renner, K.; Móczó, J.; Pukánszky, B. Modification of interfacial adhesion with a functionalized polymer in PLA/wood composites, *Eur. Polym. J.*, **2015**, *vol. 68*, pp. 592–600. DOI: 10.1016/j.eurpolymj.2015.03.032.

293. Birnin-yauri, A. U.; Ibrahim, N. A.; Zainuddin, N.; Abdan, K.; Then, Y. Y.; Chieng, B. W. Effect of maleic anhydride-modified poly(lactic acid) on the properties of its hybrid fiber biocomposites, *Polymers (Basel).*, **2017**, *vol. 9, no. 5*, pp. 1–16. DOI: 10.3390/polym9050165.

294. Drott, E. E.; Mendelson, R. A. Determination of polymer branching with gel-permeation chromatography. I. Theory, *J. Polym. Sci. Part A-2 Polym. Phys.*, **1970**, *vol. 8, no. 8*, pp. 1361–1371. DOI: 10.1002/pol.1970.160080808.

295. Dhar, P.; Tarafder, D.; Kumar, A.; Katiyar, V. Thermally recyclable polylactic acid/cellulose nanocrystal films through reactive extrusion process, *Polymer (Guildf).*, **2016**, *vol. 87*, pp. 268–282. DOI: 10.1016/J.POLYMER.2016.02.004.

296. Sin, L. T.; Rahmat, A. R.; Rahman, W. A. W. A.; Sin, L. T.; Rahmat, A. R.; Rahman, W. A. W. A. Thermal Properties of Poly(lactic Acid), in *Polylactic Acid*, *1st ed.*, Norwich, N.Y., USA: William Andrew Publishing, 2013, pp. 127–128.

297. Sütekin, S. D.; Atıcı, A. B.; Güven, O.; Hoffman, A. S. Controlling of free radical copolymerization of styrene and maleic anhydride via RAFT process for the preparation of acetaminophen drug conjugates, *Radiat. Phys. Chem.*, **2018**, *vol. 148*, pp. 5–12. DOI: 10.1016/J.RADPHYSCHEM.2018.02.012.

298. Murillo, E. A.; López, B. L. Effect of the maleic anhydride content on the structural, thermal, rheological and film properties of the n-butyl methacrylate–maleic anhydride copolymers, *Prog. Org. Coatings*, **2015**, *vol. 78*, pp. 96–102. DOI: 10.1016/J.PORGCOAT.2014.10.003.

299. Boztuğ, A.; Basan, S. Syntheses and characterization of maleic anhydride-styrene-allyl propionate terpolymer ester derivatives, *J. Appl. Polym. Sci.*, **2003**, *vol. 89, no. 2*, pp. 296–299. DOI: 10.1002/app.12080.

300. Kurmaz, S. V.; Poshchupkin, V. P.; Kochneva, I. S. IR Spectroscopy for Studying the Conversion of Double Bonds in the Radical Copolymerisation of Oligodimethacrylates with Styrene, *Int. Polym. Sci. Technol.*, **2003**, *vol. 30, no. 2*, pp. 43–48. DOI: 10.1177/0307174X0303000212.

301. Schlebrowski, T.; Beucher, L.; Bazzi, H.; Hahn, B.; Wehner, S.; Fischer, C. B. Prediction of a-C:H layer failure on industrial relevant biopolymer polylactide acide (PLA) foils based on the sp2/sp3 ratio, *Surf. Coatings Technol.*, **2019**, *vol. 368*, pp. 79–87. DOI: 10.1016/j.surfcoat.2019.03.069.

302. Tomasella, E.; Thomas, L.; Dubois, M.; Meunier, C. Structural and mechanical properties of a-C:H thin films grown by RF-PECVD, *Diam. Relat. Mater.*, **2004**, *vol. 13, no. 9*, pp. 1618–1624. DOI: 10.1016/j.diamond.2004.01.017.

303. González-López, M. E.; Robledo-Ortíz, J. R.; Manríquez-González, R.; Silva-Guzmán, J. A.; Pérez-Fonseca, A. A. Polylactic acid functionalization with maleic anhydride and its use as coupling agent in natural fiber biocomposites: a review, *Compos. Interfaces*, **2018**, *vol. 25, no. 5–7*, pp. 515–538. DOI: 10.1080/09276440.2018.1439622.

304. Piemonte, V.; Gironi, F. Kinetics of Hydrolytic Degradation of PLA, *J. Polym. Environ.*, **2013**, *vol. 21, no. 2*, pp. 313–318. DOI: 10.1007/s10924-012-0547-x.

305. Khankrua, R.; Pivsa-Art, S.; Hiroyuki, H.; Suttiruengwong, S. Grafting of poly (lactic acid) with maleic anhydride using supercritical carbon dioxide, *IOP Conf. Ser. Mater. Sci. Eng.*, **2015**, *vol. 87, no. 1*, p. 012066. DOI: 10.1088/1757-899X/87/1/012066.

306. Ellis, D. I.; Broadhurst, D.; Goodacre, R. Rapid and quantitative detection of the microbial spoilage of beef by Fourier transform infrared spectroscopy and machine learning, *Anal. Chim. Acta*, **2004**, *vol. 514, no. 2*, pp. 193–201. DOI: 10.1016/J.ACA.2004.03.060.

307. Liu, G.; Huang, Y.; Qu, X.; Xiao, J.; Yang, X.; Xu, Z. Understanding the hydrophobic mechanism of 3-hexyl-4-amino-1, 2,4-triazole-5-thione to malachite by ToF-SIMS, XPS, FTIR, contact angle, zeta potential and micro-flotation, *Colloids Surfaces A Physicochem. Eng. Asp.*, **2016**, *vol. 503*, pp. 34–42. DOI: 10.1016/J.COLSURFA.2016.05.028.

308. Losito, I.; De Giglio, E.; Cioffi, N.; Malitesta, C. Spectroscopic investigation on polymer films obtained by oxidation of o-phenylenediamine on platinum electrodes at different pHs, *J. Mater. Chem.*, **2001**, *vol. 11, no. 7*, pp. 1812–1817. DOI: 10.1039/b101626l.

309. Barrio, J.; Grafmüller, A.; Tzadikov, J.; Shalom, M. Halogen-hydrogen bonds: A general synthetic approach for highly photoactive carbon nitride with tunable properties, *Appl. Catal. B Environ.*, **2018**, *vol. 237*, pp. 681–688. DOI: 10.1016/J.APCATB.2018.06.043.

310. Zhang, Q.; Mo, Z.; Zhang, H.; Liu, S.; Cheng, S. Z. D. Crystal transitions of Nylon 11 under drawing

and annealing, *Polymer (Guildf).*, **2001**, *vol. 42, no. 13*, pp. 5543–5547. DOI: 10.1016/S0032-3861(01)00050-7.

311. Sperling, L. H. *Introduction to Physical Polymer Science*, *4th ed.* Hoboken, NJ, USA: John Wiley & Sons, Inc., 2005.

312. Sugai, N.; Asai, S.; Tezuka, Y.; Yamamoto, T. Photoinduced topological transformation of cyclized polylactides for switching the properties of homocrystals and stereocomplexes, *Polym. Chem.*, **2015**, *vol. 6, no. 19*, pp. 3591–3600. DOI: 10.1039/c5py00158g.

313. Das, R.; Bandyopadhyay, R.; Pramanik, P. Stereo-regulated Schiff base siloxane polymer coated QCM sensor for amine vapor detection, *Mater. Chem. Phys.*, **2019**, *vol. 226*, pp. 214–219. DOI: 10.1016/J.MATCHEMPHYS.2019.01.023.

314. Khan, A. A.; Hussain, R.; Khan, M. Q. Amines vapour sensing kinetics and electrical properties of synthetic Polyaniline-titanium(IV)sulphosalicylophosphate cation exchange nanocomposite, *Environ. Nanotechnology, Monit. Manag.*, **2017**, *vol. 8, no. May*, pp. 187–198. DOI: 10.1016/j.enmm.2017.06.004.

315. Shen, M. L.; Wei, Z.; Xu, L.; Liu, B.; Jiao, H. A mixed matrix Eu-4,4′-biphenyldicarboxylate coordination polymer film as a fluorescence turn-off sensor to aniline vapor, *J. Solid State Chem.*, **2019**, *vol. 269*, pp. 87–93. DOI: 10.1016/J.JSSC.2018.09.014.

316. Fiddes, L. K.; Yan, N. RFID tags for wireless electrochemical detection of volatile chemicals, *Sensors Actuators, B Chem.*, **2013**, *vol. 186*, pp. 817–823. DOI: 10.1016/j.snb.2013.05.008.

317. Lopera-Valle, A.; Elias, A. Amine Responsive Poly(lactic acid) (PLA) and Succinic Anhydride (SAh) Graft-Polymer: Synthesis and Characterization, *Polymers (Basel).*, **2019**, *vol. 11, no. 9*, p. 1466. DOI: 10.3390/polym11091466.

318. Domínguez-Aragón, A.; Olmedo-Martínez, J. A.; Zaragoza-Contreras, E. A. Colorimetric sensor based on a poly(ortho-phenylenediamine-co-aniline) copolymer for the monitoring of tilapia (Orechromis niloticus) freshness, *Sensors Actuators, B Chem.*, **2018**, *vol. 259*, pp. 170–176. DOI: 10.1016/j.snb.2017.12.020.

319. Del, J. *et al.* Dye incorporation in polyphosphate gels: synthesis and theoretical calculations, *Mater. Res.*, **2003**, *vol. 6, no. 3*, pp. 335–340. DOI: 10.1590/S1516-14392003000300006.

320. Nivedhini Iswarya, C.; Kiruba Daniel, S. C. G.; Sivakumar, M. Studies on L-histidine capped Ag and Au nanoparticles for dopamine detection, *Mater. Sci. Eng. C*, **2017**, *vol. 75*, pp. 393–401. DOI: 10.1016/j.msec.2016.11.102.

321. Yin, M.; Zhao, L.; Wei, Q.; Li, H. Rapid colorimetric detection of melamine by H2O2 - Au

nanoparticles, *RSC Adv.*, **2015**, *vol. 5, no. 42*, pp. 32897–32901. DOI: 10.1039/C5RA02717A.

322. Ismail, M.; Khan, M. A. I.; Akhtar, K.; Khan, M. A. I.; Asiri, A. M.; Khan, S. B. Biosynthesis of silver nanoparticles: A colorimetric optical sensor for detection of hexavalent chromium and ammonia in aqueous solution, *Phys. E Low-Dimensional Syst. Nanostructures*, **2018**, *vol. 103, no. June*, pp. 367–376. DOI: 10.1016/j.physe.2018.06.015.

323. Urmila, K.; Li, H.; Chen, Q.; Hui, Z.; Zhao, J. Quantifying of total volatile basic nitrogen (TVB-N) content in chicken using a colorimetric sensor array and nonlinear regression tool, *Anal. Methods*, **2015**, *vol. 7, no. 13*, pp. 5682–5688. DOI: 10.1039/c5ay00596e.

324. Zhai, H. *et al.* Biogenic amines in commercial fish and fish products sold in southern China, *Food Control*, **2012**, *vol. 25, no. 1*, pp. 303–308. DOI: 10.1016/j.foodcont.2011.10.057.